Beneficial therapeutic effects of the L-type calcium channel antagonist nimodipine in experimental autoimmune encephalomyelitis – an animal model for multiple sclerosis

Günstige therapeutische Effekte des L-Typ-Calciumkanal-Antagonisten Nimodipin in der experimentellen autoimmunen Enzephalomyelitis − einem Tiermodell der Multiplen Sklerose

Doctoral thesis for a doctoral degree
at the Graduate School of Life Sciences,
Julius-Maximilians-Universität Würzburg,
Section Neuroscience.
Submitted by

Andrea Schampel

from

Bonn

Würzburg 2017

Submitted on:

Members of the *Promotionskomitee*:

Chairperson: Prof. Dr. rer. nat. Ulrike Holzgrabe

Primary Supervisor: Prof. Dr. med. Stefanie Kürten

Supervisor (Second): PD Dr. rer. nat. Robert Blum

Supervisor (Third): Prof. Dr. med. Paul V. Lehmann

Date of Public Defence:

Date of Receipt of Certificates:

Günstige therapeutische Effekte des L-Typ-Calciumkanal-Antagonisten Nimodipin in der experimentellen autoimmunen Enzephalomyelitis − einem Tiermodell der Multiplen Sklerose

Beneficial therapeutic effects of the L-type calcium channel antagonist nimodipine in experimental autoimmune encephalomyelitis – an animal model for multiple sclerosis

Dissertation zur Erlangung des naturwissenschaftlichen Doktorgrades
der Graduate School of Life Sciences,
Julius-Maximilians-Universität Würzburg,
Fachbereich Neurowissenschaften.
Vorgelegt von

Andrea Schampel
aus
Bonn

Würzburg 2017

Eingereicht am:

Mitglieder des Promotionskomitees:

Vorsitzende/r: Prof. Dr. rer. nat. Ulrike Holzgrabe

1. Betreuer: Prof. Dr. med. Stefanie Kürten

2. Betreuer: PD Dr. rer. nat. Robert Blum

3. Betreuer: Prof. Dr. med. Paul V. Lehmann

Tag des Promotionskolloquiums:

Doktorurkunden ausgehändigt am:

Affidavit

I hereby confirm that my thesis entitled “Beneficial therapeutic effects of the L-type calcium channel antagonist nimodipine in experimental autoimmune encephalomyelitis – an animal model for multiple sclerosis” is the result of my own work. I did not receive any help or support from commercial consultants. All sources and / or materials applied are listened and specified in the thesis. Furthermore, I confirm that this thesis has not yet been submitted as part of another examination process neither in identical or similar form.

Würzburg,

Andrea Schampel

Eidesstattliche Erklärung

Hiermit erkläre ich an Eides statt, die Dissertation „Günstige therapeutische Effekte des L-Typ Calciumkanal-Antagonisten Nimodipin in der experimentellen autoimmunen Enzephalomyelitis - einem Tiermodell der Multiplen Sklerose“ eigenständig, d.h. insbesondere selbständig und ohne Hilfe eines kommerziellen Promotionsberaters angefertigt, und keine anderen als die von mir angegebenen Quellen und Hilfsmittel verwendet zu haben. Ich erkläre außerdem, dass die Dissertation weder in gleicher noch in ähnlicher Form bereits in einem anderen Prüfungsverfahren vorgelegen hat.

Würzburg,

Andrea Schampel

To friends and family.

Play is the highest form of research.
(Albert Einstein)

Once the development was ended

the founts of growth and regeneration of the axons and dendrites dried up irrevocably. In the adult centers, the nerve paths are something fixed, ended, and immutable. Everything may die, nothing may be regenerated. It is for the science of the future to change, if possible, this harsh decree.

Santiago Ramon y Cajal, 1911

Summary

Multiple sclerosis (MS) is the most prevalent neurological disease of the central nervous system (CNS) in young adults and is characterized by inflammation, demyelination and axonal pathology that result in multiple neurological and cognitive deficits. The focus of MS research remains on modulating the immune response, but common therapeutic strategies are only effective in slowing down disease progression and attenuating the symptoms; they cannot cure the disease. Developing an option to prevent neurodegeneration early on would be a valuable addition to the current standard of care for MS. Based on our results we suggest that application of nimodipine could be an effective way to target both neuroinflammation and neurodegeneration. We performed detailed analyses of neurodegeneration in experimental autoimmune encephalomyelitis (EAE), an animal model of MS, and in *in vitro* experiments regarding the effect of the clinically well-established L-type calcium channel antagonist nimodipine. Nimodipine treatment attenuated the course of EAE and spinal cord histopathology. Furthermore, it promoted remyelination. The latter could be due to the protective effect on oligodendrocytes and oligodendrocyte precursor cells (OPCs) we observed in response to nimodipine treatment. To our surprise, we detected calcium channel-independent effects on microglia, resulting in apoptosis. These effects were cell type-specific and independent of microglia polarization. Apoptosis was accompanied by decreased levels of nitric oxide (NO) and inducible NO synthase (iNOS) in cell culture as well as decreased iNOS expression and reactive oxygen species (ROS) activity in EAE. Overall, application of nimodipine seems to generate a favorable environment for regenerative processes and could therefore be a novel treatment option for MS, combining immunomodulatory effects while promoting neuroregeneration.

Zusammenfassung

Multiple Sklerose (MS) ist die häufigste neurologische Erkrankung des zentralen Nervensystems (ZNS) von jungen Erwachsenen und charakterisiert durch Inflammation, Demyelinisierung und axonale Pathologie. Diese Prozesse bewirken zahlreiche neurologische und kognitive Defizite. Der Schwerpunkt in der MS-Forschung besteht derzeit vor allem in der Modulation der Immunantwort, jedoch sind herkömmliche Therapiestrategien bislang nur in der Lage die Progression der Erkrankung zu verlangsamen und die Symptome zu lindern, die Krankheit kann jedoch immer noch nicht geheilt werden. Die Möglichkeit, den Prozess der Neurodegeneration früh aufzuhalten, würde eine wertvolle Ergänzung zu herkömmlichen Therapien darstellen. Basierend auf den Ergebnissen dieser Studie schlagen wir vor, dass die Applikation von Nimodipin eine elegante Möglichkeit wäre, um sowohl die Neuroinflammation als auch die -degeneration zu bekämpfen. Um den Effekt des klinisch gut etablierten Calciumkanal-Antagonisten Nimodipin zu untersuchen, haben wir detaillierte Analysen der Degeneration in der experimentellen autoimmunen Enzephalomyelitis (EAE), einem Tiermodell der MS, und in *in vitro* Untersuchungen durchgeführt. Applikation von Nimodipin verringerte das klinische Erscheinungsbild der EAE sowie die Histopathologie des Rückenmarkes. Außerdem förderte es die Regeneration. Die Ursache für letzteres liegt vermutlich am protektiven Effekt der Behandlung mit Nimodipin auf die Oligodendrozyten und deren Vorläuferzellen. Überraschenderweise, konnten wir Calciumkanal-unspezifische Effekte auf Mikroglia feststellen, die in Apoptose resultierten und sowohl Zelltyp-spezifisch als auch unabhängig von der Polarisierung der Mikrogliazellen waren. Apoptose wurde begleitet von reduzierten Spiegeln an Stickstoffmonoxid (NO) und der induzierbaren NO Synthase (iNOS) in Zellkultur, sowie einer reduzierten Expression von iNOS und dem geringeren Vorkommen von reaktiven oxygenen Spezies (ROS) in der EAE. Zusammenfassend gehen wir davon aus, dass die Applikation von Nimodipin eine günstige

Umgebung für regenerative Prozesse schafft. Daher stellt die Applikation dieser Substanz eine neue Behandlungsmöglichkeit für die MS dar, insbesondere da sie Möglichkeiten der Immunmodulation mit der Förderung von Neuroregeneration verbindet.

Table of contents

List of abbreviations

Aβ	amyloid β
AD	Alzheimer´s disease
ALF	anterolateral funiculus
ALS	amyotrophic lateral sclerosis
APC	adenomatous polyposis coli
APP	amyloid precursor protein
BBB	blood-brain barrier
BCL2	B cell lymphoma 2
BDNF	brain-derived neurotrophic factor
BSA	bovine serum albumin
CACNA2D2	(VGCCs) subunit Alpha2delta2
CACO	cacodylate
CFA	complete Freund´s adjuvant
CNS	central nervous system
cPARP	cleaved poly (ADP-ribose) polymerase
CPT1A	carnitine palmitoyltransferase 1A
CSF	cerebrospinal fluid
DAB	3.3'-diaminobenzidine
dHet	dihydroethidium
DMSO	dimethyl sulfoxide
DNA	deoxyribonucleic acid
DTI	diffusion tensor imaging
EAE	experimental autoimmune encephalomyelitis

EDSS	enhanced status disability score
EM	electron microscopy
ER	endoplasmic reticulum
FDR	false discovery rate
FGF2	fibroblast growth factor 2
FODOs	fields of dead oligodendrocytes
GA	glatiramer acetate
GDNF	glial cell-derived neurotraphic factor
GFAP	glial fibrillary acidic protein
GLA	glutardialdehyde
HRP	horseradish peroxidase
Iba1	ionized calcium binding adapter molecule 1
IFN-β	interferon-β
IFN-γ	interferon-γ
IGF1	insulin-like growth factor 1
IHC	immunohistochemistry
IL-1β	interleukin-1β
IL-4	interleukin-4
iNOS	inducible nitric oxide synthase
LINGO-1	leucine rich repeat and immunoglobin-like domain-containing protein 1
L-VDCC	L-type VDCC
MAG	myelin-associated glycoprotein
MAPK	mitogen activated protein kinase
MBP	myelin basic protein
MHC	major histocompatibility complex
MIP1α	macrophage inflammatory protein 1α

MOG	myelin oligodendrocyte glycoprotein
MP4	PLP and MBP fusion protein
MRS	magnetic resonance spectroscopy
MS	multiple sclerosis
NAA	*N*-acetylaspartate
NF-κB	nuclear factor kappa-light-chain-enhancer of activated B-cells
NG2	neural/glial antigen 2
NGF	nerve growth factor
NGS	normal goat serum
NMDA	N-methyl-D-aspartate
NO	nitric oxide
NOGO-A	neurite outgrowth inhibitor A
NOS	nitric oxide synthase
NOS2	nitric oxide synthase 2
NOX2	NADPH oxidase 2
NOX4	NADPH oxidase 4
NPG	n-propyl gallate
N-VDCC	N-type VDCC
Olig2	oligodendrocyte transcription factor 2
OPC	oligodendrocyte precursor cell
PBS	phosphate-buffered saline
PD	Parkinson´s disease
PEG 400	polyethyleneglycol 400
PF	posterior funiculus
PFA	paraformaldehyde
PLP	proteolipid protein

PMA	phorbol-12-myristate-13-acetate
PMSF	phenylmethylsulfonyl fluoride
PP-MS	primary progressive
PR-MS	progressive remitting
P/Q-VDCC	P/Q-type VDCC
ROS	reactive oxygen species
RR-MS	relapsing-remitting MS
RT	room temperature
R-VDCC	R-type VDCC
S1P	sphingosine-1-phosphate
SD	standard deviation
SEM	standard error of the mean
SEMA3A	semaphorin 3A
SEMA4D	semaphorin 4D
SEMA6A	semaphorin 6A
SEMA7A	semaphorin 7A
SP-MS	secondary progressive
TBS	tris-buffered saline
TBS-T	TBS containing 0.05 % Tween
TEA	tetraethylammonium
TMEV	Theiler´s murine encephalomyelitis virus
TNF-α	tumor necrosis factor-α
TRP	transient receptor potential
TRPA1	transient receptor potential cation channel subfamily A member 1
T-VDCC	T-type VDCC
VDCC(s)	voltage-dependent calcium channel(s)

VSCC	L-type voltage sensitive calcium channel(s)
WGA	wheat germ agglutinin

Annotation regarding the nomenclature of proteins/genes:

If possible, proteins were written in regular font (e.g. TRPA1) and genes were written in italics (e.g. *TRPA1*). Human proteins/genes were written in capital letters (TRPA1/*TRPA1*), murine proteins/genes in lower cases (Trpa1/*Trpa1*). Due to a better reading comprehension, or to be consistent with other studies this nomenclature may differ.

I. Introduction

I.1 Multiple sclerosis (MS)

MS is an autoimmune disease and the most prevalent disorder of the CNS in young adults [1-4]. It is characterized by inflammation, demyelination and axonal pathology, leading to multiple neurological deficits [2]. These range from motor and sensory deficits to cognitive impairment and psychological issues [5,6]. Common therapeutic strategies are able to attenuate the immune response, which can lead to milder symptoms and a slower progression of disease. Currently, there is no cure for this disease. As most therapeutic strategies do not provide persistent prevention of neurodegeneration, focusing on this area of research is an urgent need to treat all aspects of disease and could be a step towards curing MS.

I.1.1 Etiology of MS

As it causes multiple neurological and cognitive deficits, MS severely affects quality of life. However, it has a low lethality (5-10 % of all cases) [6]. The mean age to develop MS varies from 20 to 40 years. To date, primary triggers for MS are still unknown, but several factors are suspected to influence disease development [4,7]. Consensus in the field is that affected individuals have genetic risk factors that require a boost via an environmental trigger to develop the disease. Several genes on chromosome 6p21- flanking the area of the major histocompatibility complex (MHC) - are altered in MS patients [8]. In addition, polymorphisms in other alleles, like T-cell receptor genes, were identified in patients [5]. Population, family and twin studies indicate that disease prevalence is significantly increased for family members of affected individuals, underlining the genetic component of the disease. Stress, lifestyle, location of residence and infections are considered environmental risks to provoke disease development [4-6,9,10]. It has been demonstrated that human Herpes virus 6 and Epstein-Barr virus may induce MS or trigger relapses [5]. Additionally, Northern Europe,

Canada and the Northern parts of the USA have the highest incidence of MS, whereas Japan is a low risk area [5,6]. Sunlight exposure and vitamin D deficiency are suggested as potential reasons for this North-South difference in MS incidence [5]. In general, women are more likely to be affected than men (female-to-male ratio ranging from 1.6–2.0:1) [5]. This was related to different hormonal conditions. Accordingly, elevated estrogen and low progesterone levels were correlated with increased MRI disease activity and an increased susceptibility for MS [5,6]. This is supported by a lower relapse rate during pregnancy, a subsequent disease rebound and the worsening of MS during menstruation [5]. However, the precise mechanisms by which sex hormones may influence MS susceptibility are not known but estrogens seem to stimulate pro-inflammatory cytokine secretion.

Due to the multimodal etiology it is difficult to determine what the primary trigger of MS is. The broad spectrum of environmental triggers and genetic risk alleles cause a distinct heterogeneity of disease, further complicating the discovery of a curative treatment.

I.1.2 Clinical Presentation

Patients often refer to MS as the "many-faced disease". This expression depicts clearly the distinct inter-individual differences in the course and presentation of disease. Nevertheless, it is possible to distinguish two main forms. The most common form is relapsing-remitting MS (RR-MS) as it affects 80-85 % of all MS patients [11,12]. The RR-course of disease presents with repeated appearance of relapses. The second main form is primary progressive MS (PP-MS); only about 15 % of MS patients suffer from PP-MS [5,6,10]. In most of the RR-MS patients the disease progresses to a form that is called secondary progressive MS (SP-MS), characterized by steady worsening of the disease over time. Additionally, a steady decline of RR-MS with worsening attacks leads to progressive remitting (PR-MS) [13]. In approximately 50 % of patients with RR-MS progressive worsening develops 10-15 years

after initial diagnosis [4]. Neurological deficits usually increase during the relapse phase and exacerbations are followed by remissions with partial or full recovery [4,10]. Remissions are explained by changes on the cellular level, like myelination processes. Other factors may be the functional plasticity of cells that surround damaged axons as well as the plasticity of the contralateral cortical area. Relapses are characterized by subsiding of edema and decreased secretion of cytokines by inflammatory cells [10].

I.1.3 Pathogenesis of MS

Differentiation of activated $CD4^+$ T cells into a T_H1 subtype is considered the initiating event of MS pathology [5]. Autoreactive $CD4^+$ T cells are activated in the periphery, cross the blood-brain barrier (BBB) and reach the brain tissue where they are reactivated. Subsequently, other cells, like B cells, monocytes and $CD8^+$ T cells are attracted by cytokines to the inflammatory side and also cross the BBB. In healthy individuals, these cells cannot enter the brain but in MS, the BBB becomes leaky. Infiltrating cells are components of the lesions in the CNS of MS patients and cause edema [14]. Demyelination and axonal damage can be initiated following activation of microglia, which release NO and show increased glutamate production. Enhanced glutamate levels can cause over-excitation, as glutamate is the major excitatory neurotransmitter, leading to the onset of nerve fiber injury cascades e.g. by an increase in the intracellular sodium and/or calcium concentration [4,5,10-12,15-18]. Like $CD8^+$ cytotoxic T cells, NO can injure the tissue and even induce apoptosis [4,5,10]. Ongoing pathogenesis results in changes within the CNS. These include demyelination, nude axons and *ovoids* (balloon-like axonal swellings) indicating axonal transection and other indices of injured nerve fibers. These pathological changes are suspected to cause neurological impairment in patients and often correlate with irreversible clinical deficits [4,5]. Macrophages/microglia containing myelin lipids are frequently detected, indicating these cells

are involved in the clearing of myelin from damaged nerves [4]. After the acute phase of neurodegeneration, axonal sprouting can be observed within the injured area and in the surrounding tissue. Unaffected oligodendrocytes or oligodendrocyte precursors start remyelinating the demyelinated nerve fibers [5,10] but the new myelin sheath is thinner than the original sheath. This results in a reduced transmission speed of stimuli compared to healthy nerve fibers, causing slower reflexes in MS patients [5,10].

Today the understanding of MS pathology is more refined. For example, there is accumulating evidence that B cells play an important role in mediating MS pathology [15,19]. Also, the traditional paradigm of inflammation-induced neurodegeneration has recently begun to change as activated microglia and dying oligodendrocytes are observed in early, acute brain lesions in the absence of T cell infiltration [20,21]. These widespread areas of apoptotic oligodendrocytes were named FODOs ("fields of dead oligodendrocytes") by *Barnett and Prineas, 2004* [20]. Their observation suggests that MS may be a primary disease of neurons, and damaged nerve fibers and/or oligodendrocytes subsequently trigger an autoimmune reaction in response to neurodegeneration [21,22]. Now that imaging techniques have further improved, axonal pathology can be detected earlier and more precisely. These techniques are able to substantiate the histopathological findings, especially regarding the theory of an early axonal pathology at disease onset [23,24]. Interestingly, *Charcot* already described in 1868 that nerve fiber pathology is present within early acute inflammatory lesions in MS [25]. Recent findings from imaging studies led to the hypothesis that clinical progression in MS may be caused by the inability of mechanisms to compensate for axonal loss due to reduced plasticity [18,21,26]. Although the occurrence of neurodegeneration prior to inflammation as mechanism for disease pathology is still a matter of debate, latest findings underline the need to focus on early neurodegeneration in MS research.

I.1.4 Present therapeutic strategies for MS

Current therapeutic strategies aim at modulating the immune response but they cannot cure the disease. Yet, they are able to slow disease progression and to attenuate symptoms. To suppress the inflammatory reaction during acute exacerbations and relapses, glucocorticoids are commonly administered. They inhibit immune cell-migration and affect humoral immune processes [27]. Moreover, glucocorticoids are capable of inhibiting arachnoid acid metabolites and to restore the BBB [27]. As basic therapy for MS, especially for RR-MS, the administration of immunomodulatory drugs such as interferon-beta (IFN-β) or glatiramer acetate (GA) are first-line strategies [27-29]. IFN-β mainly attenuates the autoreactive T cell response, whereas GA has additional potential to influence neuroprotection. Its primary effect is based on shifting the T cell response towards a T_H2 phenotype. Thereby, it could also trigger the production of anti-inflammatory cytokines or neurotrophic factors by these cells [14,28,29]. Additionally, GA was shown to promote neurogenesis, proliferation and differentiation of OPCs, thus supporting remyelination [29]. If first-line therapies fail, monoclonal antibodies like natalizumab are an option for MS treatment. The underlying mechanism is to modulate immune cell functions, e.g. blocking of cell adhesion and subsequent infiltration of immune cells into the lesion site [27,30]. Some monoclonal antibodies like alemtuzumab can induce depletion of T cells and B cells. Alemtuzumab was able to decrease the relapse rate in patients that did not respond to first-line therapy or have not been treated with immune modulatory substances before [27]. In the US, fingolimod is a first-line therapy for MS. The metabolized substance is able to influence lymphocyte migration by binding to their sphingosine-1-phosphate (S1P) receptor and is administered orally. As it can pass the BBB easily, it is likely that it binds to neural and glial cell S1P receptors as well and further influences the disease [27]. Modulating the T cell and B cell proliferation by cytostatic agents like azathioprine, cyclophosphamide and minocycline have

not been successful enough for a treatment in patients [12,27,31]. Taken together there is still no neuroprotective treatment in first-line therapy. Only few strategies that specifically aim at protecting nerve fibers are currently available. One approach is to reduce damage induced by free radicals by reduction of ROS [12,26]. Yet another strategy is to protect axons from NO. Indeed, the sodium channel antagonist lamotrigine was able to protect axons exposed to NO [26] and might suppress the activation of innate immune cells, in particular microglia and their migratory activity [26,32]. Unfortunately the clinical trial failed, as lamotrigine did not protect against early brain atrophy. However, it should be mentioned that only patients with an advanced course of the disease were included in the study. Another approach is to restore the conduction along demyelinated axons by insertion of new sodium channels into damaged nerve fiber segments [21]. Additionally, several studies have focused on cell types that are involved in CNS regeneration. Peripheral nerve segments or olfactory glial cells are capable of regeneration and have been shown to enhance functional recovery and regeneration of axons when implanted into the lesion site [33]. Fetal rat tissue was also implanted into adult animals, but regeneration only occurred under optimized conditions (additional trophic support) [33]. An increasing number of studies deal with the effects of transplanted neural progenitor and mesenchymal stem cells. Indeed, their implantation initiated immunomodulatory responses, oligodendrogenesis, the expression of neurotrophic factors [33,34] and a reduction of clinical symptoms after transplantation was reported. Right now, some of these cellular therapies are already in clinical trials [33,34]. Other studies aim at modulating CNS damage via growth factors like insulin-like growth factor 1 (IGF1) and fibroblast growth factor 2 (FGF2). Both were shown to increase neuroregenerative processes and remyelination [1,35]. Frank *et al., 2002* [25] administered IGF1 to MS patients, but they did not find any significant improvement in MRI endpoints. However, they did not use advanced MRI techniques to assess their results. This illustrates another problem regarding

the development of regenerative strategies; there is a lack of clinical tools and biomarkers to detect and quantify regenerative processes. In general, administration of neuroprotective treatments is limited by several factors like a short half-life or the inability to cross the BBB [12,33].

I.2 The role of glia cells in neurodegenerative disease

Regarding the role of glial cell in neurodegenerative diseases, most studies focus on Alzheimer's (AD) and Parkinson's disease (PD), and little is known about their role in MS. Generally, studies focus mainly on astrocytes and microglia as they are suspected to initiate detrimental processes in the pathology of CNS diseases.

Microgliosis is a hallmark of several neurological diseases including stroke, injury, epilepsy as well as neurodegenerative diseases like PD and AD [36-38]. Under normal conditions, microglia help maintain CNS homeostasis, remove toxic products and can secrete neuroprotective factors like nerve growth factor (NGF) an essential factor for sprouting axons [38,39]. However, activated microglial cells can also do more harm in the area of injury or degeneration, e.g. by turning into scavenger cells, activating T cells, expressing cytokines, glutamate, iNOS, production of NO and production of ROS [39,40]. Along this line macrophage inflammatory protein 1α (MIP1α) was associated with the recruitment of macrophages/microglia into demyelinating lesions, and in MIP1α deficient mice a significant decrease in demyelination was detectable [40]. Furthermore, it was shown that *ovoids*, an early sign of axonal damage in various neurological disorders, are induced by microglia-released glutamate [36]. Activated microglial cells were associated with degradation of synaptic proteins and atypical phosphorylation of neurofilaments in the cerebral cortex [41]. Demyelination can be caused by expression of pro-inflammatory cytokines like tumor necrosis factor-α (TNF-α), which is secreted by microglia [42] and macrophages/microglia

have also been shown to strip myelin. As they are further capable of killing OPCs and neurons, and expression of pro-inflammatory cytokines can lead to insufficient recruitment and differentiation of OPCs [42-45], microglia can actively inhibit remyelination. Pro-inflammatory cytokines secreted by microglia (e.g. TNF-α and interferon-γ (INF-γ)) induce the release of glutamate. Excessive glutamate release leads to stimulation of the N-methyl-D-aspartate (NMDA) receptor, triggering mitochondrial death and subsequent apoptosis of oligodendrocytes and neurons [45]. To explain both the detrimental and beneficial effects of microglia, several research groups suggest that microglia show different polarization, referred to as pro (M1) - and anti (M2)- inflammatory subtype, but this concept is a matter of debate [36,46-50].

Besides microglia, astrocytes also play an ambiguous role in neurodegenerative diseases. They communicate with neurons and support them with metabolic substances and growth factors, like brain-derived neurotrophic factor (BNDF) [21,59]. In response to CNS damage they form the "glia limitans". This morphological boarder serves as natural limit for proliferation and hypertrophy but it can also limit remyelination [14]. Like microglia, they can harm other cells by the expression of glutamate, NO, cytokines and induction of ROS [36,37]. In amyotrophic lateral sclerosis (ALS) it was demonstrated that astrocytes can express mutant SOD1 which can cause excessive loss of motor neurons [37]. Overexpression of tau, which is a known feature of many neurodegenerative diseases, was found in several glial cell types like oligodendrocytes and microglia under pathological conditions in humans [51]. In oligodendrocytes and OPCs overexpression of α-synuclein and inhibitors of remyelination (e.g. neurite outgrowth inhibitor A, NOGO-A; myelin-associated glycoprotein, MAG; neural/glial antigen 2, NG2) are detected and associated with neurodegenerative diseases [14,37]. Although all glia-subtypes can contribute to pathological processes in neurological

and neurodegenerative diseases, astrocytes and particularly oligodendrocytes are associated with protective effects whereas microglial cells are mainly considered harmful.

I.3 Animal models of MS

Progress in understanding the pathology of MS is still mostly dependent on suitable animal models since specimens from MS patients are not readily available. As patients represent a heterogeneous group with a high inter- individual variability, it is easier to study mice with the same genetic background in a controllable and standardized environment. Three main animal models are used to mimic MS pathology: the cuprizone model, infection with Theiler's murine encephalomyelitis virus and immunization of animals leading to EAE.

I.3.1 Cuprizone model

The toxin cuprizone is usually administered via the food and leads to a complete loss of the myelin sheath with subsequent neoformation [52-55]. It is a good model to study de- and remyelination, but is lacking an autoimmune component [56]. The exact mechanism behind cuprizone intoxication is not understood. However, its feature to act as copper-chelator is suspected to inhibit mitochondrial enzymes of the respiratory chain, which require copper as co-factor. This leads to oxidative stress, followed by oligodendrocyte apoptosis, microglia and astrocyte activation. The first signs of oligodendrocyte apoptosis are detectable as early as two days after initiation of the cuprizone diet. Demyelination is usually complete after 4–5 weeks cuprizone application [56]. Once the cuprizone diet is replaced by regular chow strong endogenous remyelination is detectable and can be studied [52-55].

I.3.2 Theiler's murine encephalomyelitis virus (TMEV)

This type of MS model is induced by infection of the CNS with Theiler's murine encephalomyelitis virus via inoculation [57,58]. Usually the infection leads to autoimmune reactions in the CNS starting with the apoptosis of neurons, particularly in the grey matter. During the chronic phase of disease, the white matter is also affected in disease pathology, presumably by increased involvement of macrophages and glia cells in the autoimmune reaction. TMEV infection may mimic the viral infections as trigger for MS.

I.3.3 Experimental autoimmune encephalomyelitis (EAE)

EAE is the most common and the best characterized animal model for MS [59,60]. Its introduction as an animal model for MS was an important step towards gaining insights that are relevant for the therapy of patients suffering from MS. EAE is induced by the immunization of animals with antigens and adjuvants that operate encephalogenic [60]. This procedure was first used in 1855 by *Louis Pasteur* during his experiments for developing the rabies vaccination [61]. When he tried to "immunize" patients with infected spinal cords from rabbits this led to an unintended descending paresis, which is now considered the hallmark of EAE. Due to this severe side effect, this approach for vaccination was abandoned. It was not until the 1930s when *Rivers* further examined *Pasteur's* observations, and demonstrated that immunization in rabbits and rhesus macaques led to inflammation and demyelination. The idea for EAE as animal model for MS was born [61].

I.3.3.1 Induction

There are several ways to induce EAE: spontaneous models, passive/adoptive transfer and active immunization. Spontaneous models are a relatively young approach. For this approach T cell receptor transgenic mice are used, carrying a T cell receptor specific for myelin

oligodendocyte glycoprotein (MOG). Mice with SJL/J background spontaneously develop relapsing-remitting EAE, altering between different CNS tissues [62]. A more classical attempt is the passive/adoptive transfer. Here auto-reactive T cells are transferred into naïve animals. For this purpose, encephalitogenic T cells are isolated from the lymphoid tissues of an animal that has been immunized with a CNS antigen before. The T cells are re-stimulated *in vitro* and subsequently transferred into a naive recipient. The activated, now myelin-specific $CD4^+$ T cells can cross the BBB and initiate inflammation. For active immunization, spinal cord homogenates were originally used [61]. Today CNS proteins or short peptide sequences purified from the CNS are applied to induce EAE in susceptible animal stains. In this process, the selected myelin antigen is emulsified in complete Freund´s adjuvant (CFA) in order to boost the T cell response and enhance local antibody production. CFA consists of paraffin oil, mannide monooleate and inactivated *Mycobacterium tuberculosis*, triggering a pro-inflammatory immune response that induces inflammation and subsequent demyelination. Similar to MS, EAE is characterized by three hallmarks; multifocal inflammation within the CNS tissue, demyelination and axonal pathology. Clinically, EAE is characterized by an ascending paresis, starting at the tail, followed by hind limb weakness, hind limb paresis and finally resulting in fore limb paresis. In order to induce EAE, additional application of pertussis toxin to perforate the BBB to greater extent is necessary [63]. Some mice develop a so-called “atypical” EAE that is characterized by ataxia, sensomotoric deficits and spasticity [60]. Our study makes use of the active immunization with the myelin antigen MP4 dissolved in CFA.

I.3.3.2 Phenotypes of EAE

Various myelin antigens are used for the induction of EAE. In a suitable animal strain, they cause either acute, chronic or relapsing-remitting encephalomyelitis, so that immunization

with each different myelin antigen leads to a characteristic form of EAE. The most studied myelin antigens are myelin basic protein (MBP), proteolipid protein (PLP) and MOG. PLP usually causes a chronic form of disease in C57BL/6 mice, but in previous studies we observed a relapsing-remitting form in SJL/J mice. Immunization with MOG:35-55 induces a chronic and non-relapsing form of EAE and it works well in C57BL/6 mice, which are usually resistant to MBP induced EAE. Our research group introduced a new EAE model using MP4. MP4 is a fusion protein of the most abundant components of the myelin sheath (PLP and MBP). Like in MOG-induced EAE, the course of MP4-induced EAE is dependent on T cells, but additionally B cells play an important role in mediating pathology.

I.3.3.3 Specifications of the MP4 model

Our study uses MP4-induced EAE as it has several additional features compared to the conventional models. First, the MP4 model features a pathogenic contribution of B cells in the mediation of EAE pathology. Second, "*determinant spreading*" was observed in our model. This means that the immune response is not directed exclusively against a single myelin antigen, but rather includes multiple myelin antigens over the course of disease. This phenomenon is also detectable in MS patients. We decided to use SJL/J mice for our studies in order to generate a relapsing-remitting course of disease. As RR-MS is the most common form of MS in humans, an animal model that mimics this form of disease and possesses additional immunological features (like the contribution of B cells in the initiation of disease pathology and *determinant spreading*) should provide valuable insights into the underlying mechanisms of the human disease. On top of this, some mice displayed an atypical form of EAE that was already described by *Stromnes and Goverman, 2006* [60] and is characterized by sensomotoric deficits, ataxia as well as spasticity, thus mirroring additional symptoms of MS patients. Taken together, our model offers a broad spectrum of features of the human

disease, and as such is an ideal model for experimental testing of therapeutic agents, such as nimodipine.

I.4 The role of calcium in the CNS

I.4.1 Function and distribution of voltage-dependent calcium channels (VDCC) in the CNS

Calcium is one of the most important secondary messengers in the CNS and it is able to regulate numerous processes like cell growth and proliferation, gene expression, long-term potentiation, energy metabolism, neurotransmitter release, plasticity and apoptosis [33,64,65]. Voltage-dependent calcium channels (VDCCs) mediate calcium influx after membrane depolarization and regulate intracellular processes depending on their localization. For example, they regulate contraction of cardiomyocytes, secretion of hormones in endocrine cells and release of neurotransmitters in the CNS. Furthermore, they can alter gene expression [66]. The nervous system expresses various VDCCs with specific functions and distribution (summarized in Table 1). They are detectable in many brain areas such as the cortex, thalamus and the hippocampus. In the CNS the occurrence of L-(long-lasting length of activation, high voltage activated), N-(neural-type, high voltage activated)- P/Q-(Purkinje cells, high voltage activated), R-(residual, intermediate voltage activated) and T-(transient, low voltage activated) type VDCCs has been reported [66]. Especially P/Q-, T- and N-type VDCCs are widely distributed within the nervous system. Presynaptic P/Q- and N-type VDCCs induce neurotransmitter release and T-type VDCCs facilitate rhythmic burst firing of neurons. L-type VDCCs (L-VDCCs) are localized at neural cell bodies as well as at dendrites and spines. Postsynaptic L-VDCCs regulate gene expression and neuronal excitability. Although microglial cells are responsive to calcium signaling, it is still a matter of debate whether

microglial cells express calcium channels, but astrocytes, oligodendrocytes and glial precursor cells were shown to express those channels [67-70].

Channel	Current	Localization	Cellular function
$Ca_v1.1$	L	Skeletal muscle transverse tubules	Excitation-contraction coupling
$Ca_v1.2$	**L**	**Cardiac myocytes, endocrine cells, neuronal cell bodies and proximal dendrites**	**Excitation-contraction coupling, hormone release, regulation of transcription, synaptic integration**
$Ca_v1.3$	L	Endocrine cells, neuronal cell bodies and dendrites	Hormone release, regulation of transcription, synaptic integration
$Ca_v1.4$	L	Retina	Neurotransmitter release from rods and bipolar cells
$Ca_v2.1$	P/Q	Nerve terminals and dendrites	Neurotransmitter release, dendritic Ca^{2+} transients
$Ca_v2.2$	N	Nerve terminals and dendrites	Neurotransmitter release, dendritic Ca^{2+} transients
$Ca_v2.3$	R	Neuronal cell bodies and dendrites	Repetitive firing
$Ca_v3.1$	T	Neuronal cell bodies and dendrites, cardiac myocytes	Pacemaking, repetitive firing
$Ca_v3.2$	T	Neuronal cell bodies and dendrites, cardiac myocytes	Pacemaking, repetitive firing
$Ca_v3.3$	T	Neuronal cell bodies and dendrites	Pacemaking, repetitive firing

Table 1. Localisation and cellular functions of VDCC. Modified from *Catterall et al., 2005*.

1.4.2 Ca^{2+} under pathological conditions

In addition to these regulatory functions, calcium is also capable of triggering harmful cascades. These can lead to mitochondrial damage and axonal injury, resulting in axonal energy failure and apoptosis. A relatively low concentration of calcium (about 0.1 µM) is physiological within cells, while elevated concentrations are considered cytotoxic [64,71-74]. Increased levels of intracellular calcium can cause enhanced generation of free radicals via an increased activity of nitric oxide synthases (NOS) and their generation of NO, which in turn operates cytotoxic [75]. In MS/EAE increased NO levels originating from perivascular infiltrates can also induce mitochondrial hypoxia/ischemia [18,74]. This is followed by increased production of ROS and mitochondrial dysfunction that causes further dysregulation of the calcium homeostasis with an intracellular calcium overload [18,74]. Eventually an increased intracellular calcium concentration plus additional calcium release from mitochondria cause axonal energy failure and severe cellular degeneration, finally causing apoptosis of neurons and oligodendrocytes [45,74]. This effect is partially due to excessive glutamate expression and activation of NMDA receptors by calcium [45]. Indeed, in EAE blockage of glutamate release leads to attenuated disease progression [76] and increased vulnerability of hippocampal neurons with age was association with increases in NMDA receptor currents *in vitro* [77]. In general, neurons are particularly sensitive to increased calcium concentrations, and calcium is suspected to mediate neurologic dysfunction associated with age and age-dependent diseases [78,79].

I.4.2.1 Role of VDCCs in neurological disorders

Evidence from human disorders, knock-out mice and cell culture models indicate a strong contribution of VDCCs in several neurological disorders such as vascular dementia, Prion disease, AD, PD [33,80], migraine and cerebral ischemia [11,33,65]. Studying PD, *Sigh et al.*,

2016 demonstrated that dihydropyridines, potent VDCC antagonists, reduce the population risk for suffering from PD in humans [81]. Blockage of VDCCs improved ataxia in cortical cerebellar atrophy as well as ataxia-telangiectasia and is also expected to improve spinocerebellar ataxia type 6, as VDCCs play a crucial role in this disease [80]. On a mechanistic level it was shown that amyloid β (Aβ) peptides amplify the influx of Ca^{2+} in neurons via L-VDCCs [33] and that increased function of neuronal L-type voltage sensitive calcium channels (L-VSCCs) correlates with reduced synaptic plasticity in the hippocampus and subsequent impairment of memory function [78]. Moreover, L-type calcium channels are elevated during aging and in AD [82]. Most recently, it was discovered that *Cacna2d2* limits axonal regeneration [82]. *Cacna2d2* is the gene encoding the alpha2delta2 subunit of voltage-gated calcium channels. Many mechanisms of VDCC signaling remain unclear and still have to be elucidated.

I.4.2.2 Indicators of calcium-mediated damage

As described above, increased intracellular calcium levels may trigger cellular damage. Cell organelles like mitochondria and neurofilaments are particularly vulnerable to cytotoxicity [64,71-74]. Mitochondria possess different roles in organisms like generation of energy, structural integrity and apoptosis. Their damage can cause changes in mitochondrial gene expression as mitochondrial deoxyribonucleic acid (DNA) is especially vulnerable to oxidative damage [18,74,84]. For instance, inflammation and increased NO levels can alter gene expression and induce dysfunction of mitochondria. This causes further dysregulation of the calcium homeostasis (as described above), results in enhanced cellular degeneration [74] and finally apoptosis of neurons and oligodendrocytes. Histologically, an increased size (*swelling*) of mitochondria indicates mitochondrial dysfunction. In demyelinating nerve fibers, increased numbers or *swollen* mitochondria are frequently detected, reflecting an

enhanced local energy demand [18,21,85]. Furthermore they are an early sign of axonal degeneration [18,21,85]. Increased intracellular calcium also weakens neuronal integrity as it promotes breakdown of the cytoskeleton, including actin, tubulin and intermediate filaments. This can be observed histologically and ultrastructurally as cytoplasmatic *blebbing* and accumulation or dissolution of filaments [86,87]. Other detectable signs of calcium-mediated damage are dilatation of the endoplasmic reticulum (ER) and cytosolic shrinkage [86,87].

I.5 The L-type calcium channel antagonist nimodipine and its CNS applications

Nimodipine is a calcium channel antagonist that belongs to the pharmacological group of dihydropyridines and is able to bind to cardiac, smooth and skeletal muscle as well as to brain membranes [66,88]. In animals it was shown that nimodipine binds to L-type calcium channels with high affinity and selectivity and consequently the trans-membranous influx of calcium is blocked [89]. Nimodipine was originally developed to treat hypertension and other cardiovascular diseases [72,90]. As it has a high affinity for the CNS it can cross the BBB easily, especially compared to other dihydropyridines [65,71,91]. Based on this feature it is frequently used to treat migraine and vasospasms after subarachnoidal haemorrhage [72,89]. Current research trials regarding the off-label use of nimodipine in the CNS focus on examining its effect on cognitive performance, especially on improving learning and spatial working memory [88,91-94]. Its effects on synaptic plasticity in the hippocampus and aging are also being investigated [65,95,96]. All those studies report a beneficial effect of nimodipine [65,95,96]. In some studies its effect on brain injury, cerebral ischemia and epilepsy was examined. Application of nimodipine enhanced recovery after brain damage or surgery and increased neuronal repair after cerebral ischemia [33,79,97-99]. Favorable effects on brain injury or epilepsy [90,100] are mainly attributed to the effects of local vascularization [101-104]. As previously mentioned it was also shown that L-VDCCs

blockers prevent neurons from Aβ-induced apoptosis in models of AD and that they decrease the population risk of suffering from PD in humans [33,81,90]. These studies suggest that treatment with nimodipine should be considered as a valuable tool for the treatment of many CNS disorders such as brain injury, stroke and cerebral ischemia, epilepsy, dementia and age-related degenerative diseases. However, the effect of nimodipine on neurodegenerative diseases that are mediated by inflammation has not been well studied. There are few studies that aimed at examining the neuroprotective role of nimodipine *in vivo* and *in vitro*. Those describe the ability of nimodipine to reduce neuronal damage, especially induced by glutamate and stress, but also by microglia [33,90,92,93,97]. Additionally, *in vitro* studies have shown that inhibition of calcium was able to reduce damage induced by oxygen deprivation or oxidative stress [29,105].

I.6 Aim of this study

Despite extensive research in the field of MS, current therapy is not able to prevent neurodegeneration or enhance regenerative processes. In order to discover potential ways to enhance regeneration, we made use of the L-type calcium channel blocker nimodipine in this study. Nimodipine has been described to promote many beneficial processes in the CNS. However, its effect on inflammatory-mediated neurodegenerative diseases is still unclear. Using MP4-induced EAE in SJL/J mice as an animal model that mimics a broad spectrum of the features in the human disease, the, we aimed at clarifying the following questions: Does nimodipine treatment have an effect on the clinical course and severity of EAE? Does it have an effect on the three hallmarks of CNS histopathology, i.e. inflammation, demyelination and axonal pathology? Which pathways are modulated by nimodipine and is its mode of action attributable to the blockage of the Ca_v 1.2 channel? Is there any specific effect on glial cells, in particular microglia?

II. Materials and Methods

II.1 Mice

N = 104 female 6-8 week old female SJL/J mice were obtained from Janvier (France) or Harlan (The Netherlands), respectively, and maintained under specific pathogen-free conditions in the animal facilities of the Department of Anatomy, University of Cologne or the FMZ, University of Wuerzburg. Only mice with comparable phenotypes of EAE (typical or atypical EAE) were included in the study to eliminate possible differences between the strains from different vendors. Animals had free access to standard rodent diet (Altromin Cat. #1314) and tap water, both of which were autoclaved. For severely diseased EAE-animals (score 2.5 or higher), food pellets were softened with water and put into the cage to ease food uptake. Room temperature (RT) was kept between 20-22 °C, humidity was maintained at 65 %. A twelve hour light on/light off period was ensured. All animal experiments complied with the German Law on the Protection of Animals, the 'Principles of laboratory animal care' [106] and the ARRIVE guidelines. Treatments were performed in according to a protocol that was approved by the LANUV and the 'Regierung von Unterfranken', Germany (approval numbers 84-02.04.2012.A269 and 55.2-2531.01-118/13).

II.2 EAE induction and drug treatment

N = 96 female eight week old mice were immunized subcutaneously into both sides of the flank with MP4. Each mouse received 200 µg MP4 (Lot E, Alexion Pharmaceuticals Inc.) emulsified in CFA. CFA contained paraffin oil (Sigma Cat. #18512), mannide monooleate (Sigma Cat. #M8819) at a proportion of 9:1 and *Mycobacterium tuberculosis* strain H37 Ra (BD Biosciences Cat. #231141) at a concentration of 5 mg/ml. Mice were scored daily to notice the onset of EAE and to document the course of disease. For mice suffering from typical EAE, the standard EAE scoring system was used with 0 - no EAE, 0.5 - beginning tail

paresis, 1 - tail paresis, 2 - hind limb weakness, 2.5 - beginning hind limb paresis, 3 - complete hind-limb paresis, 4 - quadriplegia and 5 - death. For atypical EAE, a balance score was used to rate for sensomotoric deficits, which occurred mainly in the atypical form. For this purpose, mice were encouraged to balance over a distance of 10 cm on a metal bar and rated according to following parameters: 0 - no problems balancing, 1 - not able to balance over the whole distance but able to stay on the bar and 2 - mice falling off the bar. To compare the course of disease in the typical and atypical group the standard EAE score was used to grade atypical EAE, but it had to be modified to account for the absent tail paresis (Fig. 1), which was frequently observed in atypical EAE mice. Nimodipine (Bayer HealthCare AG) or vehicle were applied daily by subcutaneous injections. Treatment started during the first remission at day 23 after immunization. Mice were either injected with 10 mg/kg nimodipine in vehicle solution, which consisted of 5 % ethanol, 5 % dimethyl sulfoxide (DMSO, Sigma Cat. #D8418), 40 % polyethyleneglycol 400 (PEG 400, Sigma Cat. #202398) and phosphate-buffered saline (PBS) or treated with vehicle solution only. As nimodipine is light-sensitive all steps including stock preparation and administration were performed protected from light. The treatment of non-immunized animals (n = 8) was performed for a period of ten days. In all cohorts, mice were matched before the beginning of treatment so that the mean score was not significantly different between both groups. If in one treatment group EAE was slightly more developed, we used this group for nimodipine treatment to guarantee that a potential treatment effect was not biased by a worse pathology in vehicle animals. To ensure that the doses of nimodipine used in our study both *in vivo* and *in vitro* were clinically relevant, we followed recommendations by already published studies [79,81,90,98,104]. As the doses used in these studies were able to attenuate cognitive deficits in models of neurodegenerative diseases and to trigger endogenous hormone responses [79,81,99] it is most likely that sufficient levels of the drug were achieved in the CNS.

Moreover several studies on subarachnoidal hemorrhage have shown that the dosages used in animal studies are able to induce comparable effects in patients [98,99].

Typical EAE	
Classical EAE score	
0	no EAE
0.5	beginning tail paresis
1	tail paresis
2	hind limb weakness
2.5	beginning hind limb paresis
3	complete hind limb paresis
4	quadriplegia
5	death
Atypical EAE	
Modified EAE score	(A+B) / 2 *see chart*
Balance score	
0	no problems balancing
1	not able to balance over the whole distance, but able to stay on the bar
2	falling off the bar

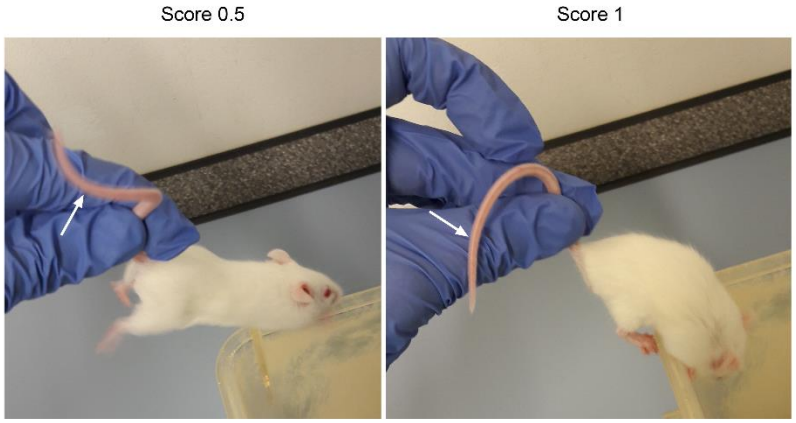

A + B

Tail paresis ?	
0	no paresis
0.5	beginning tail paresis
1	complete tail paresis

EAE score (body) ?	
0	no EAE
2	hind limb weakness
2.5	beginning hind limb paresis
3	complete hind limb paresis
4	quadriplegia

Fig. 1. Detailed explanation of the different scoring strategies for typical and atypical EAE. Typical EAE was rated according to the classic EAE score, while atypical EAE was evaluated with a balance score. Since atypical animals frequently displayed incomplete tail paresis (see image “Score 0.5”, compared to the complete tail paresis in typical EAE, see image “Score 1”) we used a modified EAE score to compare both forms of EAE among each other. For this atypical EAE scoring tail and body were rated separately and their mean was calculated as (A+B)/2.

II.3 Tissue preparation

Mice were deeply anesthetized with CO_2 and intracardially perfused for 15- 20 minutes with 4 % paraformaldehyde (PFA) and 4 % glutaraldehyde (GLA) in PBS (final pH = 7.4) for electron microscopy (EM) or 4 % PFA in PBS (final pH = 7.4) for ROS detection and immunohistochemistry (IHC). Prior to fixation, the vascular system was flushed with PBS for approximately 2 min. After the perfusion was complete, the spinal cord was fixed in perfusion solution at 4 °C for 24 h. Afterwards it was carefully removed from the vertebral canal. The lumbar part of the spinal cord was divided into three segments, which were embedded in EPON (ingredients see Table 2) for EM or in paraffin for IHC. For ROS detection the spinal cord was cut with a cryostat so it had to be cryoprotected in 10 % sucrose at 4 °C for 2-3 h, followed by 30 % sucrose at 4 °C overnight. Afterwards, spinal cord segments were stored in TissueTek (Tissue Tek O.C.T. Compound, Sakura Cat. #4583) and subsequently snap-frozen in isopentane and liquid nitrogen.

Ingredients of EPON
20 g Epoxy-embedding medium (Fluka/Sigma-Aldrich, Taufkirchen, Germany)
11 g Dodecenyl succinic anhydride (DDSA, Fluka/Sigma-Aldrich, Taufkirchen, Germany)
9 g Methyl nadic anhydride (MNA,Fluka/Sigma-Aldrich, Taufkirchen, Germany)
0.8 g 2,4,6-Tris (dimethylaminomethyl) phenol (DMP, Fluka/Sigma-Aldrich, Taufkirchen, Germany)

Table 2. List of ingredients required for the EPON solution.

II.4 Semi-thin sectioning and electron microscopy

For this purpose, the spinal cord was post-fixed overnight in 4 % PFA/ 4 % GLA after perfusion, carefully removed from the vertebral canal and the lumbar part was separated and split into three segments as described above. These segments were embedded in EPON using the following protocol: first, spinal cord segments were washed with 0.1 M cacodylate (CACO) buffer (pH = 7.35) three times on a rotating wheel for 30 min each in order to get rid of the abundant fixative. Afterwards tissue was placed into 0.1 M CACO buffer containing 2 % osmium tetroxide at RT for 3 h, deposited on a rotator and covered from light. The tissue was then washed three times (30 min each), using 0.1 M CACO buffer. On the following day, the tissue was put into 90 % ethanol at RT for 30 min, subsequently washed three times in 100 % ethanol (30 min each) and transferred into a 1:1 mixture of propylene oxide and ethanol for 30 min at RT followed by treatment with pure propylene oxide for 30 min before the final embedding in EPON. Embedded tissue was cut transversely at 500 nm with an ultra-microtome (Leica, Ultracut UCT) for semi-thin analysis. Sections were rinsed in methylene blue for approximately 1-2 min. Sections were dried on a heating plate and covered with Entellan (Merck, Germany). Digital images were acquired using a Leica DM LB2 microscope, equipped with a Zeiss camera (AxioCam MRc) and Zeiss software (AxioVision 40 4.7). ImagePro Plus software 6.0 (Media Cybernetics, Inc.) was employed to analyze six to eight images of two lumbar spinal cord sections per mouse covering both funiculi completely. For EM observations the EPON-embedded tissue was cut into 80 nm thick sections. The sections were carefully stretched with xylene while floating in a water tub and put on 150 mesh hexagonal formvar-coated copper grids (Electron Microscopy Sciences). To enhance contrast for EM analyses the sections were stained with 1 % aqueous uranyl acetate solution for 20 min and Reynold's lead citrate solution for 7 min. We used a Zeiss 902A transmission electron microscope at 80 kV acceleration voltage, equipped with an EM digital camera

system (MegaView, analysis docu 3.2; Olympus Soft Imaging Systems GmbH) at a magnification of 3000x and 7000x. The anterolateral funiculus (ALF) and the posterior funiculus (PF) were analyzed separately. In order to obtain quantifiable data for ultra-structural analyses of myelination we used the g-ratio according to *Guy et al., 1991* [107]. This parameter describes the relation between the nerve fiber and its corresponding myelin sheath. A g-ratio of one represents a nude nerve fiber. To calculate the g-ratio the smallest diameter of the axon is divided by the smallest diameter of the myelin sheath. The normal range of the g-ratio was determined by calculating the mean value of five naïve SJL/J mice $\pm$ the triple standard deviation (SD). Hereby a g-ratio of 0.57-0.77 within the PF and a g-ratio of 0.52-0.70 within the ALF were classified as normal (Fig. 2 A). A g-ratio below 0.57 (PF)/0.52 (ALF) reflects a nerve fiber in the process of demyelination (Fig. 2 B), whereas a g-ratio above 0.77 (PF)/0.79 (ALF) describes a remyelinating nerve fiber (Fig. 2 C). Axonal pathology was examined with the help of the mito-ratio, which mirrors the relation of the axon and to its mitochondria [87]. For this, the area of all mitochondria within the observed axon was divided by the area of the respective axon (Fig. 2 D). In Fig. 2 D, the upper axon images the normal condition, whereas the lower axon depicts an axon with increased mito-ratio. Again, five naïve SJL/J mice were analyzed to figure out the normal conditions. In that way a mito-ratio of $\leq$0.21 within the PF and a mito-ratio of $\leq$0.173 within the ALF were classified as normal. As only enlarged mitochondria indicate pathology [108] an upper limit and not a range (as for the g-ratio) was determined.

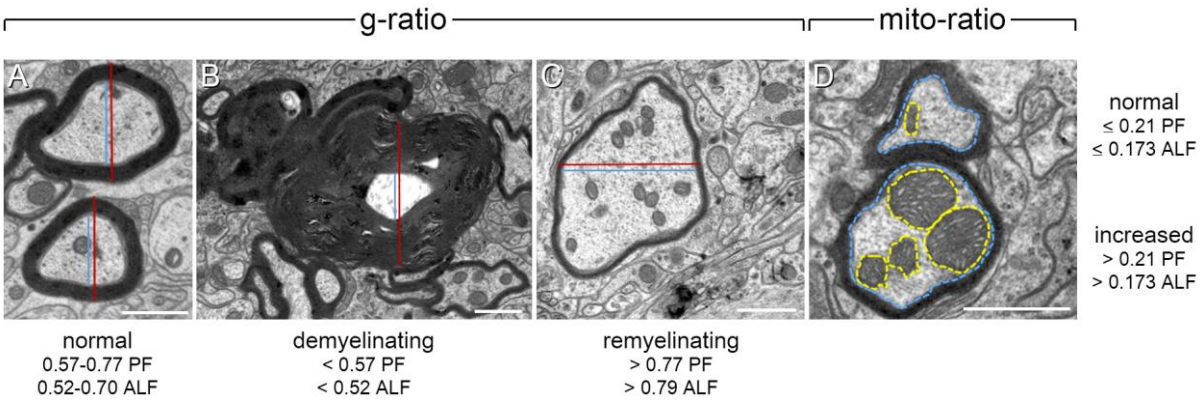

Fig. 2. Illustration of the measurements used to quantify myelination status (g-ratio) and axonal pathology (mito-ratio). Normal (*A*), demyelinating (*B*), remyelinating (*C*) nerve fibers and axons with normal and increased mito-ratio (*D*) are depicted. Scale bars represent 1µm.

II.5 Immunohistochemistry

Murine spinal cords were deparaffinized and boiled for 10 min in 10 mM citrate buffer (pH = 6) for antigen retrieval. Sections were washed with PBS, blocked with 1 % normal goat serum (NGS) in PBS at RT for 1 h, followed by incubation with the primary antibody (anti-ionized calcium binding adapter molecule 1 (Iba1), Wako Laboratories Cat. #019-19741, diluted 1:1,000 in PBS or anti-glial fibrillary acidic protein (GFAP), Sigma Cat. #G 3893, diluted 1:500 in blocking solution) at 4 °C overnight. Subsequently, sections were washed three times in PBS and incubated with the secondary antibody (Cy3-conjugated goat-anti rabbit IgG for Iba1, Cat. #111-165-003 and Cy3-conjugated goat-anti mouse IgG for GFAP, Cat. #115-165-003, both from Jackson ImmunoResearch, each diluted 1:600 in PBS) at RT for 1-2 h. After renewed washing, sections were counterstained with DAPI (1:1,000, Roche Cat. #236276), washed again and coverslipped with n-propyl gallate (NPG; Fluka Cat. #48710). For Iba1/TUNEL staining the same protocol was used, but after antigen retrieval the sections were

stained for TUNEL using the ApopTag red *in situ* apoptosis detection kit (Millipore Cat. #S7165) according to the manufacturer's instruction. Immunofluorescent images were acquired using a Keyence BZ-9000 fluorescence microscope. For light microscopic staining of oligodendrocyte transcription factor 2 (Olig2) spinal cord sections were blocked with 3 % hydrogen peroxide in distilled water at RT for 10 min. Subsequently, sections were permeabilized with 0.25 % Triton-X in PBS for 10 min before blocking them with 5 % NGS in PBS at RT for 1 h. Next, sections were rinsed with the primary antibody against Olig2 (Merck Millipore Cat. #Ab 9610, diluted 1:500 in 1 % NGS in PBS) at RT for 1 h, followed by incubation with the secondary antibody (biotinylated goat anti-rabbit IgG, Vector Laboratories Cat. #BA-1006, diluted 1:250 in 1 % NGS in PBS) at RT for 30 min. Subsequently sections were incubated for 30 min with the ABC kit (Vector Laboratories, Vectastain Elite Cat. #PK-6100 Standard) according to the manufacturer's instruction. Afterwards, the staining was developed with a 3.3'-diaminobenzidine (DAB) peroxidase substrate kit (Vector Laboratories Cat. #SK-4100, according to the manufacturer's instructions) at RT for approximately 15 min. Sections were counterstained with hematoxylin for 10 min and coverslipped with Aqua Poly/Mount (Polysciences Cat. #18606). For fluorescence double-staining of Olig2 and adenomatous polyposis coli (APC) the same protocol was used, but after blocking the primary antibody was incubated overnight at 4 °C. Subsequently, the sections were incubated with the secondary antibody (Cy5-conjugated goat-anti-rabbit IgG, JacksonImmuno Research Cat. #111-175-144, diluted 1:250 in PBS) together with DAPI (1:5,000; Roche Cat. #236276) at RT for 30 min. For APC staining, sections were again blocked with 5 % NGS in PBS at RT for 1 h. Next, the anti-APC antibody (Calbiochem Cat. #OP80) was diluted 1:100 in 1 % NGS in PBS and incubated at RT for 2 h. Subsequently, the secondary antibody (biotinylated goat anti-mouse IgG, Vector Laboratories Cat. #BA-9200) was diluted 1:250 in 1 % NGS in PBS and applied at RT for 30 min.

Afterwards NeutrAvidin DyLight 550 (ThermoScientific Cat. #84606) was diluted 1:500 in PBS and incubated at RT for 30 min. Sections were finally coverslipped with mowiol 4-88 (Roth Cat. #0713.1). Positive cell bodies were counted per mm^2 of the respective funiculus. For this purpose, six to eight images of three segments of the spinal cord per mouse were analyzed covering both funiculi completely. The depicted area was measured using ImagePro Plus software 6.0 (Media Cybernetics, Inc.).

II.6 Immunocytochemistry

Microglial cells were seeded at 250,000 cells/mm^2 on coverslips (round, diameter: 12 mm) that had been mounted with 0.001 % poly-ornithine/dH_2O (Sigma Cat. #P4957) for 2 h in advance. Cells were allowed to settle for 24 h in the incubator (37 °C, 3.5 % CO_2) and afterwards treated for up to 24 h with several doses of nimodipine or vehicle. Treatment with 10 µM nimodipine and the respective vehicle for 24 h became the standard procedure. After treatment cells were fixed with 2 % PFA at 4 °C for 2 h, washed with PBS, blocked with 3 % bovine serum albumin (BSA)/1 % NGS in PBS and incubated with anti-iNOS antibody (BD Biosciences Cat. #610432, diluted 1:150 in blocking solution) at 4 °C overnight. Subsequently, sections were washed with PBS and incubated with the secondary antibody (Cy3-conjugated goat anti-rat IgG, diluted 1:500 in blocking solution, Jackson ImmunoResearch Cat. #112-165-003). After renewed washing cells were counterstained with wheat germ agglutinin (WGA, Texas Red-X-conjugated, Invitrogen Cat. #W21405, diluted 1:200 in PBS) and DAPI (diluted 1:2,000 in PBS). Last, coverslips were turned and put on a microscope slice with mowiol 4-88 (Roth Cat. #0713.1). For the detection of the Ca_v 1.2 channel the same protocol was used. As the antibody (1:400 diluted in blocking solution, Alomone Labs Cat. #ACC-003-AG) was directly conjugated with ATTO-488 no secondary antibody was needed. As background control goat anti-rabbit FITC-conjugated IgG (Jackson

ImmunoResearch Cat. #111-095-003) was recommended by Alomone Labs and used in several dilutions (1:200, 1:400, 1:800 in blocking solution). Immunofluorescent images were acquired using a Keyence BZ-9000 fluorescence microscope. Confocal laser scanning microscopy images were taken using a Nikon A1R+ confocal microscope system equipped with an Eclipse TI-E inverse microscope with coherent sapphire lasers and a mbp communication visible fiber laser (lines: 405, 488, 561, 647 nm). Objectives Plan Apo 20x NA: 0.8, Plan Apo 60x NA: 1.4 and Apo 100x NA: 1.5 were used and detection in three simultaneous channels applied. The system was endowed with NIS-Elements Advanced Research Software (Nikon). ImageJ (1.47v, NIH) was used for editing of confocal laser scanning microscope images.

II.7 ROS detection

In order to detect the occurrence of ROS in the spinal cord, mice were treated either with 10 mg/kg nimodipine or vehicle. These mice as well as untreated immunized and non-immunized controls were subcutaneously injected with dihydroethidium (dHet; Molecular Probes by Life Technologies Cat. #D11347) 3 h before intracardial perfusion took place. Again mice were perfused with PBS first, followed by 4 % PFA in PBS. Spinal cords were removed and post-fixed in 4 % PFA at 4 °C for 24 h. Cryoprotection and snap-freezing of the tissue were performed as described above. The spinal cord was transversally cut with a Leica cryostat into 10 µm (fluorescence microscopic analyses) and 30 µm (confocal analyses) thick sections and counterstained with DAPI (1:2,000 in PBS). The protocol was adapted from *Choi et al., 2015* [109].

II.8 RNA extraction, RT-PCR and microarray analyses

Total RNA was isolated from homogenized murine tissue or murine N9 cell pellets according to the TRIzol method. First TRIzol (Invitrogen Life Technologies Cat. #15596018) was added for 5 min. Afterwards chloroform was applied to the lysate and centrifuged at 13,000 g at 4 °C for 15 min. The supernatant was precipitated by isopropanol at RT for 10 min. Next ethanol was added to the RNA pellet, mixed well and centrifuged at 7,500 g and 4 °C for 5 min. The pellet was dried and resuspended in diethyl polycarbonate (DEPC) water, stored at -80 °C for at least 1 h and quantified using spectrophotometric measurement with a Nanodrop 2000c spectrophotometer (Thermo Fisher Scientific) for each RNA extract. Subsequently, the RNA was reversely transcribed using the Qiagen QuantiTect reverse transcription kit (Qiagen Cat. #205313) according to the manufacturer's instruction. cDNA was used as a template for RT-PCR and RT-qPCR. The RT-PCR reaction mix consisted of 9.5 µl $MgCl_2$ (50 mM), 0.75 µl of each primer (concentration: 10 µM), 12.5 µl Red Taq Mix (Genaxxon Bioscience Cat. #M3029) and 1 µl template for one reaction. The RT-PCR was performed in a thermal cycler (Applied Biosystems Cat. #2720) using a total reaction volume of 25 µl. Thermocycling conditions were 95 °C for 5 min, followed by 35 cycles of 95 °C for 30 s, 60/58 °C (see Table 3) for 30 s and 72 °C for 30 s. Amplified products were separated on an 1 % agarose gel in 1x Tris/acetate/EDTA (TAE) buffer (pH 8.0) containing 0.005 % Midori Green (Biozym Cat. #617004). RT-PCR products were visualized with UV light. The house-keeping gene GAPDH was used as a loading control. RT-qPCR was performed in 0.1 ml PCR vials (Qiagen) in the Qiagen Rotor Q (Qiagen). Each reaction contained 10 µl of Qiagen Master Mix (QuantiNova SYBR Green Master PCR Kit, Qiagen Cat. #208052), gene-specific forward and reverse primer mix (final concentration of 1 µM each), RNase-free water and approximately 200 ng of cDNA/reaction. Controls without templates contained nuclease-free water instead so that the single-reaction volume came to 20 µl. As loading control GAPDH was used. Cycling

conditions were 95 °C for 2 min to activate the DNA polymerase followed by 35 cycles at 95 °C for 20 s for denaturation, 20 s of annealing at 60 °C, and 20 s of elongation at 72 °C. At the end of the amplification cycles, melting curves were used to validate RT-qPCR product specificity and all RT-qPCR runs included a negative control (no template) for each primer set. All samples were amplified in triplicates. Data were analyzed using the DD Ct method [110]. Expression levels were normalized to the Ca_v 1.2 gene expression level of IMA 2.1 cells. The relative expression of our gene of interest was defined as the ratio of expression of the gene in diverse cell types to that of IMA 2.1 cells. Primers were provided by biomers.net GmbH and Eurofins Genomics and are listed in Table 3. For microarray analyses, total RNA was isolated from murine spinal cord tissue or N9 cell pellets using the TRIzol method as described above. Prior to sample preprocessing, RNA integrity was assessed with the RNA 6000 nano kit (Agilent) using the Bioanalyzer 2100 instrument (Agilent). Each sample (100 ng) was processed with the whole transcript (WT) PLUS kit (Affymetrix), i.e. subjected to RNA amplification via reverse transcription to double-stranded cDNA and subsequent *in vitro* transcription. This was followed by an additional round of reverse transcription yielding single-stranded DNA in sense orientation. Hybridization cocktails were produced after fragmentation and biotin labeling of target DNAs. Microarray hybridization to GeneChip Mouse Gene 2.0 ST arrays (Affymetrix) was performed according to the manufacturer's protocol using the Fluidics Station 450 with the program FS450_0002. Background correction, normalization and gene-level probeset summary were performed using the Expression Console v1.2.1.20 (Affymetrix). Differentially expressed genes were determined for nimodipine- *vs.* vehicle-treated samples with the false discovery rate (FDR) of differential expression being estimated with an empirical Bayes methodology employing a lognormal normal data modeling [111]. Microarray data were deposited at Gene Expression Omnibus (GEO; http://www.ncbi.nlm.nih.gov/geo) in entry GSE87397.

Primer	Forward	Reverse	Annealing temperature
Ca_v 1.2	CGT GGA GGA GAG CAA AGA GG	GGT TCC TGA AGG AGG TGT GC	60 °C
iNOS	TGC TGT TCT CAG CCC AAC AA	TGA TGG ACC CCA AGC AAG AC	58 °C
GAPDH	CTA CCC CCA ATG TGT CCG TC	GCC GTA TTC ATT GTC ATA CCA GG	60 °C

Table 3. List of the primers used for RT-PCR and RT-qPCR.

II.9 Cell culture

N9, BV-2 and IMA 2.1 cell lines were cultured in DMEM medium (Gibco by Thermo Fisher Scientific Cat. #41966) containing 10 % FBS (Gibco by Thermo Fisher Scientific Cat. #10270), penicillin (100 IU/ml; penicillin G sodium salt, Sigma Cat. #P3032) and streptomycin (100 mg/ml; streptomycin sulfate salt, Sigma Cat. #S6501) and maintained at 37 °C and 3.5 % CO_2. Nimodipine diluted in vehicle solution or vehicle solution (consisting of DMSO, ethanol and PEG 400 analogous to treatment in mice) was added to the medium. The final concentration of DMSO and ethanol was below pro-apoptotic range. Pro-apoptotic effects of DMSO or ethanol alone were also excluded by performing corresponding vehicle control experiments. Several time-points and concentrations were tested (1 µM, 5 µM, 10 µM, 20 µM), whereas 10 µM for 24 h became the standard treatment dose. To ensure that our *in vitro* dose of nimodipine was clinically relevant we studied the literature closely and tested doses that were already used in other CNS disease models [79,81,98,104]. For instance, the dose we used in our cell culture experiments was shown in another *in vitro* study to induce equivalent effects in cell culture and patients (e.g. decreased excitotoxicity and reduced stress-mediated effects after brain surgery) [99]. Polarization of cells was triggered either with 100 ng/ml TNF-α (PeproTech Cat. #315-01A) and IFN-γ (PeproTech Cat. #345-05) each, 100 ng/nl TGF-β1 (PeproTech Cat. #100-21) or 10 ng/ml IL-4 (interleukin-4; PeproTech Cat. #214-14). For the determination of cell viability MTT was used (Vybrant MTT cell proliferation assay kit, quick protocol, Molecular Probes Cat. #V-13154) according to the vendor's instructions. The absorbance was measured at 540 nm using a Victor^3 ELISA reader (Victor^3 1420 Multilabel counter, software version 3.00 revision 5, Perkin Elmer). For nitrite quantification the Griess assay (Molecular Probes by Thermo Fisher Scientific Cat. #G-7921) was used according to the manufacturer's instruction and incubated for 30 min. Absorbance was measured at 548 nm using the same Victor^3 ELISA reader (Perkin Elmer). For the Griess

assay, cells were cultured in phenol-free DMEM medium (Gibco by Thermo Fisher Scientific Cat. #31053). Apoptosis was visualized by TUNEL assay (DeadEnd fluorometric TUNEL system, Promega Cat. #G3250) according to the provided protocol for cells.

II.10 Microglia isolation and cultivation

Microglia cells were either isolated from adult mouse brain using the Adult Brain Dissociation Kit (Miltenyi Biotec Cat. #130-107-677) or from newborns using the Neural Tissue Dissociation Kit T (Miltenyi Biotec Cat. #130-093-231). Adult brains were removed, washed in PBS, cut into sagittal slices and subsequently dissociated by enzymatic digestion on a gentleMACS Octo Dissociator (Miltenyi Biotec Cat. #130-095-937). Afterwards the cell suspension was filtered through a 70 µM cell strainer (Miltenyi Biotec Cat. #130-095-823) and washed with cold PBS (Sigma Aldrich Cat. # D8662) before debris and red blood cells were removed. In the following cells were labeled with CD11b MicroBeads (Miltenyi Biotec Cat. #130-093-634) for 15 min, washed and further processed by magnetic separation on LS columns (Miltenyi Biotec Cat. #130-042-401). Labeled cells were flushed out by pushing the plunger into the column. To increase the purity of microglial cells the magnetic separation was repeated. Cells were re-suspended in DMEM medium containing 10 % horse serum (Sigma Cat. #H1138) and 1 % penicillin/streptomycin (Pan Biotech Cat. #P06-07100) and seeded on poly-D-lysine pre-coated culture plates (0.002 %; 3 h at 37 °C; Sigma Cat. #P0899) at a density of 1 x 10^5 cells per well. Microglia from newborns was isolated with the Neural Tissue Dissociation Kit T according to the manufacturer's instructions and seeded on poly-D-lysine pre-coated culture plates for 14 days in DMEM medium (Gibco Cat. #41966-029) containing 10 % horse serum (Sigma Cat. #H1138) and 1 % penicillin/streptomycin (Pan Biotech Cat. #P06-07100). Culture medium was exchanged approximately three times a week. Microglia cells from newborn mice were likewise purified by using CD11b

MicroBeads and magnetic separation on LS columns. Purified cells were re-suspended in medium and seeded on poly-D-lysine pre-coated culture plates (3 h at 37°C) at a density of 50,000 cells per well.

II.11 Flow cytometry

Single-cell suspensions were analyzed by staining for extra- and intracellular markers. Dead cells were excluded by a fixable viability dye eFluor780 (eBioscience Cat. #65-0865-14) and Fc block was performed using αCD16/32 (eBioscience Cat. #16-0161). For intracellular cytokine staining, cells were stimulated with ionomycin (1 µM; Sigma Cat. #I3909) and phorbol-12-myristate-13-acetate (PMA; 50 ng/ml; Sigma Cat. #P1585) in the presence of monensin (2 µM; eBioscience Cat. #00-4505-51) for 4 h. Cells were stained for surface markers for 30 min at RT with the respective fluorochrome-conjugated antibodies and permeabilized using Fix/Perm (eBioscience Cat. #00-5523-00) according to the manufacturer's protocol. Intracellular cytokines were stained for 30-45 min with the respective fluorochrome-conjugated antibodies. Measurements were performed with the BD FACSCanto II flow cytometer and BD FACSDiva software (BD Bioscience) and data were analyzed with FlowJo (TreeStar). Apoptosis was determined by incubating the cells for 15 min in 500 µl annexin V binding buffer (BD Pharmingen Cat. #556454) containing 5 µl annexin V FITC (BD Pharmingen Cat. #556419) and 5 µl propidium iodide (BD Pharmingen Cat. #51-66211). Afterwards, cells were washed and analyzed with the BD FACSCanto II. The following fluorochrome-conjugated anti-mouse antibodies were used: CD4-FITC (RM4-5, eBioscience Cat. #11-0042-8), CD8a-BV510 (53-6.7, Biolegend Cat. #100752), CD11b-PE (M1/70, Biolegend Cat. #101207), CD25-PeCy5 (PC61, Biolegend Cat. #102010), CD44-PE (IM7, Biolegend Cat. #103008), CD45-V450 (30-F11, eBioscience Cat. #560501), CD45R/B220-BV510 (RA3-6B2, Biolegend Cat. #103247), CD62L-APC (MEL-14,

eBioscience Cat. #17-0621-83), FoxP3-PE (FJK-16s, eBioscience Cat. #12-5773-82), IFN-γ-APC (XMG1.2, eBioscience Cat. #17-7311-82), IL-17A-PE (eBio17B7, eBioscience Cat. #12-7177-81).

II.12 Patch clamp

N9 cells were seeded on coverslips (round, diameter: 10 mm) and allowed to settle in the incubator (37 °C, 3.5 % CO_2) for 24 h. Subsequently, cell recordings were performed at RT in a bath solution consisting of 140 mM tetraethylammonium (TEA) chloride, 2 mM $MgCl_2$, 20 mM $BaCl_2$, 10 mM glucose and 10 mM HEPES, pH 7.4. Patch pipettes were pulled from borosilicate glass capillaries (Science Products) and sharpened to give input resistances of 2-4 MΩ. The pipette recording solution consisted of 100 mM CsCl, 20 mM TEA chloride, 1 mM $MgCl_2$, 5 mM MgATP, 10 mM HEPES and 10 mM EGTA (pH = 7.3). For recordings of potassium channels the bath solution contained 135 mM NaCl, 5.4 mM KCl, 1.8 mM $CaCl_2$, 1 mM $MgCl_2$, 10 mM glucose, and 5 mM HEPES, pH 7.4 and the pipette recording solution consisted of 140 mM KCl, 0.01 mM $CaCl_2$, 2 mM $MgCl_2$, 1 mM EGTA, 1 mM Na_2ATP, 0.1 mM cAMP, 0.1 mM GTP, and 5 mM HEPES, pH 7.3. Currents were recorded with an EPC-9 patch-clamp amplifier (HEKA) and low pass-filtered at 2.9 kHz. Analyses were performed with IgorPro (WaveMetrics) and leak currents were digitally subtracted. Steady-state current voltage relations were obtained by applying voltage ramps between +60 and −150 mV. During the experiments cell resistance was measured continuously.

II.13 Immunoblotting

Total protein lysates were obtained from N9 cells by lysing the samples in cold radioimmunoprecipitation assay buffer (RIPA) buffer in the presence of phenylmethylsulfonyl fluoride (PMSF, Sigma Cat. #78830-5G) and following protease

inhibitors on ice: aprotinin (AppliChem Cat. #A2131), pepstatin A (AppliChem Cat. #A2205), leupeptin-hemisulfate (AppliChem Cat. #A2183), sodium fluoride (Merck; Cat. # 6649), and sodium orthovanadate (Sigma; Cat. # S6508). Protein concentrations were determined by BCA assay (Pierce BCA Protein Assay Kit, Thermo Fisher Scientific Cat. #23225). Western blot analyses were performed with antibodies to the following proteins: iNOS (1:500, BD Biosciences Cat. #610432), cPARP (1:1,000, Cell Signaling Cat. #Asp214), Akt 1/2/3 (H136) (1:500, Santa Cruz, Cat. #sc-8312), pAkt (1:500, Cell Signaling Cat. #Ser473) and β-actin (1:1,000, Sigma Cat. #A1978). Antibodies were diluted in blocking solution that consisted of: 1× tris buffered saline (TBS) + 0.25 % Tween (TBS-T; Tween 20, AppliChem Cat. #A1389) containing 5 % milk or 2 % BSA (anti-pAkt). All secondary antibodies were conjugated with horseradish peroxidase (HRP) and diluted at 1:1,000 in blocking solution (goat anti-rabbit IgG for cPARP, Akt and pAkt, Jackson ImmunoResearch Cat. #111-035-003; goat anti-mouse IgG for iNOS and β-actin, Jackson ImmunoResearch Cat. #115-035-068). For the detection of HRP on the immunoblots, ECL Prime Western blotting detection substrate (Amersham Cat. #RPN2232) was used and protein bands were imaged with a digital imaging system (Fusion Solo Vilber Lourmat VL-35.F0.84, Vilber).

II.14 Slice culture and staining

For organotypic slice culture mice were sacrificed by cervical dislocation. The lumbar section of the spinal cord or the spleen were quickly removed and stored in cold PBS containing 2 % penicillin/streptomycin, on ice. Subsequently, the tissue was embedded in 2 % agarose in PBS and sectioned into transversal slices (200 µm) using a vibratome (Leica VT 1000S, Leica). Sections were again stored in cold PBS containing 2 % penicillin/streptomycin and transferred into pre-warmed culture medium that consisted of DMEM with 10 % FBS, penicillin (100 IU/ml) and streptomycin (100 mg/ml). Slices were then stored in the incubator

(at 37 °C and 3.5 % CO_2) for 24 h. Drug treatment was performed in analogy to the cell culture experiments (10 µM nimodipine in vehicle solution or vehicle solution solely for 24 h). For IHC free-floating sections were washed in PBS three times, fixed in 4 % PFA in PBS at 4°C for 2 h, washed in PBS and permeabilized with 0.5 % Triton-X 100 (Sigma Cat. #T9284). Triton was replaced by the blocking solution (1 % NGS in PBS) at RT for 1 h. Afterwards slices were incubated with the primary antibody (anti-Iba1, 019-19741, Wako Laboratories, diluted 1:1,000 in PBS or anti-GFAP, G 3893, Sigma, diluted 1:500 blocking solution) at 4 °C overnight. On the next day, the antibody was replaced by fresh antibody solution for 16-20 h. Subsequently, the sections were washed three times with PBS and incubated with the secondary antibody (Cy3-conjugated goat-anti rabbit IgG for Iba1 and Cy3-conjugated goat-anti mouse IgG for GFAP, Jackson ImmunoResearch Cat. #115-165-003, each diluted 1:600 in PBS) at 4 °C for 16 h. After renewed washing sections were counterstained with DAPI (diluted 1:1,000 in PBS), washed and coverslipped with NPG. Sections were examined with a confocal microscope (Nikon A1R MP) and z-stacks were generated. Different channels were merged with the Image J 1.46r software (National Institutes of Health). For generating the organotypic slice cultures we modified the protocol of *Chatterjee et al. 2013* [112]. Slices were tested for viability using MTT according to *Connelly et al. 2000* [113].

II.15 Statistics

Standard disease parameter and day of sacrifice are presented as means ± SEM. Error bars within the graphs depict the SD. Statistical analyses were performed using GraphPad Prism (Prism 6 for Windows, version 6.01, GraphPad Software Inc.). Score data were analyzed using the unpaired Mann-Whitney test and for calculation of extended disease parameters (Table 5) Fisher's exact test was used. For all other analyses two-tailed, unpaired Student's *t* test was performed.

III. Results

III.1 Nimodipine treatment significantly attenuated clinical course of EAE

For this study, *n* = 96 female mice on the SJL/J background were immunized with MP4 in CFA at the age of eight weeks. Immunized mice showed either the typical phenotype of EAE with severe ascending motor deficits (*n* = 56 mice) or the atypical form including ataxia and spasticity (*n* = 40). Overall, immunization with MP4 resulted in a relapsing-remitting course of EAE in all animals. Disease onset in mice suffering from typical EAE occurred at day 11 after immunization (Fig. 3 A), whereas the onset of atypical EAE (Fig. 3 B) was as early as day 12. The clinical data are summarized in Table 4 and 5. Mice were treated at the beginning of the first relapse (day 23 after immunization) either with 10 mg/kg nimodipine or vehicle (5 % EtOH, 5 % DMSO, 40 % PEG 400, and 50 % sterile PBS) for 19-37, consecutive days by subcutaneous injection, depending on the experimental setting. The dose of 10mg/kg aligns with a well-established body of literature [81,104,114]. During the course of disease, the clinical score was significantly attenuated in nimodipine-treated mice with both the typical and atypical EAE (Fig. 3 A and B). Vehicle-treated mice displayed a significantly increased relapse rate compared to animals that received nimodipine (Table 5). Moreover, sensomotoric deficits, measured with the balance score, were significantly decreased in nimodipine- compared to vehicle-treated mice (Fig. 3 C).

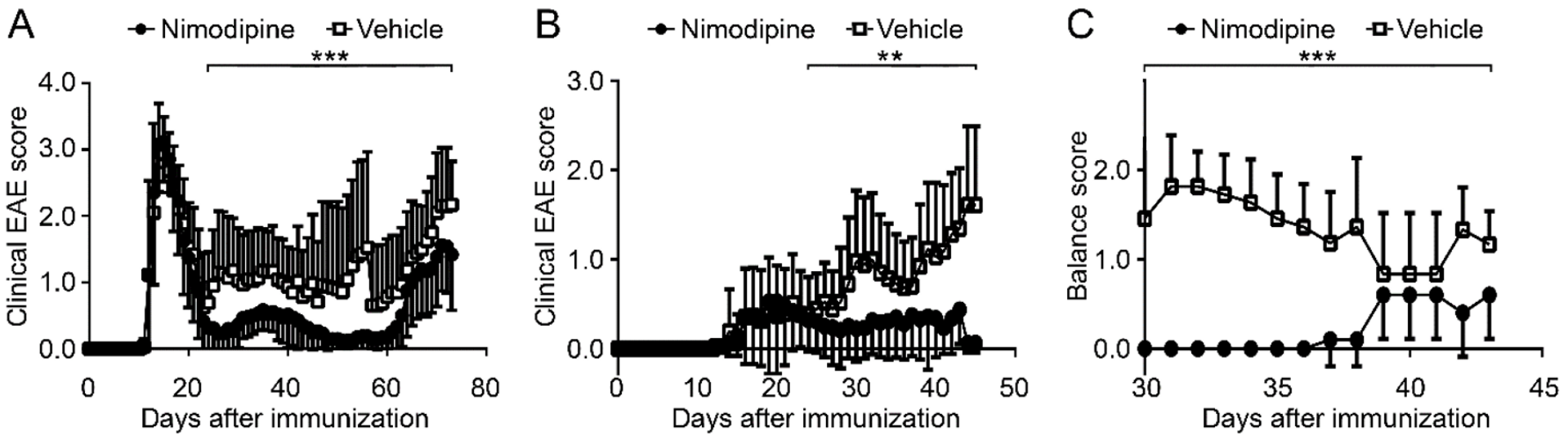

Fig. 3. Attenuated clinical course of EAE in nimodipine-treated mice. Clinical course of (*A*) typical and (*B*) atypical EAE. All animals were treated on day 23 after immunization with either nimodipine (•; $n = 32$ in the typical EAE group, $n = 18$ in the atypical EAE group) or vehicle solution (▫; $n = 24$ in the typical EAE and $n = 22$ in the atypical EAE group). Sensomotoric deficits were rated with a balance score (*C*) in $n = 10$ nimodipine- and $n = 11$ vehicle-treated mice. $^{**}P \leq 0.01$; $^{***}P \leq 0.001$, by Mann-Whitney test.

Typical EAE	**Mean onset of disease ± SEM**	**Mean treatment duration ± SEM**	**Mean score at treatment onset ± SEM**	**Mean final score ± SEM**	**Mean disease severity ± SEM**	**Mean score difference ± SEM**
Nimodipine-treated	12.48 ± 0.15	33.43 ± 3.37	0.41 ± 0.11	1.02 ± 0.16	0.75 ± 0.10	1.52 ± 0.24
Vehicle-treated	12.79 ± 0.21	27.23 ± 3.79	0.63 ± 0.17	1.93 ± 0.20	1.26 ± 0.07	0.34 ± 0.20
P value	n.s. (0.27)	n.s. (0.39)	n.s. (0.57)	< 0.01	< 0.001	< 0.001
Atypical EAE	**Mean onset of disease ± SEM**	**Mean treatment duration ± SEM**	**Mean score at treatment onset ± SEM**	**Mean final score ± SEM**	**Mean disease severity ± SEM**	**Mean score difference ± SEM**
Nimodipine-treated	16.89 ± 0.68	19.06 ± 0.59	0.38 ± 0.09	0.37 ± 0.11	0.28 ± 0.02	0.32 ± 0.18
Vehicle-treated	17.15 ± 0.82	19.30 ± 0.62	0.39 ± 0.11	1.40 ± 0.15	0.70 ± 0.07	0.68 ± 0.19
P value	n.s. (0.86)	n.s. (0.57)	n.s. (0.59)	< 0.001	< 0.001	< 0.001

Table 4. Standard disease parameters for both treatment groups, separated by typical and atypical EAE phenotypes.

Typical EAE			
	Occurrence of relapse (at least score 1)	**Regain of hind limb mobility** (after five days of treatment)	**Regain of hind limb mobility** (day of sacrifice)
Nimodipine-treated	**40.63 %** (13/32)	**96.88 %** (31/32)	**62.5 %** (20/32)
Vehicle-treated	**95.84 %** (23/24)	**58.34 %** (14/24)	**37.5 %** (9/24)
P value	< 0.01	< 0.01	n.s. (0.10)
Atypical EAE			
	Occurrence of relapse (at least score 1)	**Regain of hind limb mobility** (after 5 days of treatment)	**Regain of hind limb mobility** (day of sacrifice)
Nimodipine-treated	**16.67 %** (3/18)	**88.89 %** (16/18)	**88.89 %** (16/18)
Vehicle-treated	**86.36 %** (19/22)	**86.36 %** (19/22)	**22.73 %** (5/22)
P value	< 0.01	n.s. (1.0)	< 0.01

Table 5. Extended disease parameters in both treatment groups, separated by typical and atypical EAE phenotypes.

III.2 Nimodipine treatment decreased neurodegeneration and increased remyelination

To investigate whether the differences in the course of disease after nimodipine treatment were also reflected by a reduced histopathology, ultrastructural analyses of the spinal cord were performed. For that purpose, n = 12 nimodipine- and n = 9 vehicle-treated mice were sacrificed during chronic EAE (day 69.60 ± 0.98 for vehicle- and day 70.33 ± 0.59 for nimodipine-treated mice) after a treatment duration of 46.60 ± 0.98 for vehicle treatment and 47.33 ± 0.59 days for nimodipine treatment. In order to quantify de- and remyelinated nerve fibers in EM analyses, we used the g-ratio according to *Guy et al., 1991* [107]. This ratio relates the diameter of the myelin sheath to the diameter of the respective nerve fiber, whereby a g-ratio of one represents a nude nerve fiber. Analyses of five naïve SJL/J mice allowed us to determine the normal range of the g-ratio in the spinal cord of SJL/J mice. Analyses were performed separately for each funiculus and each individual segment. In analogy to the g-ratio, we developed the mito-ratio, which describes the relationship of mitochondria size within a nerve fiber to the respective axoplasm [87]. Additionally, the total number of nerve fibers was calculated to determine axonal loss. Our parameters indicate that nimodipine treatment causes significantly less neurodegeneration as treated animals exhibited a reduction in demyelinated nerve fibers in both the ALF and PF compared to their vehicle-treated littermates (Fig. 4 A). Moreover, the number of nerve fibers showing mitochondrial *swelling* was decreased (Fig. 4 B), particularly in the PF, and the total number of normal appearing nerve fibers per mm² was increased in nimodipine-treated mice (Fig. 4 C). In response to treatment with nimodipine, the number of remyelinating nerve fibers was significantly increased in both funiculi (Fig. 4 D), suggesting neuroregenerative effects of the drug.

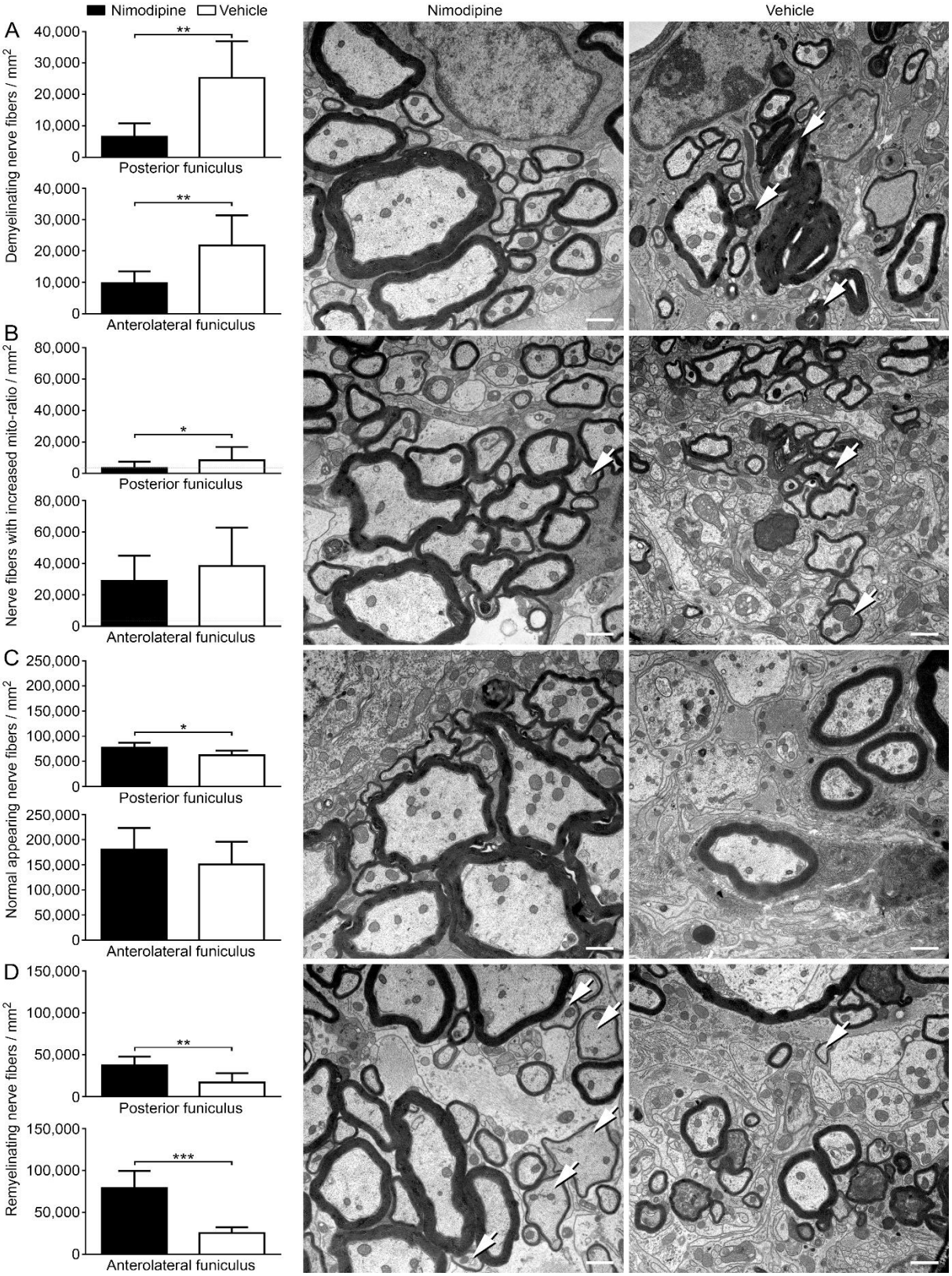
Nimodipine
Vehicle
Nimodipine
Vehicle
A
Demyelinating nerve fibers / mm2
40,000
30,000
20,000
10,000
0
**
Posterior funiculus
**
Anterolateral funiculus
B
Nerve fibers with increased mito-ratio / mm2
80,000
60,000
40,000
20,000
0
*
Posterior funiculus
Anterolateral funiculus
C
Normal appearing nerve fibers / mm2
250,000
200,000
150,000
100,000
50,000
0
*
Posterior funiculus
Anterolateral funiculus
D
Remyelinating nerve fibers / mm2
150,000
100,000
50,000
0
**
Posterior funiculus
***
Anterolateral funiculus

Fig. 4. Reduced nerve fiber pathology and increased remyelination in nimodipine-treated mice. The PF and ALF of $n = 12$ nimodipine- and $n = 9$ vehicle-treated mice were analyzed ultra-structurally. For these analyses, mice were sacrificed on day 68 or 72 after immunization, respectively. For our analyses, demyelinating nerve fibers (*A*), the number of nerve fibers with increased mito-ratio (*B*), axonal loss (*C*) and the number of remyelinated nerve fibers (*D*), were analyzed per mm². Scale bars indicate 1 µm. Arrows point to representative features of the respective panels. $*P \leq 0.05$; $**P \leq 0.01$; $***P \leq 0.001$; by two-tailed, unpaired Student's *t* test.

III. 3 Nimodipine treatment protects oligodendrocytes from EAE-induced loss

For further observation of the remyelination process, we studied the oligodendrocyte population. Our results demonstrate that the number of $Olig2^+$ cells was significantly elevated in nimodipine- compared to vehicle-treated mice. In fact, the number of oligodendrocytes was restored to the level of non-immunized controls in both funiculi (Fig. 5 A). In addition, the number $Olig2^+APC^+$ cells was significantly increased in nimodipine-treated mice (Fig. 5 B). Given that Olig2 labels oligodendrocytes in general and APC is transiently expressed during oligodendrocyte development and myelination [115], our observation of oligodendroglial regeneration, as seen by increased numbers of $Olig2^+APC^+$ cells, strongly supports the EM data regarding increased remyelination after nimodipine treatment.

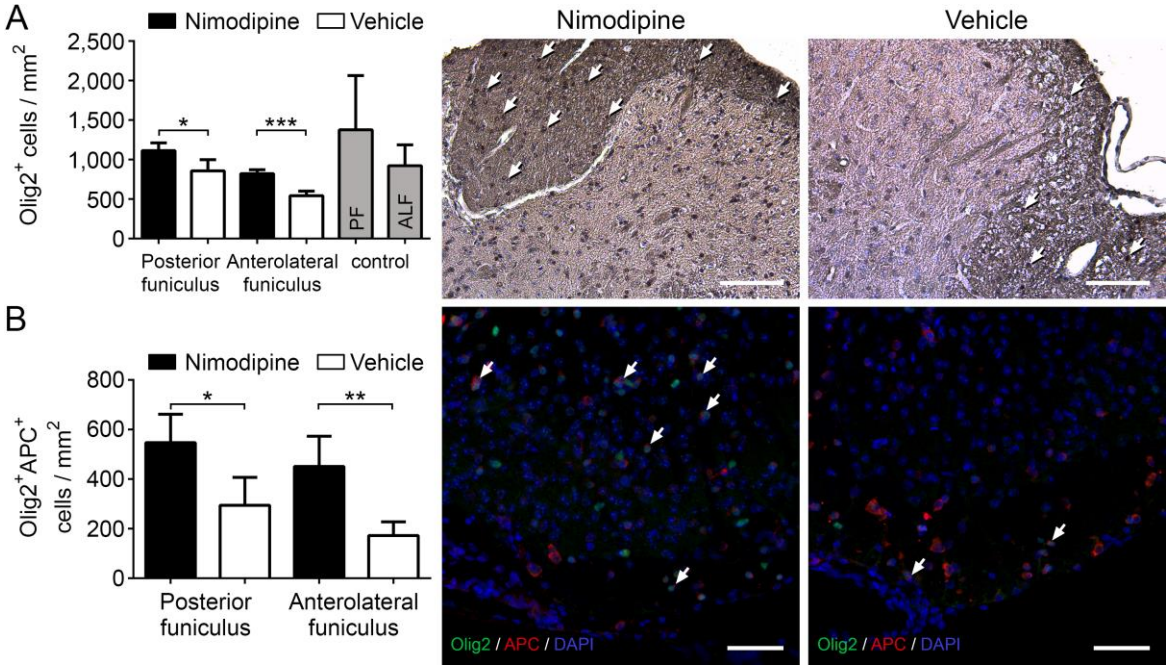

Fig. 5. Nimodipine treatment results in increased numbers of oligodendrocytes and APC^+ cells. (*A*) Number of $Olig2^+$ oligodendrocytes in the spinal cord of MP4-immunized nimodipine- or vehicle-treated mice (n = 4 per group). Mice were sacrificed on day 29 post-immunization after a treatment duration of six days. (*B*) Number of $Olig2^+APC^+$ cells per mm². Arrows highlight stained cells in the respective panels. Scale bars represent 100 µm in (*A*) and 50 µm in (*B*). *$P \leq 0.05$; **$P \leq 0.01$; ***$P \leq 0.001$; by two-tailed, unpaired Student's *t* test.

III.4 The extent of inflammation did not differ between treatment groups

In addition to studying demyelination and axonal pathology as hallmarks for MS and EAE, we also investigated inflammation as third hallmark. First, we measured the infiltrate size in $n = 7$ nimodipine- and $n = 5$ vehicle-treated MP4-immunized mice on day 68 or 72 after immunization, respectively, in methylene blue-stained semi-thin sections (Fig. 6). There were no differences between nimodipine- and vehicle-treated animals in the size of spinal cord infiltrates. In general, the PF was affected more severely than the ALF in both groups. This reflects the presence of sensomotoric deficits in our MP4/SJL model. Next, we performed flow cytometry for T cells, T cell subsets, T cell activation, and B cells in the spinal cord and spleen of immunized mice during relapse (on day 5 after treatment onset) with $n = 5$ nimodipine- and $n = 5$ vehicle-treated mice (Fig. 7). Again, there was no difference in the T cell compartment in nimodipine- and vehicle-treated mice, while the number of $B220^+$ B cells was increased in the spinal cord but not the spleen of nimodipine-treated mice. Microarray analysis of the inflammatory response in the spinal cord of MP4-immunized mice at the beginning of the second relapse (after a treatment duration of 15 or 20 days) did not reveal a difference between the two groups ($n = 3$ mice were tested per group) (Fig. 8). These results confirm our histological analyses. A list of all analyzed genes can be found at Gene-Ontology-Terms Class: GO:0006954, inflammatory response.

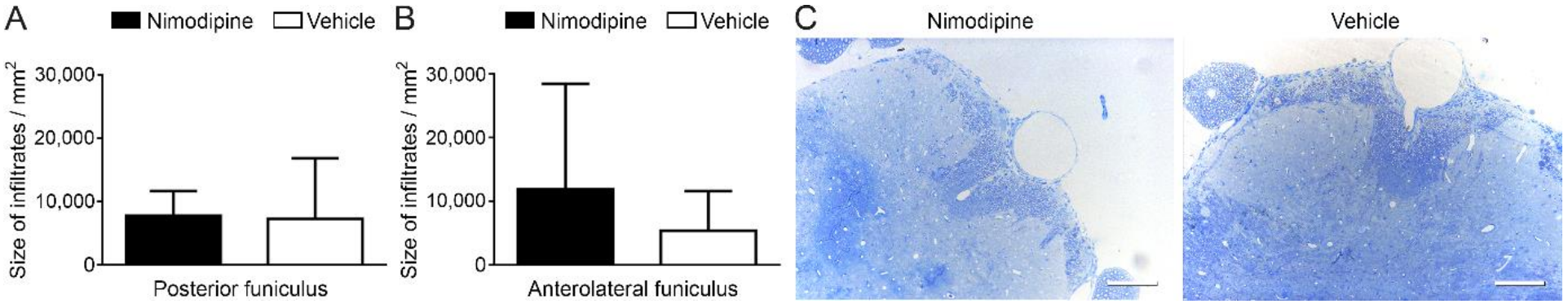

Fig. 6. The extent of inflammation does not differ between groups. Analysis of methylene blue-stained semi-thin spinal cord sections of *n* = 7 nimodipine- (*A*) and *n* = 5 vehicle-treated (*B*) mice. Representative images are depicted in (*C*) (left image: nimodipine treatment, right image: vehicle treatment). Scale bars indicate 100 µm.

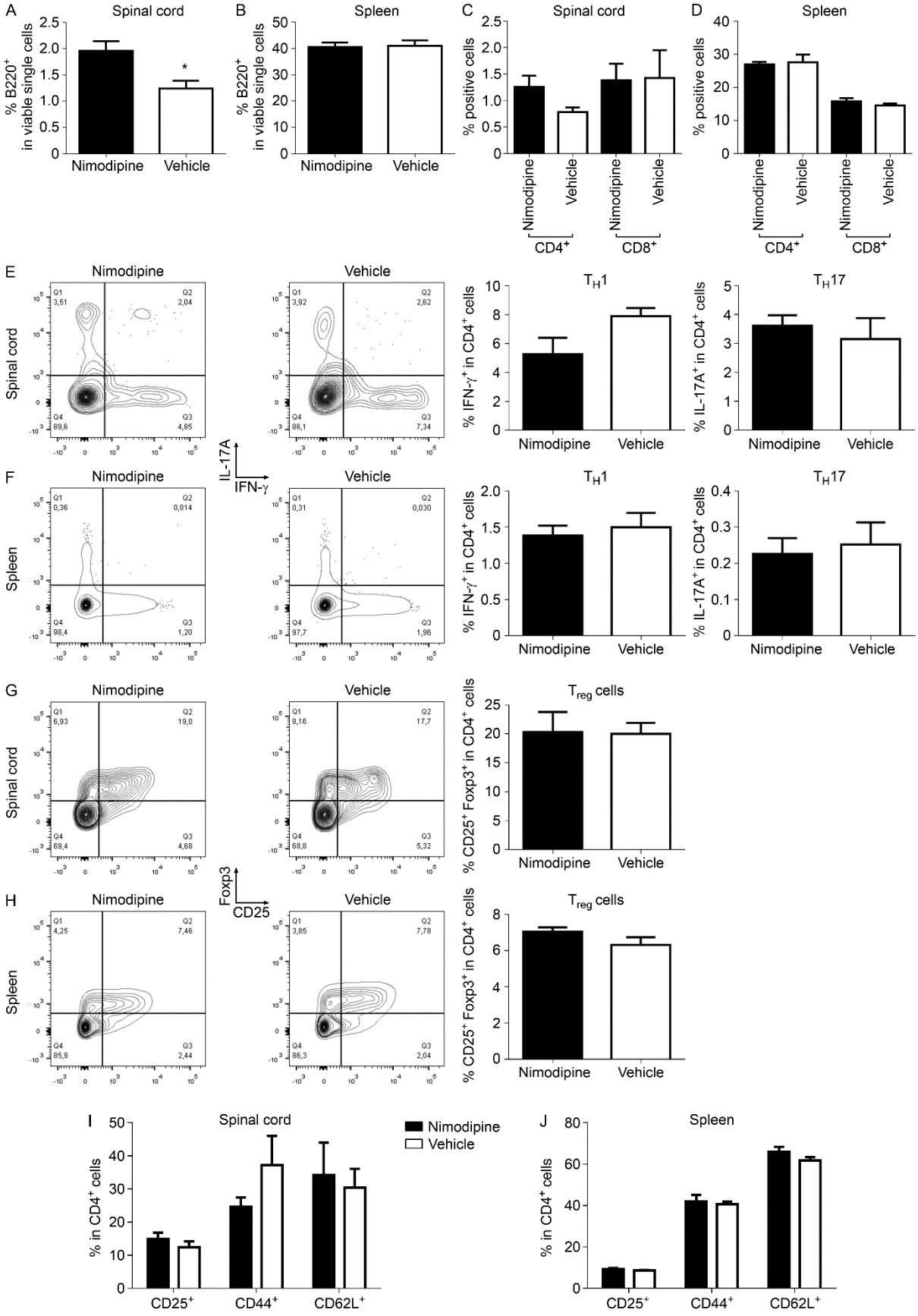
A
Spinal cord
% B220+ in viable single cells
Nimodipine
Vehicle
B
Spleen
% B220+ in viable single cells
Nimodipine
Vehicle
C
Spinal cord
% positive cells
Nimodipine
Vehicle
CD4+
CD8+
D
Spleen
% positive cells
CD4+
CD8+
E
Nimodipine
Vehicle
Spinal cord
IL-17A
IFN-γ
TH1
% IFN-γ+ in CD4+ cells
TH17
% IL-17A+ in CD4+ cells
F
Spleen
G
Spinal cord
Treg cells
% CD25+ Foxp3+ in CD4+ cells
H
Spleen
Foxp3
CD25
I
Spinal cord
% in CD4+ cells
CD25+
CD44+
CD62L+
J
Spleen

Fig. 7. Flow cytometric analyses of spinal cord inflammation in nimodipine- and vehicle-treated mice. MP4-immunized nimodipine- (n = 5) or vehicle-treated (n = 5) mice were sacrificed during the first relapse (on day 5 after treatment onset). Percentage of $B220^+$ B cells in spinal cord (*A*) and spleen (*B*). Percentage of $CD4^+$ and $CD8^+$ T cells in spinal cord (*C*) and spleen (*D*). T_H1/T_H17 cells infiltrating in the spinal cord (*E*) and spleen (*F*) and regulatory T cells in spinal cord (*G*) and spleen (*H*) all in percent. Measurement of T cell activation in spinal cord (*I*) and spleen (*J*). $*P \leq 0.05$; by two-tailed, unpaired Student's t test. Flow cytometry experiments and analyses were kindly performed by S. Jörg.

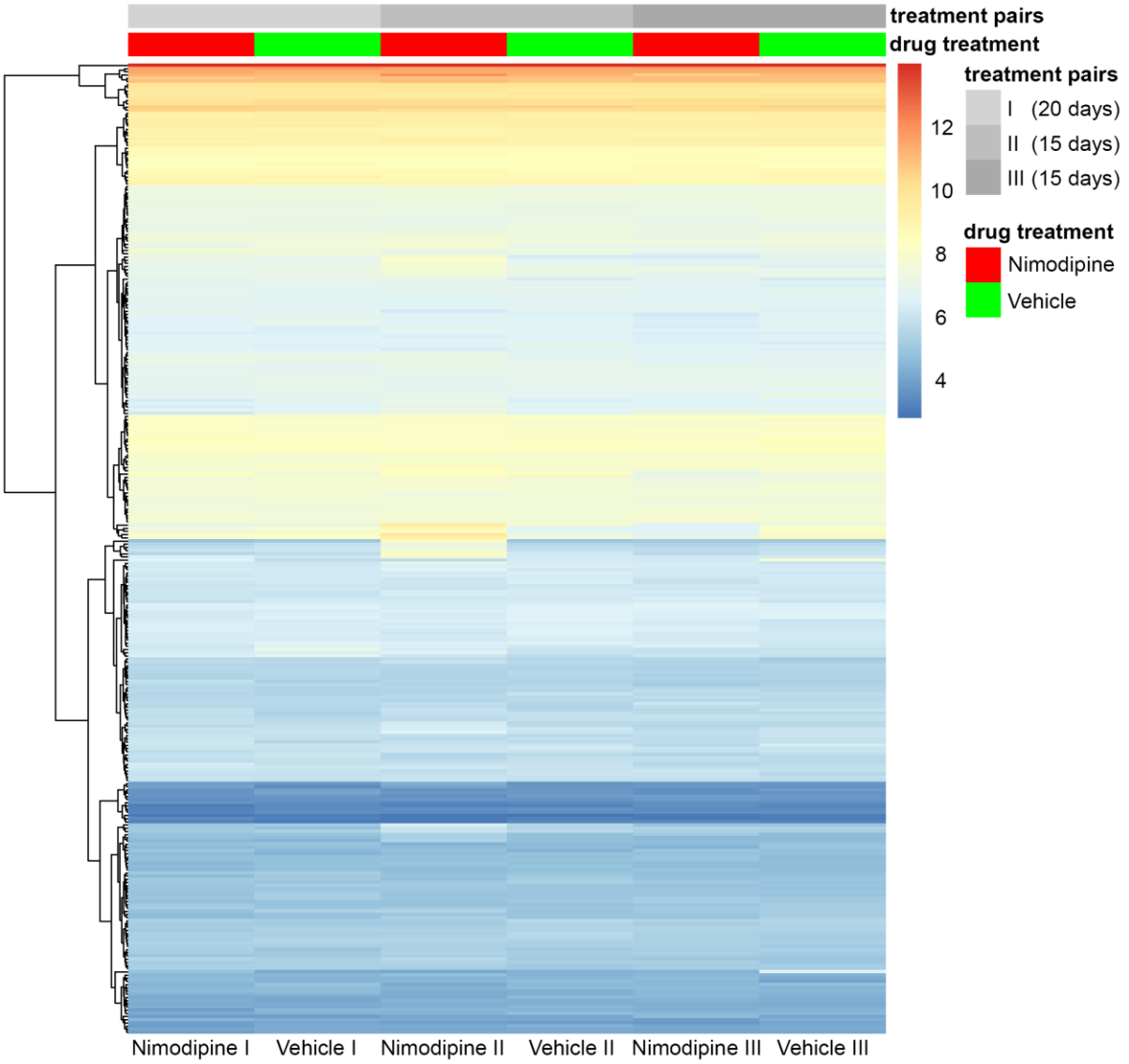

Fig. 8. Heat map of the inflammatory response (according to the gene card inflammatory response: Gene-Ontology-Terms Class: GO:0006954) in nimodipine- (n = 3; sample names: Nimodipine I, II and III) *vs.* vehicle-treated littermates (n = 3; sample names: Vehicle I, II and III). Investigations took place at the onset of the second relapse after 20 (Nimodipine I and Vehicle I; day 42 after immunization) or 15 days of treatment (Nimodipine II + III and Vehicle II + III day 37 after immunization). Microarray analysis was kindly performed by Dr. C.J. Scholz.

III.5 Nimodipine treatment resulted in decreased cell viability, shrinkage, and apoptosis of microglial cells

Despite an unaltered extent of lymphocyte infiltration, nimodipine treatment caused differences in microglial distribution. Nimodipine-treated mice showed a significantly decreased number of $Iba1^+$ cell bodies in both funiculi of the spinal cord on day 29 after immunization compared to vehicle-treated mice (n = 4 in both groups; Fig. 9 A and B). Consistently, we discovered significantly more annexin V^+ cells by flow cytometry in the spinal cord of mice sacrificed on 29 post- immunization after a treatment duration of five days with either nimodipine (n = 5) or vehicle (n = 5) (Fig. 10). In flow cytometry, annexin V is commonly used to detect apoptotic cells. To detect apoptosis we also stained $TUNEL^+Iba1^+$ microglia in the spinal cord of nimodipine- and vehicle-treated MP4-immunized mice (n = 5 per group). Animals received nimodipine or vehicle for two (n = 1 per group) or six days (n = 4 per group), respectively. We observed a higher number of double positive cells in the nimodipine-treated group (Fig. 10), but the generally low number of double positive cells in the spinal cord in both groups did not allow statistical assessment. As the earlier time point (2 days) was more convincing, perhaps an even earlier time point could be more suitable in future examinations. Non-immunized mice displayed a reduction of $Iba1^+$ cells in the spinal cord following nimodipine treatment, confirming our hypothesis of increased microglial apoptosis induced by nimodipine. This effect was not significant, possibly due to the lower number of $Iba1^+$ cells in naïve animals (Fig. 11). Organotypic slice culture of the spinal cord confirmed our *in vivo* results and was furthermore used to verify the dosage used for cell culture studies. Treatment with 10 µM nimodipine for 24 h in slice culture of the spinal cord caused a significant reduction of $Iba1^+$ cells (Fig. 9 C and D). These results initiated further examination of nimodipine-mediated effects on microglia. For that purpose, two different microglia cell lines (N9 and BV-2) were cultured. N9 and BV-2 cell lines are well studied and

reported to be comparable to primary cells with regard to calcium signaling, cytokine production, and cell-cell interaction [116,117]. By administering different doses of nimodipine to N9 and BV-2 cultures for 24 h we were able to detect a concentration-dependent loss of cells. A dose of 1 µM nimodipine did not lead to significant differences compared to vehicle-treated cells, but in both cell lines a dose of 5 µM significantly reduced the number of microglial cells (Fig. 9 E and F). The effect was most stable for 10 µM, which was also seen in MTT assays (Fig. 9 G). Doses were chosen according to previous studies [77,84,118]. Results from the cell lines were confirmed by using primary CD11b-sorted cell cultures of adult and newborn murine microglia (Fig. 12). Many cells showed rounding of the cytoplasm and shrinkage in response to treatment with 10 µM nimodipine (Fig. 9 H). Additionally TUNEL staining was positive in most nimodipine-treated microglia cells after 24 h (Fig. 9 I). In order to exclude a general toxic effect, astrocyte cultures (IMA 2.1 cell line) were used as glia cell control. Here we did not detect apoptosis or parameters of cellular stress (Fig. 13 A and B). In line with this, staining of $GFAP^+$ cells in spinal cord and slice culture did not show any evidence of cytotoxic nimodipine effects on astrocytes (Fig. 13 C). Accordingly, the apoptosis-inducing effect of nimodipine seemed to be specific for microglia. Organotypic slice culture of murine spleens indicated further specificity among macrophage populations, as $F4/80^+$ macrophages were not harmed by nimodipine treatment (Fig. 13 D). Interestingly, nimodipine-induced apoptosis was independent of microglial polarization towards a pro-inflammatory (stimulation with TNF-α/IFN-γ) or anti-inflammatory (stimulation with IL-4 or TGF-β1) phenotype (Fig. 14). Next, we tested whether the apoptosis-inducing effect was specific for nimodipine. For that purpose, we treated N9 cells with different doses of other drugs. First we studied the effect of nifedipine, another Ca_v 1.2 dihydropyridine antagonist *(*Fig. 15 A and D), which did not result in any toxic effects. To exclude nonspecific blockade of potassium channels by high doses of nimodipine [119,120],

the potassium channel antagonist 4-AP was applied to N9 cells (Fig. 15 B and E). Again, we did not observe any effect on cell viability. The Ca_v 1.2 agonist Bay K8644, (Fig. 15 C) did not influence cell viability likewise. Effects regarding the loss of cells were confirmed in BV-2 cells (Fig. 16).

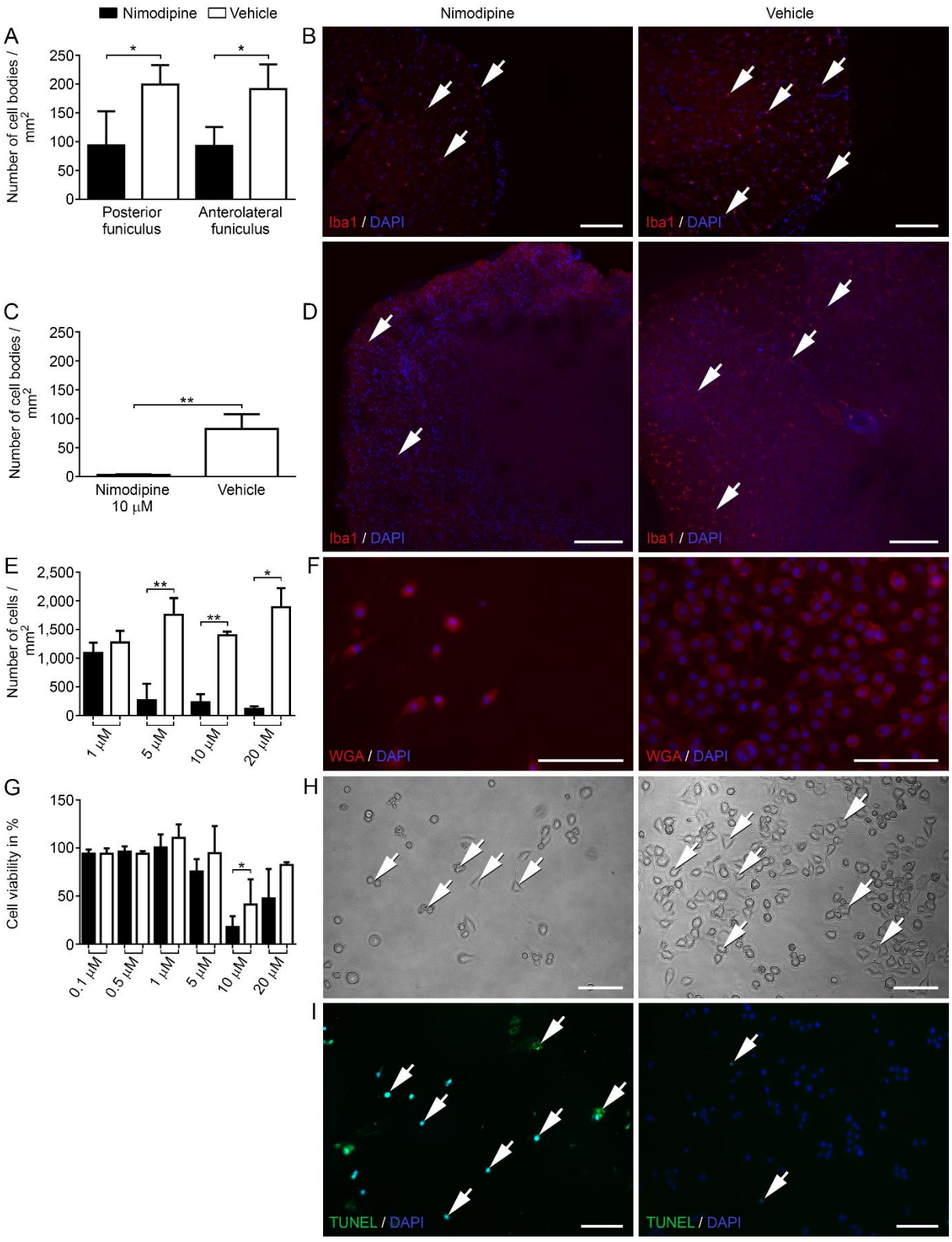
Nimodipine
Vehicle
A
Number of cell bodies / mm²
250
200
150
100
50
0
*
*
Posterior funiculus
Anterolateral funiculus
B
Nimodipine
Vehicle
Iba1 / DAPI
Iba1 / DAPI
C
Number of cell bodies / mm²
250
200
150
100
50
0
**
Nimodipine 10 μM
Vehicle
D
Iba1 / DAPI
Iba1 / DAPI
E
Number of cells / mm²
2,500
2,000
1,500
1,000
500
0
**
**
*
1 μM
5 μM
10 μM
20 μM
F
WGA / DAPI
WGA / DAPI
G
Cell viability in %
150
100
50
0
*
0.1 μM
0.5 μM
1 μM
5 μM
10 μM
20 μM
H
I
TUNEL / DAPI
TUNEL / DAPI

Fig. 9. Nimodipine treatment results in microglial cell shrinkage, rounding, and apoptosis and in reduced Iba1$^+$ cells in spinal cord tissue and organotypic culture. (*A*) Number of Iba1$^+$ cell bodies/mm² in the spinal cord of animals with EAE. (*B*) Representative images of nimodipine-treated (n = 4) *vs.* vehicle-treated mice (n = 3). (*C* and *D*) display results from organotypic slice cultures after treatment with 10 µM nimodipine for 24 h (n = 4) or vehicle (n = 3). (*E* and *F*) Number and representative images of WGA-stained cells/mm² in both groups. (*G*) Viability of N9 cells after treatment with 10 µM nimodipine for 24 h as measured by MTT assay. Representative images of cultured cells shown in (*H*). Arrows mark cells that display rounding, shrinkage, and pathological vesicles. (*I*) Apoptosis was visualized by TUNEL assay. Arrows point to positive cells in the respective panels. Scale bars indicate 100 µm. Cell culture data were obtained from at least three independent experiments. *$P \leq 0.05$; **$P \leq 0.01$; by two-tailed, unpaired Student's *t* test.

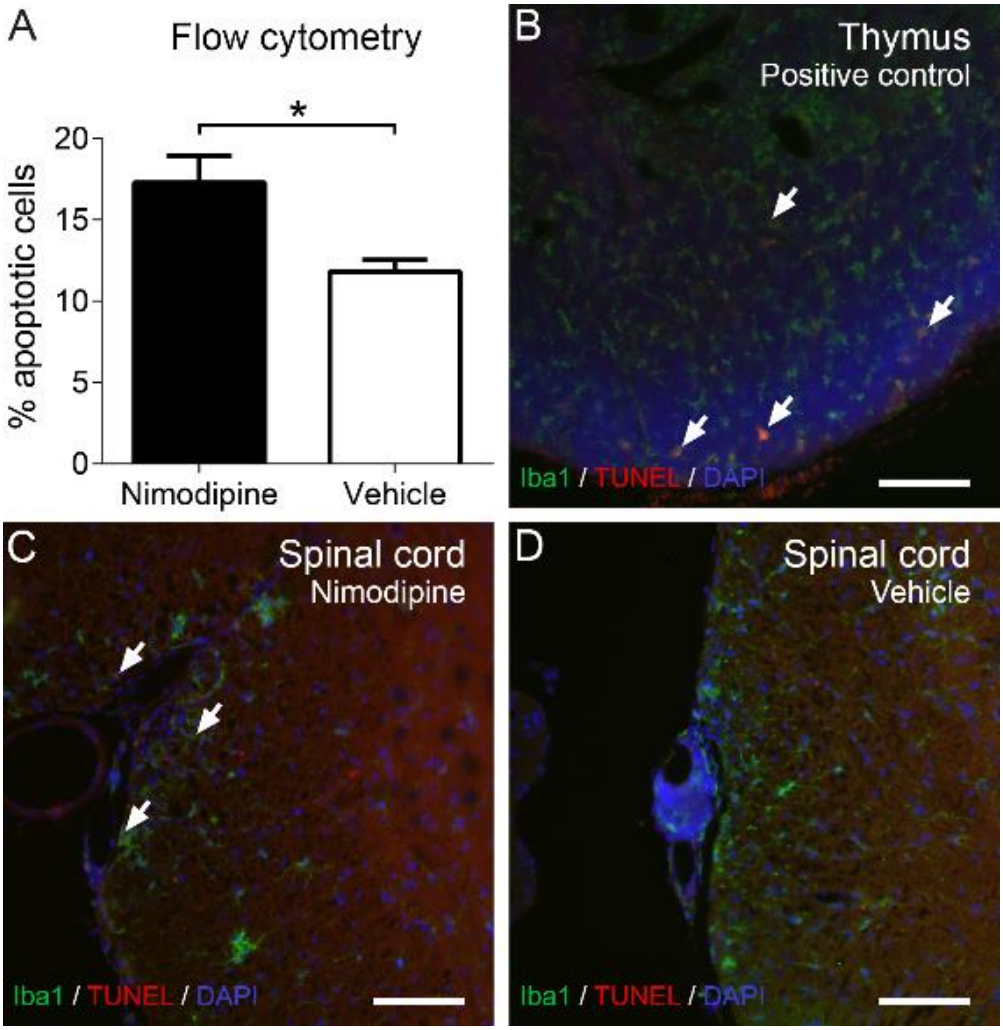

Fig. 10. Elevated apoptosis in the spinal cord following nimodipine treatment. (*A*) Flow cytometric analysis of the spinal cord after a treatment duration of five days (28 days post-immunization). TUNEL and Iba1 staining of (*B*) thymus as positive control and the spinal cord of nimodipine- (*C*) *vs.* vehicle-treated animals (*D*). The depicted immunohistochemistry of MP4-immunized mice was performed after two days of treatment. Arrows point out double positive cells in the respective panels. Scale bars represent 100 µm. *$P \leq 0.05$; by two-tailed, unpaired Student's *t* test.

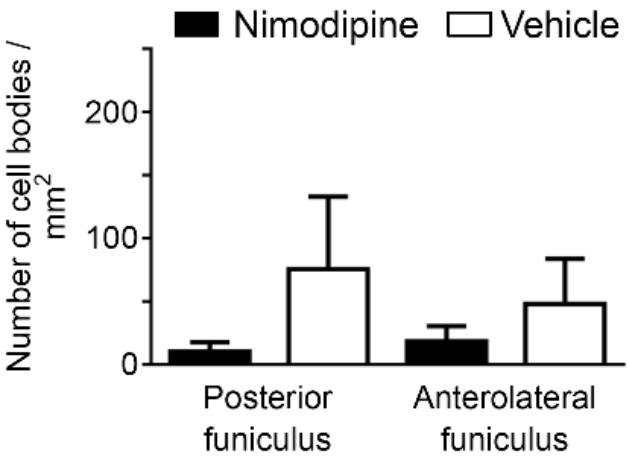

Fig. 11. Reduced number of Iba1$^+$ cells in the spinal cord of naïve SJL/J mice in response to nimodipine. Non-immunized SJL/J mice were treated with nimodipine (n = 4) or vehicle (n = 4) for 10 days to detect Iba1$^+$ microglia in the spinal cord.

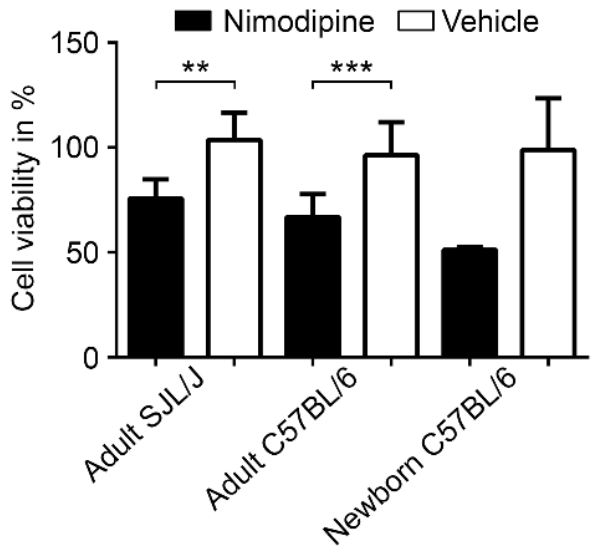

Fig. 12. Decreased viability after treatment with 10 µM nimodipine in CD11b$^+$ microglial primary culture. Isolated adult SJL/J, C57BL/6 and newborn C57BL/6 cells were purified for CD11b$^+$ cells. The experiment on adult C57BL/6 cells was done three times in triplicates. The experiments on adult SJL/J and newborn C57BL/6 cells were performed once in triplicates. $^{**}P \leq 0.01$; $^{***}P \leq 0.001$; by two-tailed, unpaired Student's t test. Cell isolation of primary microglial cells was kindly performed by S. Seubert.

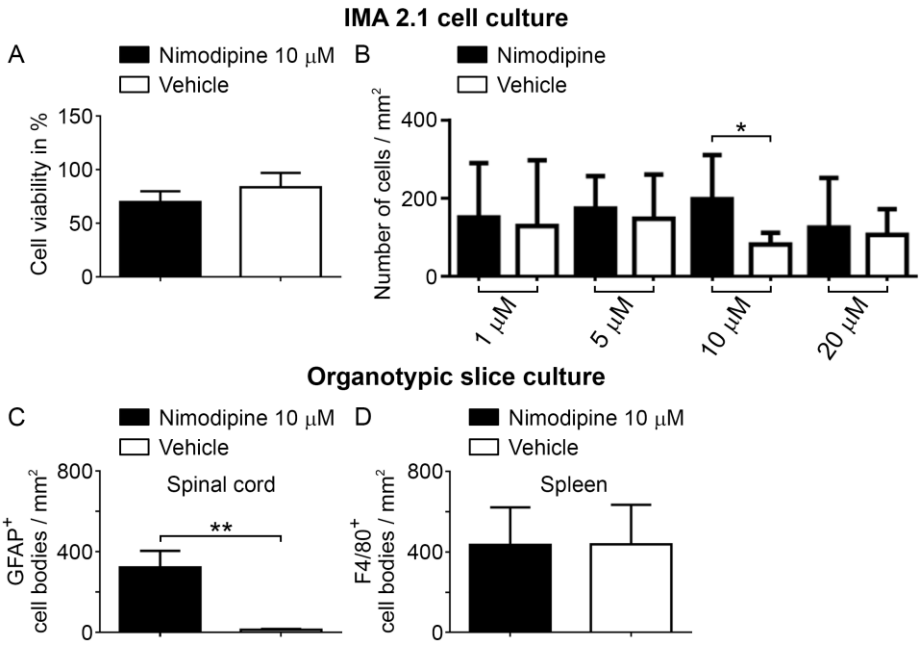

Fig. 13. Induction of apoptosis by nimodipine is cell type-specific. (*A*) Cell viability and (*B*) number of astrocytes (IMA 2.1 cell line) after treatment with 10 µM nimodipine. (*C*) Number of $GFAP^+$ cell bodies after treatment with nimodipine (10 µM) in organotypic slice cultures of the spinal cord. (*D*) Number of $F4/80^+$ macrophages in spleen organotypic slice cultures after treatment with nimodipine (10 µM). All experiments were performed at least three times in parallel with vehicle-treated controls. $*P \leq 0.05$; $**P \leq 0.01$; by two-tailed, paired Student's *t* test.

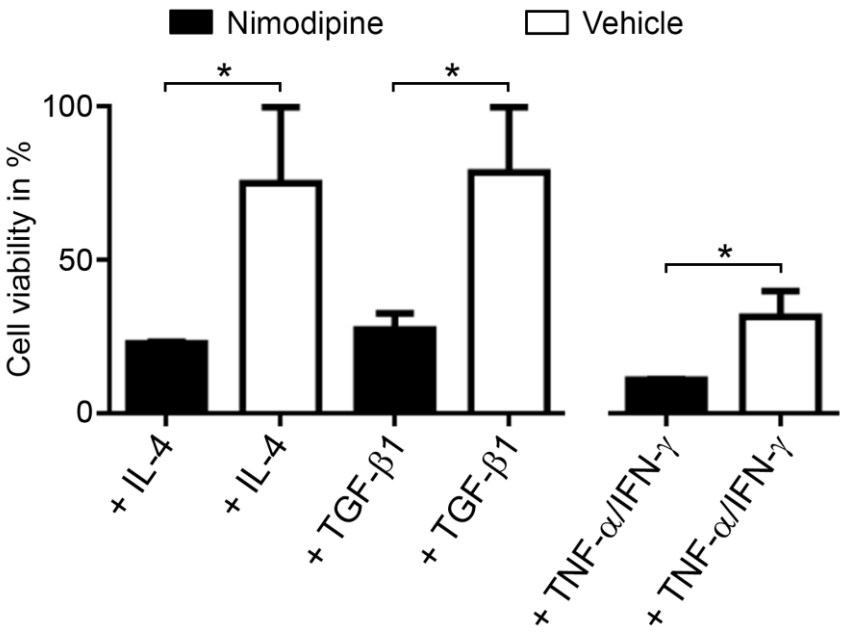

Fig. 14. Microglial polarization does not influence the nimodipine-induced decrease in cell viability. N9 cells were polarized towards an anti-inflammatory phenotype using IL-4 (10 ng/ml) or TGF-β1 (100 ng/ml) or towards a pro-inflammatory phenotype using TNF-α/IFN-γ (100 ng/ml each). Cells were subsequently incubated with 10 µM nimodipine or vehicle for 24 h. *$P \leq 0.05$; by two-tailed, unpaired Student's *t* test. Data are representative of three independent experiments, each done in triplicate.

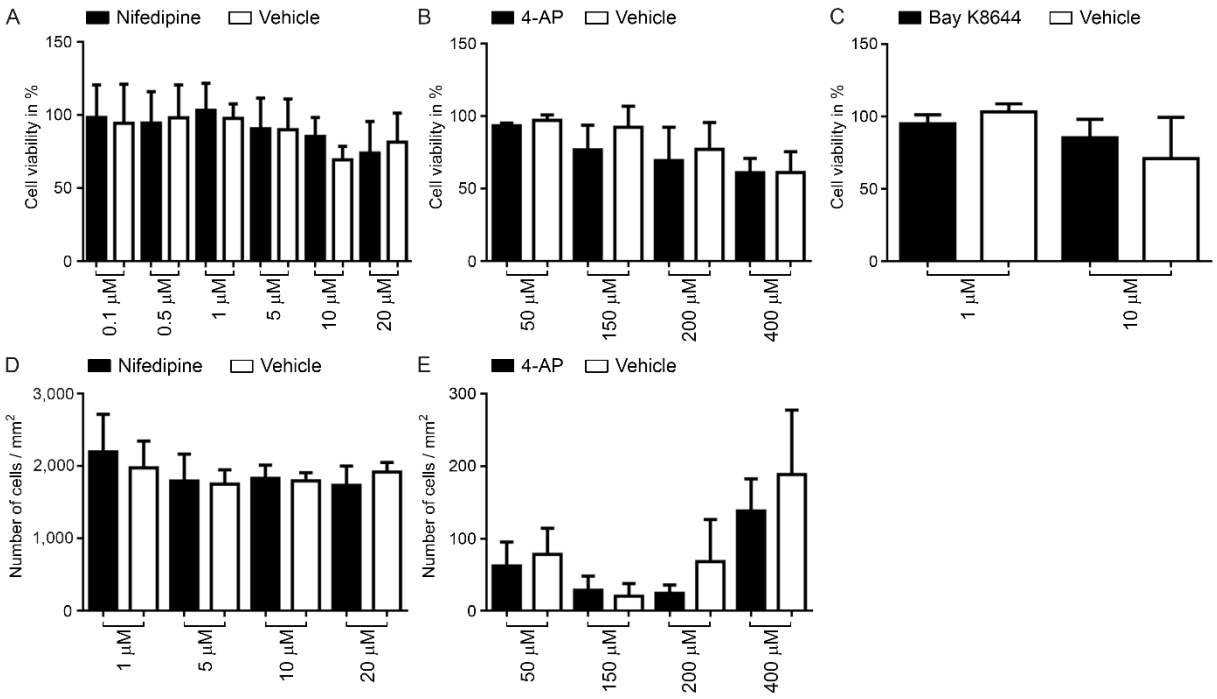

Fig. 15. Nimodipine-mediated induction of microglial apoptosis is drug-specific. N9 cells were incubated with varying doses of the second Ca_v 1.2 antagonist (nifedipine; *A* and *D*) as well as the non-specific potassium channel blocker 4-AP (*B* and *E*) and the Ca_v 1.2 agonist Bay K8644 (*C*) for 24 h. Cell viability (*A* to *C*) and the number of cells/ mm² (*D* and *E*) were assessed. Cell viability experiments were repeated three to four times and experiments regarding the cell number/mm² were performed at least five times.

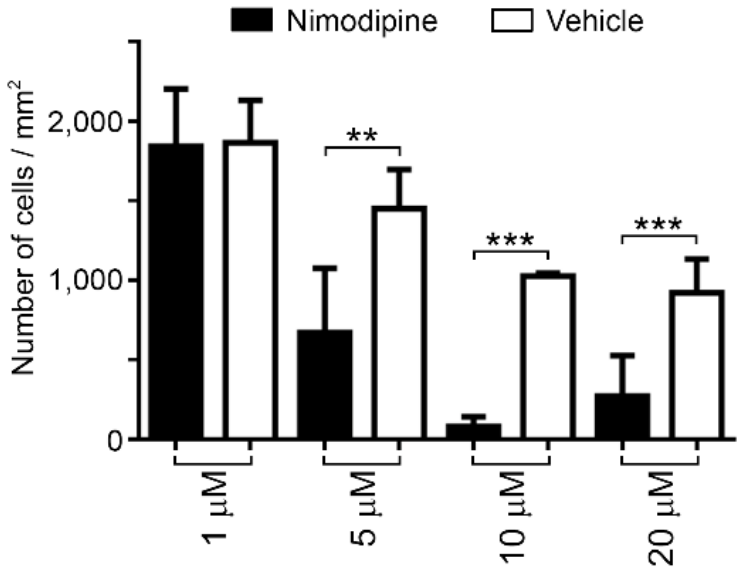

Fig. 16. Nimodipine treatment results in a decreased number of BV-2 microglial cells. BV-2 cells were used to verify effects observed in N9 cells. The number of cells/mm² was counted after 24 h of incubation with 5 µM, 10 µM, or 20 µM nimodipine. The experiment was repeated at least four times. $^{**}P \leq 0.01$; $^{***}P \leq 0.001$; by two-tailed, unpaired Student's *t* test.

III.6 Nimodipine induced a decrease in NO production and iNOS expression in microglia and spinal cord and was accompanied by decreased ROS *in vivo*.

Aside from triggering microglial apoptosis, nimodipine was also capable of reducing NO levels in cell culture of N9 cells. NO levels were quantified with the Griess detection method (Fig. 17 A). We investigated whether microglia apoptosis alone was the reason for the reduction in NO release. However, a similar effect was observed for nifedipine (Fig. 17 B), which we did not influence cell viability. 4-AP (Fig. 17 C) and Bay K8644 (Fig. 17 D) did not have any effect on NO production, suggesting a drug-specific effect of dihydropyridine calcium channel blockers. Microarray analyses of N9 cells treated with 10 µM nimodipine for 24 h revealed a significantly reduced expression of *Nos2* (synonymous with *iNOS*) (Fig. 18). Additionally, we observed reduced staining of iNOS in surviving N9 cells (Fig. 17 E to F) and found decreased *iNOS* expression in nimodipine-treated EAE mice using RT-PCR (Fig. 17 G). Here only 16.7 % (1/6) of the tested mice that received nimodipine treatment showed an *iNOS* mRNA band in the spinal cord whereas 60 % (3/5) of vehicle-treated mice displayed a respective mRNA band. In EAE lesions, *iNOS* expression levels were too low to detect lesion-specific effects in RT-qPCR analyses of the spinal cord. Instead, we chose to investigate ROS, which are massively produced in EAE lesions. For this, we made use of the dHet detection method [109]. Our data demonstrate significantly reduced activity of ROS in both funiculi of the spinal cord after treatment with nimodipine (Fig. 17 H and J) compared to vehicle-treated animals (Fig. 17 I and J). In an attempt to elucidate the mechanism behind nimodipine-mediated apoptosis induction we performed further microarray analyses of nimodipine- *vs.* vehicle-treated N9 cells and observed both significantly decreased *Pik3r3* expression and significantly increased mRNA expression of the anti-apoptotic factor *Bcl2* (Fig. 18). *Pik3r3* expression is upstream to *Akt* in the apoptosis pathway and a reduction of *Akt2* and *Akt3* expression levels was likewise detectable (Fig. 18). This is why we studied

Akt/phosphorylated Akt in extensive western blot analyses together with iNOS and cleaved poly (ADP-ribose) polymerase (cPARP) as a marker for apoptosis (Fig. 17 K). To this end, N9 cells were incubated with either vehicle or 10 µM nimodipine for 24 h and continuously observed. Doses of 0.1, 0.5 and 1 µM were tested additionally, but coherent with the other experiments effects were most stable at 10 µM. Cell lysates were collected and blotted for iNOS, cPARP and phospho-Akt/total Akt. Protein expression levels of phospho-Akt/total Akt were reduced after 24 h in some blots, but this reduction was not consistently detectable throughout all experimental repetitions. However, we detected a reduction in iNOS protein expression levels after treatment for 24 h, confirming our prior results. Protein expression levels of cPARP were increased already 3 h after treatment onset. After 24 h, a difference in cPARP expression was no longer detectable.

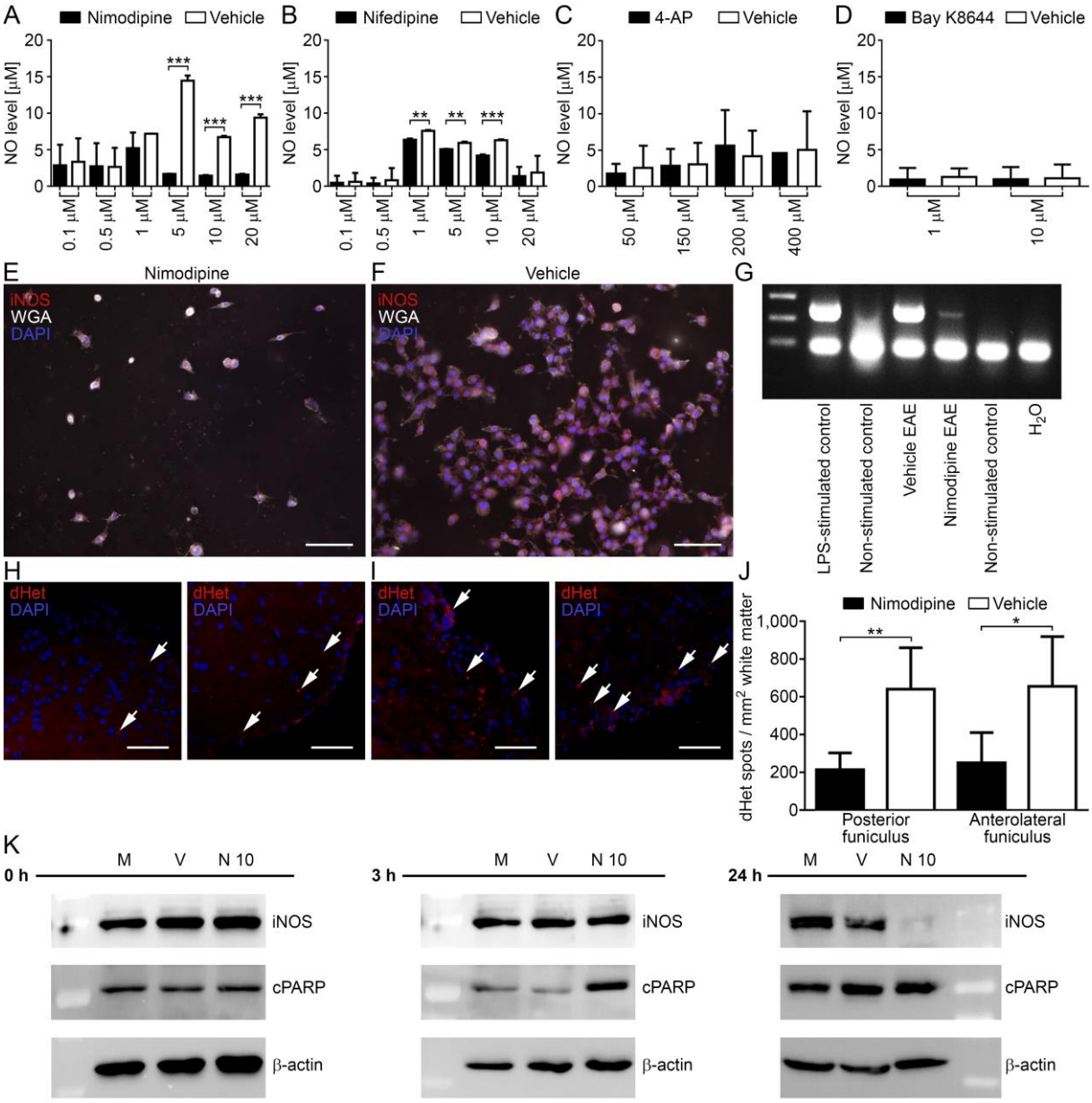
A
Nimodipine
Vehicle
NO level [µM]
0.1 µM
0.5 µM
1 µM
5 µM
10 µM
20 µM
B
Nifedipine
Vehicle
C
4-AP
Vehicle
50 µM
150 µM
200 µM
400 µM
D
Bay K8644
Vehicle
E
Nimodipine
F
Vehicle
iNOS
WGA
DAPI
G
LPS-stimulated control
Non-stimulated control
Vehicle EAE
Nimodipine EAE
Non-stimulated control
H2O
H
I
dHet
DAPI
J
Nimodipine
Vehicle
dHet spots / mm2 white matter
Posterior funiculus
Anterolateral funiculus
K
0 h
3 h
24 h
M
V
N 10
iNOS
cPARP
β-actin

Fig. 17. Nimodipine treatment results in reduced NO levels in cell culture, decreased expression of iNOS *in vivo* and *in vitro,* and reduced ROS activity in spinal cord. (*A* to *D*) NO concentration in µM after treatment of N9 cells with different concentrations in µM of nimodipine (*A*), nifedipine (*B*), 4-AP (*C*), and Bay K8644 (*D*) determined with the Griess detection method. (*E*) iNOS immunoreactivity in N9 cells after treatment with 10 µM nimodipine compared to vehicle (*F*), both counterstained with WGA and DAPI. Gene expression of *iNOS* in nimodipine-treated mice suffering from EAE compared to vehicle-treated EAE mice (*G*). (*H*) shows representative images of ROS distribution in both funiculi of the spinal cord after treatment with nimodipine ($n = 5$) compared to vehicle-treated animals (*I*, $n = 6$ mice). The left image depicts the PF and right image the ALF in (*H*) and (*I*). Arrows point out dHet spots. (*J*) Quantification of the dHet spots within the white matter per mm^2 visualizing ROS expression. (*K*) iNOS and cPARP protein expression after nimodipine treatment (10 µM; N10) at three different time points (0 h, 3 h and 24 h after treatment) compared to vehicle treatment (V) and medium control (M). Scale bar indicates 100 µm in (*E*) and (*F*) and 50 µm in (*H*) and (*J*). Cell culture data were obtained from at least three independent experiments, each done in triplicates. $*P \leq 0.05$; $**P \leq 0.01$; $***P \leq 0.001$; by two-tailed, unpaired Student's *t* test.

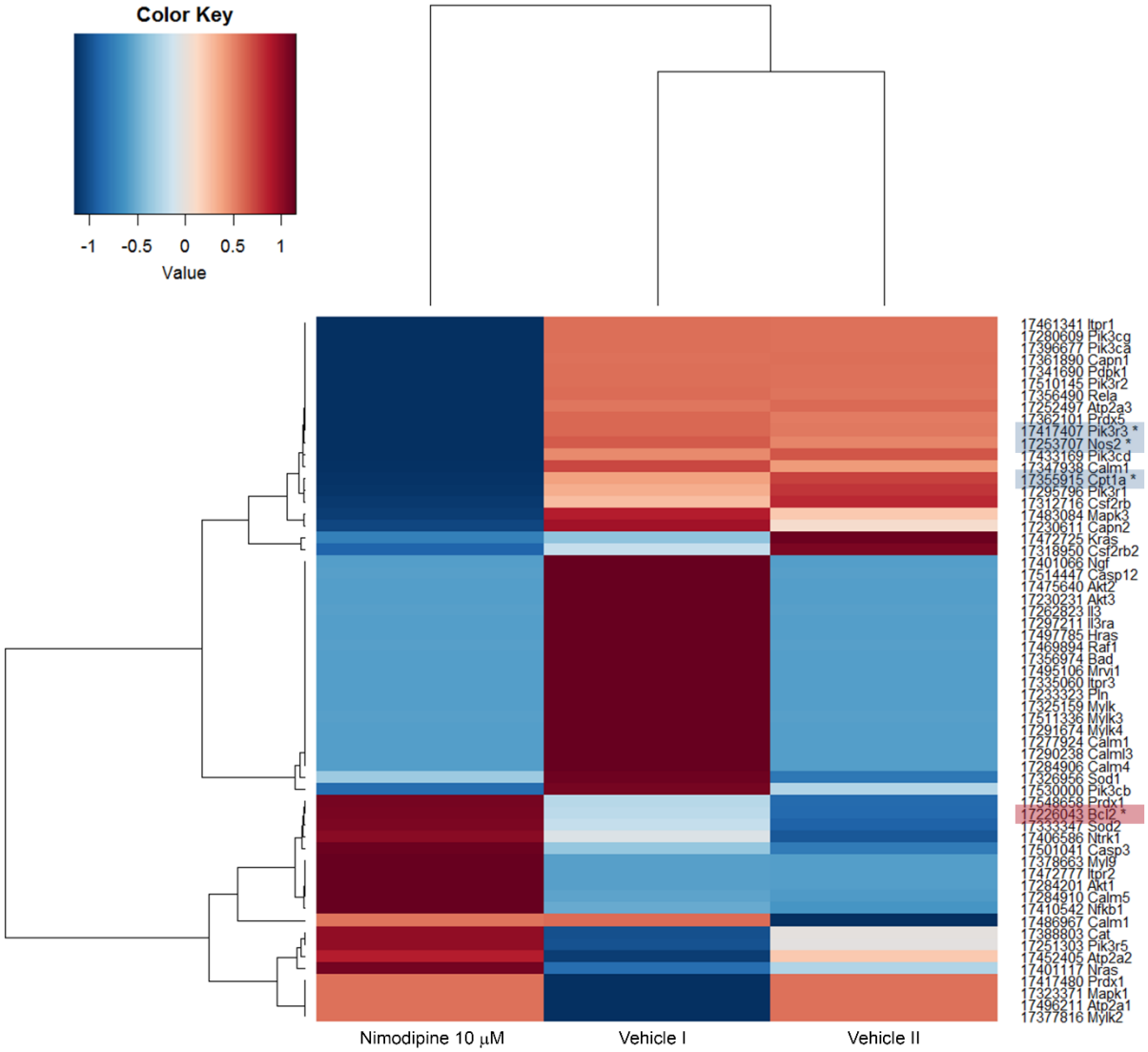

Fig. 18. Heat map of relevant microarray data obtained after treatment of N9 cells with either 10 µM nimodipine (one sample) or vehicle control (two samples: Vehicle I and Vehicle II) for 24 h. We did not detect any changes in calcium-channel dependent apoptosis pathways. A significant reduction in *Pik3r3*, *Nos2* and *carnitine palmitoyltransferase 1A* (*Cpt1A*) gene expression (highlighted in blue), indicating a decrease in microglial activity, was detectable. Additionally, *Bcl2* gene expression was significantly increased (highlighted in red) and *Akt2* and *Akt3* expression were decreased. Microarray analysis was kindly performed by Dr. C. J. Scholz.

III.7 Effects of nimodipine treatment on microglia are independent of Ca_v 1.2 channel blockage

Microarray analyses suggested that changes in the apoptosis pathway induced by treatment with 10 µM nimodipine were independent of calcium, as typical Ca^{2+}-modulated gene expression in apoptosis was not significantly changed (Fig. 18). Consequently, we aimed at determining if the Ca_v 1.2 channel is present in microglial cells. To this end we performed RT-PCR (Fig. 19 A), RT-qPCR (Fig. 19 *B*) and IHC (Fig. 19 C to D). While we found Ca_v 1.2 channel expression in the heart, astrocytes and oligodendrocytes (Oli-neu cells) (Fig. 19 A to C), it was absent in microglia. Stimulation with TNF-α/IFN-γ did not provoke Ca_v 1.2 channel expression either (Fig. 19 A). Additionally, we performed patch-clamp ramp (Fig. 19 E, upper graph) and IV-recordings (Fig. 19 E, lower graph) that did not provide convincing evidence for the existence of Ca_v 1.2 in microglia. Patch-clamp ramp recordings in the presence of TEA (Fig. 19 F) were performed to exclude the possibility that apoptosis could be induced by unspecific blockage of potassium channels. The measurements displayed a TEA-sensitive outward current with a reversal potential of -76 mV (Fig. 19 F upper panel). Long-term recording with a holding potential of +30 mV showed the TEA-sensitive fraction of the outward current (Fig. 19 F, lower panel), indicating none or only few scattered potassium channels that are most unlikely physiologically relevant. Thus, nonspecific blockage of these channels can be neglected as a major cause of apoptosis.

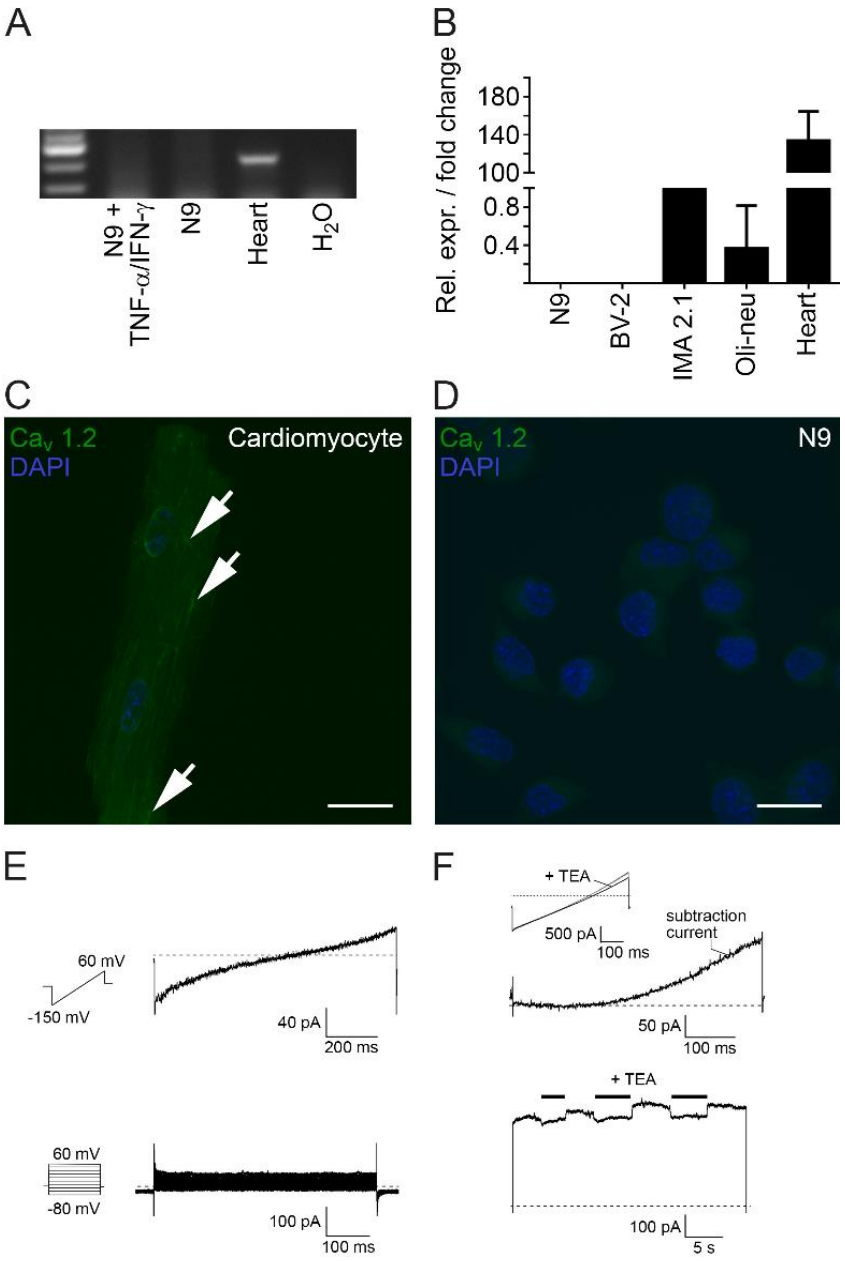

Fig. 19. Microglia do not express the Ca_v 1.2 channel. We were not able to detect the channel in (*A*) RT-PCR, (*B*) RT-qPCR (normalized to IMA 2.1 cells) and (*C* to *D*) IHC (arrows point-out positive staining). Additional (*E*) patch-clamp ramp and IV-recordings as well as (*F*) patch-clamp ramp recordings with TEA infusion were also not able to proof the existence of the Ca_v1.2 channel or potassium channels in N9 cells. Scale bars depict 20 µm. Data are representative of three independent experiments. For patch-clamp analyses, 10 cells were measured. Patch-clamp analyses were kindly performed by Prof. Dr. rer. nat. E. Wischmeyer.

IV. Discussion

IV. 1 Study design and summary of the results

The aim of our study was to create conditions as comparable to MS as possible in order to develop neuroprotective strategies for the treatment of MS patients. This is why we used the MP4 EAE model in SJL/J mice, which causes a relapsing-remitting course of disease. This model is unique as it includes many features of MS, like a B cell component and *determinant spreading*. In addition to the classic phenotype of EAE, immunization with MP4 led to sensomotoric impairment and ataxia in some mice, which is more inclusive of MS symptoms than traditional EAE models. Hence, we strongly believe that it is well suited to reflect the human conditions and to test treatment strategies.

Our hypothesis was that the calcium-channel antagonist nimodipine has a beneficial effect on MP4-induced EAE, as an increase in calcium levels was shown to trigger harmful cascades in other neurodegenerative diseases. Additionally, beneficial effects of nimodipine have been reported on cognitive dysfunction, synaptic plasticity and recovery after brain injury. In order to examine our hypothesis, mice were injected daily with either 10mg nimodipine / kg or vehicle solution for 19-24 days (as described in Table 4). The dosing regimen was chosen according to previous studies, which demonstrated its clinical relevance [79,104]. Following treatment several examinations were performed. The clinical course of disease was closely monitored and the three hallmarks of MS/EAE, namely inflammation, demyelination and axonal damage/loss were investigated. Ultimately, our results led to extensive *in vivo* and *in vitro* studies of glial cells.

The most important finding was that nimodipine significantly attenuated the clinical course of disease. This observation manifested itself for example in a lower relapse rate (Table 5) and a reduced clinical score in typical and atypical EAE (Fig. 3). The second finding was that this beneficial effect was mirrored by the extent of CNS histopathology. The

degree of demyelination and axonal pathology/loss was significantly reduced, and the extent of remyelination was significantly increased, which can be explained by increased numbers of oligodendrocytes/OPCs after treatment with nimodipine. Additionally, we observed increased numbers of $GFAP^+$ astrocytes that could be responsible for enhanced secretion of neurotrophic factors compared to vehicle controls. Regarding inflammation, we could neither detect a difference in the two groups in the extent of inflammation nor the inflammatory response in microarray analyses. Interestingly, we observed a reduced number of $Iba1^+$ cells in the spinal cord of nimodipine-treated mice. This effect was confirmed in organotypic slice culture of the spinal cord and in cell culture using two microglial cell lines (N9, BV2) and primary microglial culture. Induction of apoptosis was drug- and cell-specific and was not dependent on the polarization of the microglial cells. Additionally, the observed effects could not be linked to unspecific blockage of potassium channels [119-122]. Apoptosis did not seem to be mediated via a Ca_v 1.2 channel-dependent mechanism, as we were not able to detect Ca_v 1.2 channels in the microglia cells lines with several techniques. This is the most astonishing aspect of our study as we expected blockage of calcium channels to be the primary target of nimodipine. It is still a matter of debate whether microglia expresses Ca_v channels [123]. Our results provide further evidence that this is not the case.

IV.2 Effects on inflammation

In this study, we were not able to detect differences in the extent of inflammation between the groups as the size of infiltrates was comparable. Interestingly, infiltration was more present in the PF in both groups compared to the ALF, which can be related to the generally increased pathology in this funiculus. This could reflect the distinct sensomotoric deficits as detected specifically in our model. Microarray analyses of the inflammatory response also did not reveal differences between the two groups. Additional flow cytometric analyses confirmed

our results for the T cell compartment in nimodipine- and vehicle-treated mice as there was no difference detectable. Interestingly, the number of $B220^+$ B cells was increased in the spinal cord, but not in the spleen of nimodipine-treated mice. As the $B220^+$ B cells were not investigated in greater detail it is unclear which B cell subsets are increased. An increase of regulatory B cells could confirm our results for instance. This will be investigated in further studies. It is described that B cells are activated by an increase in intracellular calcium [124] and that B cells isolated from rats express a channel that shares similarities with the L-type channel in excitable tissues [125] and is also sensitive to dihydropyridines [125]. Therefore, our effect might be a response to nimodipine-mediated blockage of this channel.

IV.3 Effects on nerve fiber histopathology

In general, multiple mechanisms contribute to CNS histopathology in MS. After initial inflammatory damage, ongoing processes like dysfunction of mitochondria, generation of free radicals and oligodendrocyte death lead to demyelination, failure of regeneration and progression of the disease over time [126]. Based on our observations we suggest that nimodipine treatment is capable of addressing several of these events. Application of nimodipine reduced the expression of iNOS and ROS activation. This is reflected in less mitochondrial pathology. To quantify mitrochondrial pathology we used the mito-ratio in accordance to the g-ratio. The mito-ratio describes the size and number of the mitochondria in relation to the respective axoplasm. It is a significant indicator for increased oxidative stress [18,127]. Studying this parameter is of great relevance as mitochondrial DNA is especially vulnerable to oxidative damage [18,74,84], and damaged mitochondrial DNA is detectable in MS patients [108]. Furthermore an increased mito-ratio also correlates with early axonal pathology [18,21,74,84,85] as non-stationary mitochondria are often transported to degenerating axons as compensatory mechanisms to keep up with the enhanced energy

demand [74]. Indeed, we found less nerve fibers with increased mito-ratio after nimodipine-treatment, which was significant in the PF. Interestingly increased numbers of normal appearing nerve fibers per mm² in nimodipine-treated mice were likewise only significant in the PF, which could be related to reduced oxidative stress after nimodipine-treatment. In addition to effects on mitochondria and oxidative stress, treatment of MP4-immunized SJL/J mice with nimodipine also reduced the number of demyelinating nerve fibers per mm² and increased the number of remyelinating nerve fibers per mm² significantly. It is important to know that remyelination is not a common but rather a rare phenomenon [26]. The exact mechanism of the remyelination process is still unknown, but oligodendrocytes/OPCs play the main role in this event [26,128,129]. In response to processes as axonal injury, OPCs divide, migrate to the site of injury and differentiate into mature oligodendrocytes and enable remyelination [26,128,129]. OPC-induced enhancement of remyelination was demonstrated by Ruckh *et al., 2012* [130]. They were able to show that an age-related decline in remyelination was reversible by heterochronic parabiosis in adult animals. In our study nimodipine seems to protect oligodendrocytes/OPCs, as nimodipine treatment led to increased number of oligodendrocytes and OPCs, which could explain the increased remyelination in the treated mice. In *in vitro* models of CNS injury, increased calcium levels were shown to induce death of oligodendrocyte and axons [131] and oligodendrocyte survival was enhanced by the removal of Ca^{2+} [131]. This leads to the conclusion that oligodendrocytes in our model may directly be protected by decreased intracellular calcium levels due to nimodipine treatment. Our findings regarding the protection of oligodendrocytes/OPCs are of great relevance, as experiments to transplant additional or younger OPCs into the lesion site were only partially successful, presumably because of the disseminated distribution of MS lesions in patients [26]. Additionally, it is hard to estimate the correct amount of OPCs needed for efficient remyelination. Treatment with a drug would reach all lesions and address intrinsic

OPCs. The successful *in vitro* application of OPC differentiation inhibitors e.g., humanized monoclonal antibodies against leucine rich repeat and immunoglobulin-like domain-containing protein 1 (LINGO-1) and other inhibitory proteins [26,50] as well as agonists of OPC differentiation (for example the retinoid X receptor-γ agonist) [12,132] support our hypothesis. Although anti-LINGO-1 did not meet the pre-specified primary endpoint in a most recent clinical trial with RR-MS and SP-MS patients, improvement in the anti-LINGO-1 group was still detectable and will be further investigated [133]. Currently, restoring oligodendrocytes by implantation of stem cells is considered as possible neuroprotective strategy [34] and has become more popular. Nevertheless, it is hard to estimate long-term effects of this treatment, and it is certainly more invasive than nimodipine-treatment. A long-term application of nimodipine could be considered as low-risk as it is a well-known cardiovascular drug and typically used for long-term treatment in hypertension. As MS patients are usually young and their circulatory system is robust, the occurrence of severe side effects in response to treatment is unlikely. However, the use of nimodipine for the treatment of MS will have to be investigated in detail in clinical trials, eventually in combination with one of the already existing immune modulatory drugs.

Oligodendrocytes are involved in functions beyond remyelination. For instance, they are involved in axonal survival and they are capable of modulating fast axonal transport. In addition, they protect the integrity of the axonal cytoskeleton [26,128]. Minor changes in oligodendrocytes and myelin composition can have dramatic effects on the axon, like organelle accumulation and axonal atrophy, finally resulting in axonal loss [26]. Additionally, oligodendrocytes are known to transfer trophic factors to the axon and release neuronal growth factors (at least *in vitro*) [12,26,50,128]. Retaining these processes via protection of oligodendrocytes could explain the significantly reduced number of demyelinating nerve fibers per mm^2 and the decreased axonal loss after treatment with

nimodipine. As the capacity to remyelinate decreases with age, probably as consequence of a decreased ability of OPCs in the elderly to differentiate [26], some of the beneficial effects described for nimodipine regarding aging might be explained this way.

IV.4 Effects on glial cells

Oligodendrocytes and OPCs are not the only contributors to neuroprotection. Astrocytes have been shown to secrete neuroprotective factors like BDNF and glial cell-derived neurotrophic factor (GDNF) [21,50]. Nimodipine could be able to influence the expression of these factors as it increases the numbers of $GFAP^+$ cells in our study. We tried to detect BDNF in our sections via IHC but we were only able to detect BDNF in positive controls, but not in the spinal cord of our animals. This could be due to the embedding conditions or to a generally low expression of BDNF. We aim to investigate the expression pattern of neurotrophic factors in our future studies. Astrocytes can have detrimetal effects in MS as well [134], which seem to be triggered by an inflammatory environment [134]. Hence, nimodipine could be able to support the protective effects of astrocytes by promoting a less toxic environment (e.g. by reducing inflammatory processes). This will be investigated in mixed cultures in future studies. For this study, we decided to focus on microglia cells. These cells are reported to have opposing effects in the context of CNS inflammation and injury, which led to the concept of different phenotypes, the pro- (M1) and the anti-inflammatory phenotype (M2) [46,49]. When we first studied inflammation we detected that $Iba1^+$ cells were significantly reduced *in vivo*. We confirmed this effect in organotypic slice cultures of the spinal cord as well as in primary microglial culture and in microglia cell lines (N9 and BV2). Nimodipine-induced apoptosis was specific for this cell type. Nimodipine even increased the numbers of $GFAP^+$ cells in vivo and astrocytes cell lines (IMA2.1) *in vitro*. To fall back on the M1/M2 concept we hypothesized that nimodipine could lead a specific microglia cell type into

apoptosis, but this was not the case. However, the concept of a M1 or M2 phenotype is currently questioned [135,136] so it might be impossible to target one type of microglial cells. We did not observe a total depletion of microglial cells, which would be questionable as microglia also have beneficial effects, like increasing expression of anti-inflammatory cytokines, release of neurotrophic factors and clearance of myelin debris and toxic products [39,137]. Interestingly in studies on the optic nerve, beneficial effects on neuronal survival and axonal regeneration were ascribed to the secretion of a calcium-binding protein, called oncomodulin, by activated macrophages/microglia [138]). This indicates a potential beneficial role for microglial in the context of regeneration, mediated via enhancement of calcium binding. Another interesting study discovered that microglia mediate neurogenic hypertension and their depletion led to significantly attenuated blood pressure [139]. Triggering microglia apoptosis could be an unidentified reason why nimodipine-treatment is highly effective in the treatment hypertension in patients. In general, studies regarding depletion of microglia showed controversial results. Some studies reported an improved functional outcome following axonal loss and decreased disease progression in Alzheimer's-like disease [140,141]. Other studies claim that depletion of microglia aggravates post-ischemic inflammation and inflammatory processes in brain injury [142]. In early-life development, microglia depletion causes persistent changes in social, mood-related, and locomotor behavior in rats [143]. However, decreased numbers of microglia as consequence of treatment with nimodipine did not lead to comparable effects in our model. As we observed a beneficial effect on the clinical course and the symptoms of EAE, it is more likely that nimodipine decreases the detrimental effects of microglia, such as turning into scavenger cells, and increasing expression of cytokines and glutamate [39,76]. In addition, nimodipine treatment could prevent synaptic pathology, as the latter was correlated with the presence of activated microglia in relapsing-remitting EAE [41], and protect oligodendrocytes from apoptosis as

microglia were also shown to target oligodendrocytes in EAE lesions [43]. According to our results, nimodipine also strongly interferes with NO and ROS production. Our results are in accordance with other studies. For example *Huang et al., 2014* have shown in studies on BV-2 cells that nicardipine, another dihydropyridine calcium channel blocker, significantly inhibited migration of microglial cells, their release of NO and expression of iNOS [38]. Studying the effect of nimodipine on microglia in more detail, we discovered that nimodipine modulates the pro-inflammatory activity of surviving microglial cells in several ways. First, gene expression levels of *Tlr6*, *Tlr7* and *Tlr13* were decreased in microarray analyses of N9 cells. These genes are known to induce the release of inflammatory cytokines [144]. Additionally, gene expression of *Cpt1a* and *NADPH oxidase 4 (Nox4)* were decreased in nimodipine-treated N9 cells (Fig. 18). Most recently, Nox4 and Cpt1a expression were linked to the activation of the inflammasome in macrophages [145]. In EAE mice inhibition of NADPH oxidase activation reduced the pathology by reducing NADPH oxidase-mediated ROS production [109]. In our studies, nimodipine was similarly capable of reducing the production of ROS in the spinal cord. Furthermore, it reduced NO production and iNOS expression in microglial cells. These results are important in the context of MS, as other studies found excessive NO production and peroxynitrite formation in MS and EAE lesions, which harmed oligodendrocytes and axons [74,146,147]. Additionally, iNOS expression and NO release have been associated with inflammation and neurodegenerative diseases in general [147,148]. Underlying the significance of our findings regarding pathological events, NO metabolites were found in the cerebrospinal fluid (CSF) of MS patients [147]. Current attempts to protect nerve fibers aim at reducing damage by clearing reactive oxygen and nitrogen species [12,26]. For instance, lamotrigine, a sodium channel antagonist, was effective to protect axons from exposure to NO [26]. In addition, lamotrigine is suggested to suppress the activation and migratory activity of innate immune cells, in particular microglia,

in patients. Unfortunately, the drug failed in clinical testing, as it did not prevent brain atrophy later in disease [13,32]. Nimodipine has similar effects, but has already been demonstrated to restore cognitive function, which could make it more effective [92,95,96]. Overall, the effect of nimodipine on microglia in our study can be rated as positive for the severity of EAE. However, its effect in MS patients still needs to be examined. Taken together, nimodipine provides a more favorable environment for regenerative processes by reducing the number of microglia and hence harmful molecules and ROS. Targeting the regulation of microglial activity specifically and enhancing their phagocytic clearance could be an important step to enhance effective regeneration and hence be a valuable therapeutic option [131].

Interestingly we were not able to relate the effects on microglial cells to a calcium channel dependent mechanism. Our results provide further evidence that microglia cells do not express the $Ca_v1.2$ channels. Again, this is in line with the findings of *Huang et al., 2014.* They claim that anti-neuroinflammatory responses of microglia evoked by nicardipine are most likely not to be mediated by blockage of calcium channels, but their effects are rather due to reduction of pro-inflammatory transcription factors like Akt, nuclear factor kappa-light-chain-enhancer of activated B-cells (NF-κB) and mitogen activated protein kinase (MAPK) [39]. Indeed, we found evidence for a reduction of *Mapk* pathways in microarray studies of N9 cells treated with 10 µM nimodipine as *Mapk11*, *Map3k1* (gene encoding the mitogen-activated protein kinase kinase kinase 1) and *Map2k6* (gene encoding the mitogen-activated protein kinase kinase 6) were strongly reduced. We also found reduced *Akt2* and *Akt3* gene expression (Fig. 18) and hints for a reduction of Akt protein expression in treated N9 cells, but as previously described the protein expression was not consistent within all blots. Regarding *NF-κB* gene expression we did not find significant changes in microarray analyses. However, these pathways will be subject of further investigations.

IV.5 Additional alterations in gene expression

In the spinal cord of nimodipine-treated mice, we were also able to detect effects linked to calcium channel-dependent events in neurons, in particular a decreased *Cacna2d2* gene expression, which was recently attributed to limit regeneration by negative regulation of axonal growth [83]. Microarray analyses also revealed that nimodipine strongly reduced gene expression of semaphorins in the spinal cord (Fig. 20 A) and in N9 cells (Fig. 20 B). Semaphorins help to establish the neuronal network by regulating neuronal wiring under normal conditions, but during degenerative processes they were shown to interfere with regeneration as they affect axonal outgrowth and can be toxic to the oligodendrocyte lineage [149,150]. Most studies deal with semaphorin 3A (SEMA3A) and 7A (SEMA7A), but other semaphorins like Sema6A were shown to have negative effects on regeneration *in vivo* [149,151]. Moreover, SEMA4D is suggested to compromise the BBB, inhibit OPC differentiation and activate microglia [152]. In EAE, anti-SEMA4D was shown to improve clinical scores, to preserve myelination and to promote OPC migration to the lesion side [152], confirming our results.

A

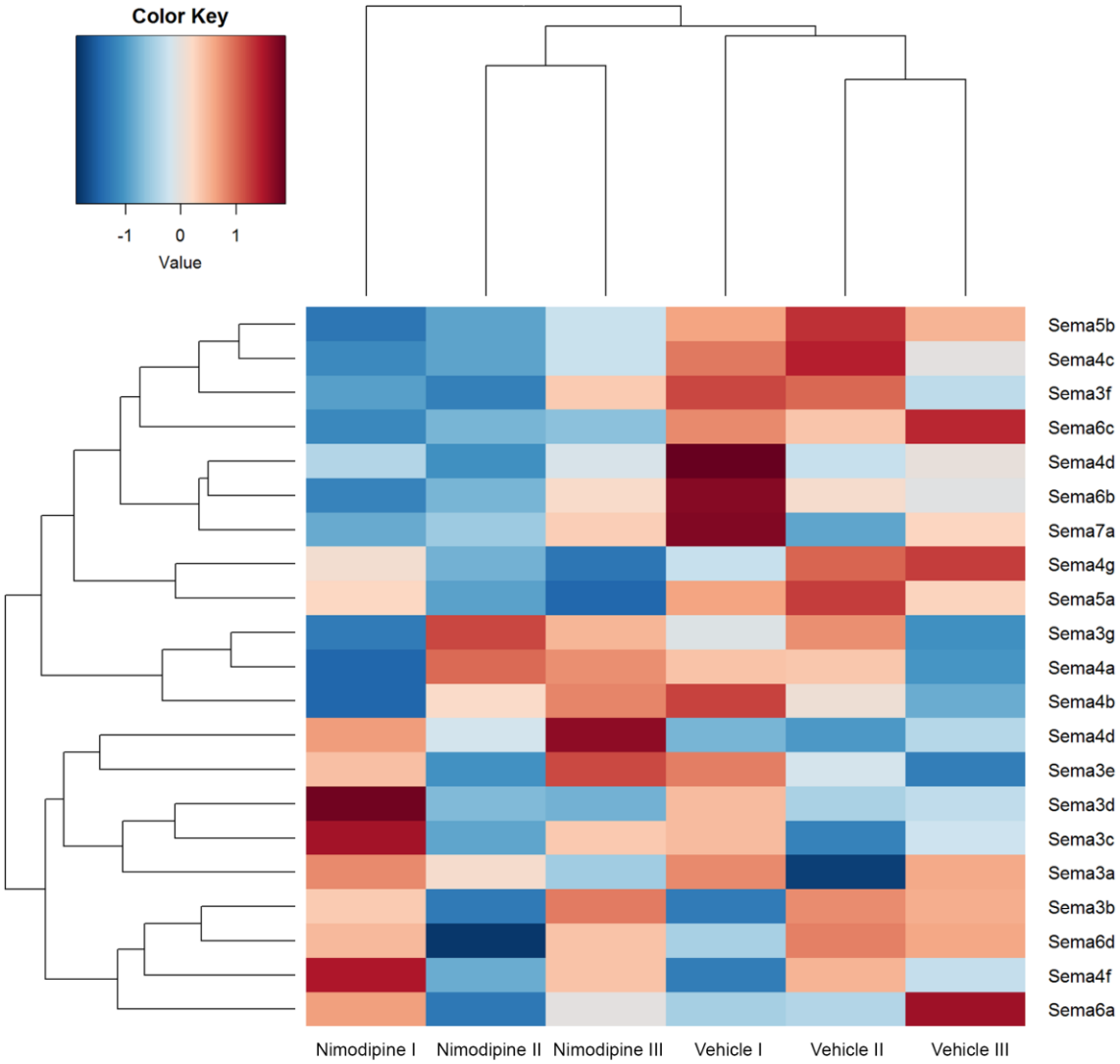

B

Gene expression in N9 cells treated with 10 µM nimodipine for 24 h compared to vehicle-treated controls	
Value	**Gene**
1.855545205	Sema4g
1.890088361	Sema6b

Fig. 20. Microrray analyses of semaphorins. (A) Heatmap of spinal cord of nimodipine-treated (*n* = 3; sample names: Nimodipine I, II and III) *vs.* vehicle-treated mice (*n* = 3; sample names: Vehicle I, II and III). Investigations took place at the onset of the second relapse after 20 (Nimodipine I and Vehicle I; day 42 after immunization) or 15 days of treatment (Nimodipine II + III and Vehicle II + III day 37 after immunization). (B) Table of strongly reduced gene expression in N9 cells treated either with 10 µM nimodipine (one sample) or the vehicle control (two samples: Vehicle I and Vehicle II) for 24 h. Microarray analysis was kindly performed by Dr. C. J. Scholz.

IV.6 Outlook and future studies

Our findings are preliminary results that warrant further investigations in order to be able to use our treatment strategy for patients. The exact mechanism how nimodipine triggers apoptosis and influences NO levels, iNOS expression and activity of ROS are unknown, and it would be useful to elucidate the mechanisms behind these observations. First targets could be BCL2 expression and glutamate-mediated excitotoxicity. It would be interesting to perform further observations in comparison with other dihydropyridines and calcium antagonists from other pharmacological groups, like verapamil. This could clarify whether potential effects are due to alterations in intracellular calcium levels or to dihydropyridine-specific effects. Some studies claim that nimodipine also has a low affinity for Ca_v 1.3 channel [153], which could be studied in comparison as well. However, microglia do not seem to express any voltage-gated calcium channels according to our analysis. Yet, it is known that they express transient receptor potential (TRP) channels [153,154], which seem to regulate microglial function [155], so it would be worth studying the effect of nimodipine on these channels in greater detail. In mammalian cells, some of the TRP family subtypes (TRPC and TRPM, in particular TRPM2) are highly expressed and activated during oxidative stress [156]. However, the effect of TRPs regarding apoptosis is complex and can vary between TRP sub-types and within different cell-types [154] so studies on the potential role for TRP channels in nimodipine neuroprotection should be carefully targeted. In microarray analyses we detected decreased expression of *Trpa1*. As TRPA1 channels are directly activated by calcium [156] this could be a potential mechanism behind the effects of nimodipine and explain our clinical observations, especially as TRPA1 antagonists were also shown to be effective in blocking pain behaviors induced by inflammation [156]. Studying the influence of nimodipine on microglial migration could be an additional approach, as nicardipine inhibits this function [39]. We have also just begun to study the role of oligodendrocytes. As they are

the main player in myelination we will start microarray and viability studies on this cell types. They are also known to express high-voltage calcium channels [67]. Between neuron and glial cells, as well as between different glial cell types, distinct communication (*cross-talk*) [67,157,158] takes place. This is why we should also investigate the effect of nimodipine in mixed cultures. On that note astrocytes should be studied as they are capable of *cross-talk*. For instance in co-culture with neurons they promoted Ca^{2+}, Na^{2+} and K^{+} channel activity [157]. Here we could focus on the influence of *cross-talk* on the expression of neurotrophic factors (BDNF, NGF) and inhibitors of regeneration.

In order to get a complete view of the potential effects of nimodipine in MS with its diverse manifestations, it would be interesting to examine its effects in other models of MS, like a chronic EAE model, and on B cells. Our results shown an significant influence of nimodipine on the number of $B220^{+}$ cells in the spinal cord. An increase in regulatory B cells could confirm our results of decreased pathological processes and should be examined in futher studies. Notably, B cells isolated from rats express a channel that shares similarities with the L-type channel and is in fact sensitive for dihydropyridines [125], so it is possible that nimodipine could influence this cell type directly.

As described earlier, microarray analyses have revealed alterations in *Cacna2d2*, *Akt* and *Mapk* gene expression, as well as in gene expression of semaphorins. We plan to investigate this in future studies.

Our findings are also important for other neurodegenerative diseases. NO production by iNOS combined with superoxide forms the toxic peroxnitrite, which was directly linked to oxidative damage and neuroinflammation in PD [155]. Immunoreactivity for iNOS was likewise increased in patients with PD [155]. The NADPH oxidase pathways influences dopaminergic neurodegeneration, a hallmark of PD, and inhibitors of NOX2 were shown to be protective in preclinical models of PD, however limitations like BBB permeability and the

lack of specificity impeded the clinical development of NOX2 inhibitors [155]. Nimodipine with its high affinity for the CNS could be a good alternative. *In vitro* experiments provide evidence that nimodipine might serve as neuroprotective agent in AD as well [90,94]. AD is marked by aggregation of the Aβ peptide and neurofibrillary tangles, associated with marked neuronal loss [70,159]. Continuous Aβ deposition in AD triggers a chronic inflammatory reaction, characterized by recruitment and proliferation of microglia followed by secretion of several inflammatory mediators, like interleukin 1β (IL-1β) [70,90,94,160] which can be considered as main players in AD. Indeed, IL-1β was shown to be neurotoxic and elevated levels of this cytokine have been detected in patients suffering from AD [94]. Despite the inhibition of microglial activation and the related decrease of NO and TNF-α, nimodipine proved to be a blocker of IL-1β secretion [90,94], hence serving as powerful inhibitor of intracellular IL-1β accumulation [94]. For a long time the protective effect of nimodipine in AD has been attributed to its ability to increase brain perfusion, solely. Our results confirm studies on AD regarding a new, direct effect of nimodipine by modulating microglial activation and secretion [90,94]. An additional mechanism of action in AD disease was introduced by *Yang et al., 2009* [161]. In this study, calcium signaling and amyloid precursor protein (APP) were closely linked for instance by constructing the hypothesis that APP is involved in the intracellular trafficking of $Ca_v1.2$. Hence, impaired APP processing may contribute to alterations in L-type calcium channel expression, followed by dysregulation of calcium homeostasis, synaptic dysfunction and AD pathogenesis [161]. Interestingly, L-type calcium channels are elevated during aging and in AD [82], which could be correlated to reduced soluble APP extracellular protein in the elderly population [162], indicating a beneficial effect of nimodipine for both aging and AD.

In order to measure the effects of nimodipine or other therapeutic drugs in patients and to optimize treatment strategies, there is still a great need of a marker of the myelination

status, and the ability to evaluate therapeutic benefit [12,26]. Therapeutic benefit in MS patients is usually determined by the assessment of the enhanced status disability score (EDSS), the annual relapse rate and MRI lesion activity. An additional parameter that attempts to detect axonal and neuronal loss is the measurement brain atrophy [14,21,23,24]. This parameter has been used to rate the outcome for clinical research trials for a long time. However, it did not only reflect the loss of nerve fibers and myelin, but also changes in the tissue fluid and vessel or glial structure, so that measurements of brain atrophy often resulted in conflicting results. A more specific method to rate the clinical outcome and to predict disease activity could be the measurement of neurofilament levels in the CSF or serum. This method is currently investigated [163], but still awaits further validation. It could be supplemented with an additional marker, for example *N*-acetylaspartate (NAA), which detects neuronal/axonal dendritic integrity and can be used in magnetic resonance spectroscopy (MRS) to measure the extent of axonal loss [21,24]. Another option is diffusion tensor imaging (DTI) to characterize nerve fiber pathology. However, it is still difficult to detect early axonal loss with imaging techniques. Thus, the development of adequate markers that can be used early or even before disease onset are essential so that the development of these markers goes hand in hand with successful treatment strategies.

IV.7 Concluding remarks

After nearly 150 years since the discovery of nerve fiber pathology in MS lesions by *Charcot* [25], there is still no available therapeutic option to attenuate nerve fiber pathology and to prevent progressive axonal loss. This is astonishing as an early treatment with neuroprotective agents could attenuate and/or prevent irreversible damage of axons, resulting in milder symptoms. Combining anti-inflammatory therapy and neuroprotection should be the most desirable goal for future treatment. Moreover, neuroprotective strategies developed for the

treatment of MS may also be beneficial for the treatment of other neurological diseases. Combined beneficial effects on oligodendrocytes, neurons and the presumed reduction of toxic neuroinflammation and oxidative stress, finally promoting regeneration, make nimodipine a highly promising candidate for future clinical trials. Additionally, its ability to decrease destructive processes in EAE pathology via reducing the number of microglial cells without completely depleting this cell type could result in a successful treatment of MS. Future studies will focus on the translation of our data to the setting of MS itself. Overall, our study raises hopes that nimodipine might serve as the first treatment option for MS that successfully combines immune modulatory features with enhanced neuroregeneration in the absence of severe side effects.

V. References

1. Rottlaender A, Villwock H, Addicks K, Kuerten S (2011) Neuroprotective role of fibroblast growth factor-2 in experimental autoimmune encephalomyelitis. *Immunology* 133(3):370-378.

2. Trapp BD, Nave KA (2008) Multiple sclerosis: an immune or neurodegenerative disorder? *Ann Rev Neurosci* 31:247-269.

3. Kuerten S, Lichtenegger FS, Faas S, Angelov DN et al. (2006) MBP-PLP fusion protein-induced EAE in C57BL/6 mice. *J Neuroimmunol* 177(1-2):99-111.

4. Trapp BD, Peterson J, Ransohoff RM, Rudick R et al. (1998) Axonal transection in the lesions of multiple sclerosis. *New Engl J Med* 338(5):278-285.

5. Sospedra, M, Martin, R (2005) Immunology of multiple sclerosis. *Annu Rev Immunol* 23:683–747.

6. Soyka, D. Kurzlehrbuch der Neurologie (1991) pp 232–239 (Soyka, Dieter: Stuttgart-New York, F.K. Schattauer Verlag (UTB).

7. Kuerten S, Gruppe TL, Laurentius L, Kich C et al. (2011) Differential patterns of spinal cord pathology induced by MP4, MOG peptide 35-55, and PLP peptide 178-191 in C57BL/6 mice. *APMIS* 119:336–46.

8. GAMES. Transatlantic Multiple Sclerosis Genetic Cooperative. (2003) A meta-analysis of whole genome linkage screens in multiple sclerosis. *J Neuroimmunol* 143(1-2):39-46.

9. Teuschner C, Noubade R, Spach K, McElvany B et al. (2006) Evidence that the Y chromosome influences autoimmune disesase in male and female mice. *Proc Natl Acad Sci USA* 103:8024–29.

10. Buddeberg BS, Kerschensteiner M, Schwab ME (2003) Die Bedeutung der axonalen Schädigung bei multipler Sklerose. *Schweiz Med Forum* 38:904–908.

11. Lidster K, Jackson SJ, Ahmed Z, Munro P et al. (2013) Neuroprotection in a novel mouse model of multiple sclerosis. *PLoS ONE* 4:8(11).

12. Hauser SL, Chan JR, Oksenberg JR (2013) Multiple sclerosis: Prospects and promise. *Ann Neurol* 74:317-327.

13. Dutta R, Trapp BD (2014) Relapsing and progressive forms of multiple sclerosis-insights from pathology. *Curr Opin Neurol* 27(3): 271–278.

14. Rottlaender A, Kuerten S. (2015) Stepchild or prodigy? Neuroprotection in multiple sclerosis research. *Int J Mol Sci* 16(7):14850-14865.

15. Magliozzi R, Howell O, Vora A, Serafini B et al. (2007) Meningeal B-cell follicles in secondary progressive multiple sclerosis associate with early onset of disease and severe cortical pathology. *Brain* 130:1089–104.

16. Kuerten S, Pauly R, Rottlaender A, Rodi M et al. (2011) Myelin-reactive antibodies mediate the pathology of MBP-PLP fusion protein MP4-induced EAE. *Clin Immunol* 140(1):54-62.

17. Lassmann H. (2016) Axonal injury in multiple sclerosis. *J Neurol Neurosurg Psychiatry* 74:695–697.

18. Waxman SG (2006) Axonal conduction and injury in multiple sclerosis: The role of sodium channels. *Nat Rev Neurosci* 7:932-941.

19. Kuerten S, Schickel A, Kerkloh C, Recks MS et al. (2012) Tertiary lymphoid organ development coincides with determinant spreading of the myelin-specific T cell response. *Acta Neuropathol* 124:861–73.

20. Barnett MH, Prineas JW (2004) Relapsing and remitting multiple sclerosis: Pathology of the newly forming lesions. *Ann Neurol* 55:458–468.

21. Dhib-Jalbut S, Arnold DL, Cleveland DW, Fischer, M et al. (2006) Neurodegeneration and neuroprotection in multiple sclerosis and other neurodegenerative diseases. *J Neuroimmunol* 176:198–215.

22. Bø L, Vedele CA, Nyland HI, Trapp BD et al. (2003) Intracortical multiple sclerosis lesions are not associated with increased lymphocyte infiltration. *Mult Scler J* 9:223-331.

23. De Stefano, N, Matthews PM, Filippi M (2003) Evidence of early cortical atrophy in MS: Relevance to white matter changes and disability. *Neurology* 60:1157–1162.

24. Filippi M, Rocca MA, de Stefano N, Enzinger C et al. (2001) Magnetic resonance techniques in multiple sclerosis. *Arch Neurol* 68:1514–1520.

25. Charcot JM (1868) Histologie de la sclérose en plaques (1868) *Gaz Hop civils et militaires* 140:554-555 and 141:557-558 and 143:566.

26. Franklin RJM, ffrench-Constant C, Edgar JM, Smith KJ (2012) Neuroprotection and repair in multiple sclerosis. *Nat Rev Neurol* 8:624-634.

27. Winkelmann A, Loebermann M, Reisinger EC, Zettl UK (2014) Multiple sclerosis treatment and infectious issues: update 2013. *Clin Exp Immunol.* 175(3):425-38.

28. Yong VW, Giuliani F, Xue M, Bar-Or A et al. (2007) Experimental models of neuroprotection relevant to multiple sclerosis. *Neurology* 68(Suppl. 3):32–37.

29. Aharoni R, Eilam R, Domey H, Labunskay G et al. (2005) The immunomodulatory glatiramer acetate augments the expression of neurotrophic factors in brains for experimental autoimmune encephalomyelitis mice. *Proc Natl Acad Sci USA* 102:19045–19050.

30. Léger OJ, Yednock TA, Tanner L, Horner HC et al. (1997) Humanization of a mouse antibody against human alpha-4 integrin: a potential therapeutic for the treatment of multiple sclerosis. *Hum Antibodies* 8:3-16.

31. Louveau A, Smirnov I, Keyes TJ, Eccles JD et al. (2015) Structural und functional features of central nervous system lymphatic vessels. *Nature* 16:523(7560):337-41.

32. Craner MJ, Damarjian TG, Liu S, Hains BC (2005) Sodium channels contribute to microglia/macrophage activation and function in EAE and MS. *Glia* 9:220-229.

33. Yagami T, Kohma H, Yagamoto Y (2012) L-type voltage-dependent calcium channels as therapeutic targets for neurodegenerative diseases. *Curr Med Chem* 19:4816–27.

34. Dulamea A (2015) Mesenchymal stem cells in multiple sclerosis-translation to clinical trials. *J Med Life* 8:24-27.

35. Frank, JA, Richert N, Lewis B, Bash, C et al. (2002) A pilot study of recombinant insulin-like growth factor-1 in seven multiple sclerosis patients. *Mult Scler J* 8:24–29.

36. Takeushi H (2013) Roles of glial cells in neuroinflammation and neurodegeneration. *Clin Exp Neuroimmunol* 4:(1):2–16.

37. Miller DW, Cookson MR, Dickson DW (2004) Glial cell inclusions and the pathogenesis of neurodegenerative diseases. *Neuron Glia Biol* 1(1):13–21.

38. Huang BR, Chang PC, Yeh WL, Lee CH et al. (2014) Anti-neuroinflammatory effects of the calcium channel blocker nicardipine on microglial cells: Implications for neuroprotection. *PLoS One* 9(3):e91167.

39. Rawji KS, Yong VW (2013) The benefits and detriments of macrophages/microglia in models of multiple sclerosis. *Clin Dev Immunol* 2013:948976.

40. McMahon EJ, Cook DN, Suzuki K, Matsushima GK (2001) Absence of macrophage-inflammatory protein-1alpha delays central nervous system demyelination in the presence of an intact blood-brain barrier. *J Immunol* 1:167(5):2964-71.

41. Rasmussen S, Wang Y, Kivisäkk P, Bronson RT et al. (2007) Persistent activation of microglia is associated with neuronal dysfunction of callosal projecting pathways and multiple sclerosis-like lesions in relapsing--remitting experimental autoimmune encephalomyelitis. *Brain* 130(Pt 11):2816-29.

42. Olah M, Amor S, Brouwer N, Vinet J et al. (2012) Identification of a microglia phenotype supportive of remyelination. *Glia* 60:306–321.

43. Peterson JW, Bö L, Mörk S, Chang A et al. (2002) VCAM-1-positive microglia target oligodendrocytes at the border of multiple sclerosis lesions. *J Neuropathol Exp Neurol* 61(6):539-46.

44. Merrill JE, Zimmerman RP (1991) Natural and induced cytotoxicity of oligodendrocytes by microglia is inhibitable by TGF beta. *Glia* 4(3):327-31.

45. Takeuchi H, Mizuno T, Zhang G, Wang J et al. (2005) Neuritic beading induced by activated microglia is an early feature of neuronal dysfunction toward neuronal death by inhibition of mitochondrial respiration and axonal transport. *J Biol Chem* 18:280(11):10444-54.

46. David S, Kroner A (2011) Repertoire of microglial and macrophage responses after spinal cord injury. *Nat Rev Neurosci* 15:12(7):388-99.

47. Mantovani A, Sica A, Sozzani S, Allavena P et al. (2004) The chemokine system in diverse forms of macrophage activation and polarization. *Trends Immunol* 25(12):677-86.

48. Martinez FO, Helming L, Gordon S (2009) Alternative activation of macrophages: an immunologic functional perspective. *Annu Rev Immunol* 27:451-83.

49. Prinz M, Priller J, Sisodia SS, Ransohoff RM (2011) Heterogeneity of CNS myeloid cells and their roles in neurodegeneration. *Nat Neurosci* 27:14(10):1227-35.

50. Batchelor PE, Howells DW (2003) CNS regeneration: Clinical possibility or basic science fantasy? *J. Clin. Neurosci* 10:523–534.

51. Komori T (1999) Tau-positive glial inclusions in progressive supranuclear palsy, corticobasal degeneration and Pick's disease. *Brain Pathol* 9(4):663-79.

52. Blakemore WF (1973) Remyelination of the superior cerebellar peduncle in the mouse following demyelination induced by feeding cuprizone. *J Neurol Sci* 20:73-83.

53. Ludwin SK (1978) Central nervous system demyelination and remyelination in the mouse: an ultrastructural study of cuprizone toxicity. *Lab Invest* 39:597-612.

54. Matsushima GK, Morell P (2001) The neurotoxicant, cuprizone, as a model to study demyelination and remyelination in the central nervous system. *Brain Pathol* 11(1):107-16.

55. Kipp M, Clarner T, Dang J, Copray S, Beyer, C (2009) The cuprizone animal model: new insights into an old story. *Acta Neuropathol* 118:723–36.

56. Kipp M, Nyamoya S, Hochstrasser T, Amor S (2017) Multiple sclerosis animal models: a clinical and histopathological perspective. *Brain Pathol* 27:2:121-245.

57. Olezak EL, Chang JR, Friedman H, Katsetos CD, Platsoucas CD (2004) Theiler's virus infection: a model for multiple sclerosis. *Clin Microbiol Rev* 17:174-207.

58. Tsunoda I, Fujinami RS (2010) Neuropathogenesis of Theiler's murine encephalomyelitis virus infection, an animal model for multiple sclerosis. *J Neuroimmune Pharmacol* 5:355-369.

59. Goverman J, Brabb T (1996) Rodent models of experimental allergic encephalomyelitis applied to the study of multiple sclerosis. *Lab Anim Sci* 46:482-492.

60. Stromnes IM, Goverman JM (2006) Active induction of experimental allergic encephalomyelitis. *Nat Protoc* 1(4):1810-1819.

61. Baxter AG (2007) The origin and application of experimental autoimmune encephalomyelitis. *Nat Rev Immunol* 7:904-912.

62. Pöllinger B, Krishnamoorthy G, Berer K, Lassmann H et al. (2009) Spontaneous relapsing-remitting EAE in the SJL/J mouse: MOG-reactive transgenic T cells recruit endogenous MOG-specific B cells. *J Exp Med* 8:206(6):1303–1316.

63. Hofstetter HH, Shive CL, Forsthuber TG (2002) Pertussis toxin modulates the immune response to neuroantigens injected in incomplete Freund's adjuvant: induction of Th1 cells and experimental autoimmune encephalomyelitis in the presence of high frequencies of Th2 cells. *J Immunol* 169:117-125.

64. Swarnkar, S, Goswami P, Karmat PK, Gupta S et al. (2012) Rotenone-induced apoptosis and role of calcium: a study on Neuro-2a cells. *Arch Toxicol* 86:1387–97.

65. Kumar N, Singh N, Jaggi AS (2012) Anti-stress effects of cilnidipine and nimodipine in immobilization subjected mice. *Physiol Behav* 105(5):1148-1155.

66. Catterall WA, Perez-Reyes E, Snutch TP, Striessnig J (2005) International Union of Pharmacology. XLVIII. Nomenclature and Structure-Function Relationships of Voltage-Gated Calcium Channels *Pharmacol Rev* 57 (4):411-425. 12.

67. Verkhratsky A, Kettenmann H (1996) Calcium signalling in glial cells. *Trends Neurosci* 19(8):346-52.

68. Casamassima F, Hay AC, Benedetti A, Lattanzi L et al. (2010) L-type calcium channels and psychiatric disorders: A brief review. *Am J Med Genet B Neuropsychiatr Genet* 5:53B(8):1373-90.

69. Triggle DJ (2007) Calcium channel antagonists: clinical uses--past, present and future. *Biochem Pharmacol* 30:74(1):1-9.

70. Silei V, Fabrizi C, Venturini G, Salmona M et al. (1999) Activation of microglial cells by PrP and beta-amyloid fragments raises intracellular calcium through L-type voltage sensitive calcium channels. *Brain Res* 6:818(1):168-70.

71. Stys PK, Jiang Q (2002) Calpain-dependent neurofilament breakdown in anoxic and ischemic rat central axons. *Neurosci Lett* 328:150–4.

72. Takano Y, Ohguro H, Dezawa M, Ishikawa H et al. (2004) Study of drug effects of calcium channel blockers on retinal degeneration of rd mouse. *Biochem Biophys Res Commun* 313(4):1015-1022.

73. Damaj MI, Martin BR (1993) Calcium agonists and antagonists of the dihydropyridine type: effect on nicotine-induced antinociception and hypomotility. *Drug Alcohol Depend* 32(1):73-79.

74. Gonsette RE (2008) Oxidative stress and excitotoxicity: a therapeutic issue in multiple sclerosis? *Mult Scler* 14(1):22-34.

75. Raddassi K, Berthon B, Petit JF, Lemaire G (1994) Role of calcium in the activation of mouse peritoneal macrophages: induction of NO synthase by calcium ionophores and thapsigargin. *Cell Immunol* 153(2):443-55.

76. Shijie J, Takeuchi H, Yawata I, Harada Y et al. (2009) Blockade of glutamate release from microglia attenuates experimental autoimmune encephalomyelitis in mice. *Tohoku J Exp Med* 217(2):87-92.

77. Brewer LD, Thibault O, Staton J, Thibault V et al. (2007) Increased vulnerability of hippocampal neurons with age in culture: temporal association with increases in NMDA receptor current, NR2A subunit expression and recruitment of L-type calcium channels. *Brain Res* 1151:20-31.

78. Thibault O, Pancani T, Landfield PW, Norris CM (2012) Reduction in neuronal L-type calcium channel activity in a double knock-in mouse model of Alzheimer's disease. *Biochim Biophys Acta* 1822(4):546–549.

79. Shen AN, Cummings C, Pope D, Hoffman D (2016) A bout analysis reveals age-related methylmercury neurotoxicity and nimodipine neuroprotection. *Behav Brain Res* 15(311):147-159.

80. Gazulla J, Tintoré M (2007) The P/Q-type voltage-dependent calcium channel: a therapeutic target in spinocerebellar ataxia type 6. *Acta Neurol Scand* 115:356–36.

81. Sigh A, Verma P, Balaji G, Samantaray S (2016) Nimodipine, an L-type calcium channel blocker attenuates mitochondrial dysfunctions to protect against 1-methyl-4-phenyl-1,2,3,6-tetrahydropyridine-induced Parkinsonism in mice. *Neurochem Int* 99:221-232.

82. Thibault O, Hadley R, Landfield PW (2001) Elevated postsynaptic [Ca2+]i and L-type calcium channel activity in aged hippocampal neurons: relationship to impaired synaptic plasticity. *J Neurosci* 15:21(24):9744-56.

83. Tedeschi A, Dupraz S, Laskowski CJ, Xue J et al. (2016**)** The calcium channel subunit alpha2delta2 suppresses axon regeneration in the adult CNS. *Neuron* 19:92(2):419-434.

84. Zambonin JL, Zhao C, Ohno N, Campbell GR et al. (2011) Increased mitochondrial content in remyelinated axons: implications for multiple sclerosis. *Brain* 134:1901–13.

85. Dutta R, McDonough J, Yin X, Peterson J et al. (2006) Mitochondrial dysfunction as a cause of axonal degeneration in multiple sclerosis patients. *Ann Neurol* 59:478–489.

86. Trump BF, Berezesky IK (1995) Calcium-mediated cell injury and cell death. *FASEB J* 9(2):219-28.

87. Recks MS, Stormanns ER, Bader J, Arnold S et al. (2013) Early axonal damage and progressive myelin pathology define the kinetics of CNS histopathology in a mouse model of multiple sclerosis. *Clin Immunol* 149(1):32-45.

88. Scriabine A, Schuurman TTJ (1989) Pharmalogical basis for the use of nimodipine in central nervous system disorders. *The FASEB Journal* 3, 1799–1806.

89. Bayer Vital GmbH Fachinformation Nimodipin, Gelbe Liste Pharmindex.
Information as of June 2014.

90. Li Y, Hu X, Liu Y, Bao Y, An L (2009) Nimodipine protects dopaminergic neurons against inflammation-mediated degeneration through inhibition of microglial activation. *Neuropharmacology* 56(3):580-589.

91. Levy A, Kong RM, Stillman MJ, Shukitt-Hale-B et al. (1991) Nimodipine improves spatial working memory and elevates hippocampal acetylcholine in young rats. *Pharmacol Biochem Behav* 39(3):781-786.

92. Taya K, Watanabe Y, Kobayashi H, Fujiwara M (2000) Nimodipine improves the disruption of spatial cognition induced by cerebral ischemia. *Physiol Behav* 70(1-2): 19-25.

93. LeVere TE, Brugler T, Sandin M, Gray-Silva, S (1989) Recovery of function after brain damage: facilitation by the calcium entry blocker nimodipine. *Behav Neurosci* 103:561–5.

94. Sanz JM, Chiozzi P, Colaianna M, Zotti M et al. (2012) Nimodipine inhibits IL-1β release stimulated by amyloid β from microglia. *Br J Pharmacol* 167(8):1702-11.

95. Kusztos RD, Ingram DK, Spangler EL, London ED (1996) Effects of aging and chronic nimodipine on hippocampal binding of [3H]CGS 19755. *Neurobiol Aging* 17(3):453-457.

96. de Jong GI, Buwalda B, Schuurman T, Luiten PG (1992) Synaptic plasticity in the dentate gyrus of aged rats is altered after chronic nimodipine application. *Brain Res* 596(1-2)345-348.

97. Krieglstein J, Seif el Nasr M, Lippert K (1997) Neuroprotection by memantine as increased by hypothermia and nimodipine. European Journal of Pharmaceutical Sciences 5, 71–77.

98. Herzfeld E, Strauss C, Simmermacher S, Bork K (2014) Investigation of the neuroprotective impact of nimodipine on Neuro2a cells by means of a surgery-like stress model. *Int J Mol Sci* 15:18453-18465.

99. Wang H, James ML, Venkatraman TN, Wilson LJ (2014) pH-sensitive NMDA inhibitors improve outcome in a murine model of SAH. *Neurocrit Care* 20:119-131.

100. Khosla P, Pandhi P (2000) Anticonvulsant effect of Nimodipine alone and in combination with Diazepam on PTZ induced status epilepticus. *Methods Find Exp Clin Pharmacol* 22(10):731-6.

101. Barnett GH, Bose B, Little JR, Jones SC et al. (1986) Effects of nimodipine on acute focal cerebral ischemia. *Stroke* 17: 884–90.

102. Barnes NY, Li L, Yoshikawa K, Schwartz LM et al. (1998) Increased production of amyloid precursor protein provides a substrate for caspase-3 in dying motoneurons. *J Neurosci* 18(15):5869–80.

103. Babu CS, Ramanathan M (2011) Post-ischemic administration of nimodipine following focal cerebral ischemic-reperfusion injury in rats alleviated excitotoxicity, neurobehavioural alterations and partially the bioenergetics. *Int J Dev Neurosci* 29:93–105.

104. Pileblad E, Carlsson A (1986) In vivo effects of Ca2+-antagonist nimodipine on dopamine metabolism in mouse brain. *J Neural Transm* 66:177-187.

105. Talbot JD, David G, Barrett EF, Barrett JN (2012) Calcium dependence of damage to mouse motor nerve terminals following oxygen/glucose deprivation. *Exp Neurol* 234:95–104.

106. National Research Council (2011) Guide for the Care and Use of Laboratory Animals (National Academies Press, Washington, DC), 8th Ed.

107. Guy J, Ellis EA, Hope GM, Emerson S (1991) Maintenance of myelinated fibre g ratio in acute experimental allergic encephalomyelitis. *Brain* 114 (Pt 1A):281-294.

108. Mao P, Reddy PH (2010) Is multiple sclerosis a mitochondrial disease? *Biochim Biophys Acta* 1802(1):66-79.

109. Choi BY, Kim JH, Kho AR, Kim IY et al. (2015) Inhibition of NADPH oxidase activation reduces EAE-induced white matter damage in mice. *J Neuroinflammation* 12:104.

110. Livak KJ, Schmittgen TD (2001) Analysis of relative gene expression data using real-time quantitative PCR and the 2(-Delta Delta C(T)) Method. *Methods* 25(4):402-408.

111. Kendziorski CM, Newton MA, Lan H, Gould MN (2003) On parametric empirical Bayes methods for comparing multiple groups using replicated gene expression profiles. *Stat Med* 22(24):3899–3914.

112. Chatterjee D, Biswas K, Nag S, Ramachandra SG, Das Sarma J (2013) Microglia play a role in direct viral induced demyelination. *Clin Dev Immunol* 2013:510396.

113. Connelly CA, Chen LC, Colquhoun S (2000) Metabolic activity of cultured rat brainstem, hippocampal and spinal cord slices. *J Neurosci Methods* 99(1-2):1-7.

114. Bishnoi M, Chopra K, Kulkarni SK (2008) Protective effect of L-type calcium channel blockers against haloperidol-induced orofacial dyskinesia: a behavioural, biochemical and neurochemical study. *Neurochem Res* 33(9):1869-1880.

115. Lang J, Maeder Y, Bannermann P, Xu J et al. (2013) Adenomatous polyposis coli regulates oligodendroglial development. *J Neurosci* 33(7):3113–3130.

116. Henn A, Lund S, Hedtjärn, Schrattenholz A et al. (2009) The suitability of BV2 cells as alternative model system for primary microglia cultures or for animal experiments examining brain inflammation. *ALTEX* 26(2):83-94.

117. Stansley B, Post J, Hensley K (2012) A comparative review of cell culture systems for the study of microglial biology in Alzheimer's disease. *J Neuroinflammation* 9:115.

118. Furukawa T, Yamakawa T, Midera T, Sagawa T et al. (1999) Selectivities of dihydropyridine derivatives in blocking Ca(2+) channel subtypes expressed in Xenopus oocytes. *J Pharmacol Exp Ther* 291(2):464-473.

119. Wulff H, Castle NA, Pardo LA (2009) Voltage-gated potassium channels as therapeutic targets. *Nat Rev Drug Discov* 8(12)982-1001.

120. Grissmer S, Nguyen AN, Aiyar J, Hanson DC et al. (1994) Pharmacological characterization of five cloned voltage-gated K+ channels, types Kv1.1, 1.2, 1.3, 1.5, and 3.1, stably expressed in mammalian cell lines. *Mol Pharmacol* 45(6):1227-1234.

121. Chandy KG, DeCourseyTE, Cahalan MD, McLaughlin C, Gupta S (1984) Voltage-gated potassium channels are required for human T lymphocyte activation. *J Exp Med* 160(2):369-385.

122. Wulff H, Kolski-Andreaco A, Sankaranarayanan A, Sabatier JM, Shakkottai V (2007) Modulators of small- and intermediate-conductance calcium-activated potassium channels and their therapeutic indications. *Current Med Chem* 14(13):1437-1457.

123. Färber K, Kettenmann H (2005) Physiology of microglial cells. *Brain Res Brain Res Rev* 48(2):133-143.

124. Lyubchenko T (2010) Ca2+ Signaling in B Cells. *ScientificWorldJournal* 10:2254–2264.

125. Sadighi Akha AA, Willmott NJ, Brickley K, Dolphin AC et al. (1996) Anti-Ig-induced calcium influx in rat B lymphocytes mediated by cGMP through a dihydropyridine-sensitive channel. *J Biol Chem* 271:13:7297–7300.

126. Leuner K, Müller WE, Reichert AS (2012) From mitochondrial dysfunction to amyloid beta formation: novel insights into the pathogenesis of Alzheimer's disease. *Molecular neurobiology* 46:186–93.

127. Mahad D, Lassmann H, Turnbull D (2008) Review: Mitochondria and disease progression in multiple sclerosis. *Neuropathol Appl Neurobiol* 34(6):577-89.

128. Wilkins A, Majed H, Layfield R, Compston A, et al. (2003) Oligodendrocytes promote neuronal survival and axonal length by distinct intracellular mechnisms: A novel role for oligodendrocyte-derived glial cell line-derived neurotrophic factor. *J Neurosci* 23:4967–4974.

129. Kotter MR, Li WW, Zhao C, Franklin RJ (2006) Myelin impairs CNS remyelination by inhibiting oligodendrocyte precursor cell differentiation. *J Neurosci* 26:328–332.

130. Ruckh JM, Zhao JW, Shadrach JL, van Wijngaardeb P et al. (2012) Rejuvination of regeneration in the aging central nervous system. *Cell Stem Cell* 10:96–103.

131. Tekkök, SB, Goldberg MP (2001) AMPA/kainate receptor activation mediates hypotoxic oligodendrocyte death and axonal injury in cerebral white matter. *J Neurosci* 21:4237-4248.

132. Huang JK, Fancy SP, Zhao C, Rowitch DH et al. (2011) Myelin regeneration in multiple sclerosis: Targeting endogenous stem cells. *Neurotherapeutics* 8:650–658.

133. Mellion M, Edwards KR, Hupperts R, Drulović L et al. (2017) Efficacy results from the phase 2b SYNERGY study: Treatment of disabling multiple sclerosis with the anti-LINGO-1 monoclonal antibody opicinumab (S33.004). *Neurology* 88:16S33.004.

134. Nair A, Frederick TJ, Miller SD (2008) Astrocytes in multiple sclerosis: a product of their environment. *Cell Mol Life Sci* 65(17):2702-2720.

135. Ransohoff RM (2016) A polarizing question: do M1 and M2 microglia exist? *Nat Neurosci* 19:987–991.

136. Mittelbronn M (2014) The M1/M2 immune polarization concept in microglia: a fair transfer? *Neuroimmunol Neuroinflammation* 1(1):6-7.

137. Kettenmann H, Hanisch U-K, Noda M, Verkhratsky A (2011) Physiology of microglia. *Physiol Rev* 91(2):461-553.

138. Yin Y, Cui Q, Gilbert HY, Yang Y et al. (2009) Oncomodulin links inflammation to optic nerve regeneration *Proc Natl Acad Sci USA* 17:106(46):19587–19592.

139. Shen XZ, Li Y, Li L, Shah KH et al. (2015) Microglia participate in neurogenic regulation of hypertension. *Hypertension* 66(2):309-316.

140. Olmos-Alonso A, Schetters ST, Sri S, Askew K (2016) Pharmacological targeting of CSF1R inhibits microglial proliferation and prevents the progression of Alzheimer's-like pathology. *Brain* 139(Pt 3):891-907.

141. Rice RA, Spangenberg EE, Yamate-Morgan H, Lee RJ et al. (2015) Elimination of microglia improves functional outcomes following extensive neuronal loss in the hippocampus. *J Neurosci* 8:35(27): 9977–9989.

142. Jin WN, Xiang-Yu Shi S, Li Z, Li M et al. (2017) Depletion of microglia exacerbates postischemic inflammation and brain injury. J Cereb Blood Flow Metab 1:271678X17694185. doi: 10.1177/0271678X17694185. [Epub ahead of print]

143. Nelson LH, Lenz KM (2017) Microglia depletion in early life programs persistent changes in social, mood-related, and locomotor behavior in male and female rats. *Behav Brain Res* 1:316:279-293.

144. Pradhan VD, Das S, Surve P, Ghosh K (2012) Toll-like receptors in autoimmunity with special reference to systemic lupus erythematosus. *Indian J Hum Genet* 18(2):155-160.

145. Moon JS, Nakahira K, Chung KP, DeNicola GM et al. (2016) NOX4-dependent fatty acid oxidation promotes NLRP3 inflammasome activation in macrophages. *Nat Med* 22(9):1002-1012.

146. Stadelmann C, Wegner C, Brück W (2011) Inflammation, demyelination, and degeneration - recent insights from MS pathology. *Biochim Biophys Acta* 1812(2): 275-282.

147. Giovannoni G, Heales SJ, Land JM, Thompson EJ (1998) The potential role of nitric oxide in multiple sclerosis. *Mult Scler* 4(3):212-216.

148. Hobbs AJ, Higgs A, Moncada S (1999) Inhibition of nitric oxide synthase as a potential therapeutic target. *Annu Rev Pharmacol Toxicol* 39:191-220.

149. Pasterkamp RJ, Verhaagen J (2001) Emerging roles for semaphorins in neural regeneration. *Brain Res Brain Res Rev* 35(1):36-54.

150. Costa C, Martínez-Sáez E, Gutiérrez-Franco A, Eixarch H et al. (2015) Expression of semaphorin 3A, semaphorin 7A and their receptors in multiple sclerosis lesions. *Mult Scler* 21(13):1632-43.

151. Rünker AE, Little GE, Suto F, Fujisawa H et al. (2008) Semaphorin-6A controls guidance of corticospinal tract axons at multiple choice points. *Neural Dev* 8:3:34.

152. Smith ES, Jonason A, Reilly C, Veeraraghavan J et al. (2015) SEMA4D compromises blood-brain barrier, activates microglia, and inhibits remyelination in neurodegenerative disease. *Neurobiol Dis* 73:254-68.

153. Xu W, Lipscombe D (2001) Neuronal Ca(V)1.3alpha(1) L-type channels activate at relatively hyperpolarized membrane potentials and are incompletely inhibited by dihydropyridines. *J Neurosci* 15:21(16):5944-51.

154. Miller BA (2006) The role of TRP channels in oxidative stress-induced cell death. *J Membrane Biol* 209:31-41.

155. Richardson JR, Hossain MM (2013) Microglial ion channels as potential targets for neuroprotection in Parkinson's disease. *Neural Plast* 2013:587418.

156. Klionsky L, Tamir R, Gao BX , Wang W (2007) Species-specific pharmacology of Trichloro(sulfanyl)ethylbenzamides as transient receptor potential ankyrin 1 (TRPA1) antagonists. *Mol Pain* 3:39 published online doi: 10.1186/1744-8069-3-39.

157. Karshin A, Wischmeyer E, Davidson N, Lester HA (1994) Fast inhibition of inwardly rectifying K^+ channels by multiple neurotransmitter receptors in oligodendroglia. *Eu J Neurosci* 6:1756-1764.

158. Domingues HS, Portugal CC, Socodato R, Relvas JB (2016) Oligodendrocyte, astrocyte and microglia crosstalk in myelin development, damage, and repair. *Front Cell Dev Biol* 4:71.

159. Ballard C, Gauthier S, Corbett A, Brayne C et al. (2011) Alzheimer's disease. *Lancet* 19:377(9770):1019-31.

160. Michelucci A, Heurtaux T, Grandbarbe L, Morga E et al. (2009) Characterization of the microglial phenotype under specific pro-inflammatory and anti-inflammatory conditions: Effects of oligomeric and fibrillar amyloid-beta. *J Neuroimmunol* 29:210(1-2):3-12

161. Yang L, Wang Z, Wang B, Justice NJ et al. (2009) Amyloid precursor protein regulates Cav1.2 L-type calcium channel levels and function to influence GABAergic short-term plasticity. *J Neurosci* 16:29(50):15660-8.

162. Palmert MR, Usiak M, Mayeux R, Raskind M et al. (1990) Soluble derivatives of the β amyloid protein precursor in cerebrospinal fluid: alterations in normal aging and in Alzheimer's disease. *Neurology* 40:7:1028.

163. Håkansson I, Tisell A, Cassel P, Blennow K et al. (2017) Neurofilament light chain in cerebrospinal fluid and prediction of disease activity in clinically isolated syndrome and relapsing-remitting multiple sclerosis. *Eur J Neurol* 24(5):703-712. doi: 10.1111/ene.13274. Epub 2017 Mar 6.

VI. Annex

Acknowledgments

I would like to thank Alla Ganscher, Eleonora Emilia Maier, Silvia Seubert and Dr. Nicole Wagner, Dr. Claus-Jürgen Scholz and Prof. Dr. Erhard Wischmeyer for technical support. Lina Koetzner for her committed work at the animal facility as well as Helena Batoulis, Tobias Koeniger, Robert Blum and Heike Wulff for good advice and fruitful discussions. I am very grateful to Michael Christof for excellent support with figure design as well as his patience in constantly changing figure details. Thanks to Reuven Stein, Regina Piske, Helmut Kettenmann, Jacqueline Trotter and Stefan Schildknecht for providing the cell lines and to Lea Seidlmayer for donating cardiomyocytes as control tissue for our stainings. Thanks to our collaboration partners and to Dr. Thomas Glaser for providing nimodipine and his enthusiasm for the study. The mice I had to sacrifice shall not go unmentioned here. Moreover, I would like to thank my colleagues - I really enjoyed working with you. Thanks to my trainers everywhere (Cologne, Halifax, Bonn, Kristianstad, Davis) but especially to Piet from Crossfit Wuerzburg for giving me the opportunity to work off stress and teaching me lessons also for my professional life. The 1. FC Koeln taught me to find the silver lining in every cloud- a quality absolutely needed for a scientist. Special thanks to the GSLS Wuerzburg for constant support and enthusiasm as well as to Prof. Dr. Stefanie Kuerten, for being optimistic to the core in every situation. Thanks a lot to Olivia Buonarati and Frances Shaffo for correcting the manuscript and for bringing California home to me (this holds true for Tyler as well). Most thanks belong to my whole family and friends for their constant support. Thank you for understanding that I had to spent so much time at work and missed some special days. Thanks a lot for sharing the enthusiasm for my work with me and most of all for the great time I do have with all of you. Dr. Ernst Schampel still inspires me with his passion for life-long

learning. We miss you. The biggest thanks are due to my husband Alexander Schampel. I am truly grateful for your constant support to achieve my goals, but you should know that you are my biggest victory.

Publications list

Schampel A., Volovitch O, Koeniger T, Scholz CJ et al. (2017) Nimodipine fosters remyelination in a mouse model of multiple sclerosis and induces microglia-specific apoptosis. *Proc Natl Acad Sci USA* 114 (16):E3295-E3304.

The publication `Schampel et al., 2017´ is based on this thesis, hence part of the figures is also published in PNAS.

Rottlaender A., Kuerten S. (2015) Stepchild or Prodigy? Neuroprotection in Multiple Sclerosis (MS) Research. *Int J Mol Sci* 16(7):14850–65.

Lehmann PV, **Rottlaender A**, Kuerten S (2015) The autoimmune pathogenesis of multiple sclerosis. *Pharmazie* 70(1):5–11.

Batoulis H, Wunsch M, Birkenheier J, **Rottlaender A** et al. (2015) Central nervous system infiltrates are characterized by features of ongoing B cell-related immune activity in MP4-induced experimental autoimmune encephalomyelitis. *Clin Immunol* 158(1):47–58.

Rottlaender A, Villwock H, Addicks K, Kuerten S (2011) Neuroprotective role of fibroblast growth factor-2 in experimental autoimmune encephalomyelitis. *Immunology* 133(3):370–378.

Kuerten S, Pauly R, **Rottlaender A**, Rodi M et al. (2011). Myelin-reactive antibodies mediate the pathology of MBP-PLP fusion protein MP4-induced EAE. *Clin Immunol* 140(1):54–62.

Kuerten S, Pauly R, Blaschke S, **Rottlaender A** et al. (2011) The significance of a B cell-dependent immunopathology in multiple sclerosis. *Fortschr Neurol Psychiatr* 79(2):83–91.

Kuerten S, **Rottlaender A**, Rodi M, Schroeter M et al. (2010) The clinical course of EAE is reflected by the dynamics of the neuroantigen-specific T cell compartment in the blood. *Clin Immunol* 137:422–432.

Kuerten S, Sparing R, **Rottlaender A**, Rodi M et al. (2009) Die Durafistel – ein unscheinbares morphologisches Korrelate mit großen Konsequenzen. *Fortschr Neurol Psychiatr* 77:679–707.

Curriculum vitae Andrea Schampel